Critical velocities and mutual friction in 3He-4He mixtures at temperatures below 100 mK

Citation for published version (APA):
Zeegers, J. C. H. (1991). *Critical velocities and mutual friction in 3He-4He mixtures at temperatures below 100 mK*. [Phd Thesis 1 (Research TU/e / Graduation TU/e), Applied Physics]. Technische Universiteit Eindhoven. https://doi.org/10.6100/IR345261

DOI:
10.6100/IR345261

Document status and date:
Published: 01/01/1991

Document Version:
Publisher’s PDF, also known as Version of Record (includes final page, issue and volume numbers)

Please check the document version of this publication:

• A submitted manuscript is the version of the article upon submission and before peer-review. There can be important differences between the submitted version and the official published version of record. People interested in the research are advised to contact the author for the final version of the publication, or visit the DOI to the publisher's website.
• The final author version and the galley proof are versions of the publication after peer review.
• The final published version features the final layout of the paper including the volume, issue and page numbers.

Link to publication

General rights
Copyright and moral rights for the publications made accessible in the public portal are retained by the authors and/or other copyright owners and it is a condition of accessing publications that users recognise and abide by the legal requirements associated with these rights.

- Users may download and print one copy of any publication from the public portal for the purpose of private study or research.
- You may not further distribute the material or use it for any profit-making activity or commercial gain
- You may freely distribute the URL identifying the publication in the public portal.

If the publication is distributed under the terms of Article 25fa of the Dutch Copyright Act, indicated by the “Taverne” license above, please follow below link for the End User Agreement:

www.tue.nl/taverne

Take down policy
If you believe that this document breaches copyright please contact us at:

openaccess@tue.nl

providing details and we will investigate your claim.

Download date: 24. Aug. 2022

CRITICAL VELOCITIES AND MUTUAL FRICTION

IN ^3He-^4He II MIXTURES AT TEMPERATURES BELOW 100 mK

Jos Zeegers

CRITICAL VELOCITIES
AND
MUTUAL FRICTION

IN ^{3}He–^{4}He MIXTURES
AT TEMPERATURES BELOW 100 mK

PROEFSCHRIFT

ter verkrijging van de graad van doctor aan de Technische Universiteit Eindhoven, op gezag van de Rector Magnificus, prof. ir. M. Tels, voor een commissie aangewezen door het College van Dekanen in het openbaar te verdedigen op vrijdag 25 januari 1991 te 14.00 uur.

door

JOSEPHUS CATHARINA HENRICUS ZEEGERS

geboren te Oss

Druk: Letru, Helmond, 04920-37797

Dit proefschrift is goedgekeurd door
de promotor: prof. dr. H.M. Gijsman
en de copromotor: dr. A.T.A.M. de Waele

The work described in this thesis was carried out at the Physics Department of the Eindhoven University of Technology and was partly supported by the Dutch Foundation for the Fundamental Research on Matter (FOM), which is financially supported by the Dutch Organization for the Advancement of Research (NWO).

"In experimental philosophy we are to look upon propositions inferred by general induction from phenomena as accurately or very nearly true, notwithstanding any contrary hypotheses that may be imagined, till such time as other phenomena occur, by which they may either be made more accurate, or liable to exceptions".
Sir Isaac Newton, Principia (1686, 1713, 1725), Rule IV of book three, The system of the world. Motte's translation (1729).

"Every man is a valuable member of society who by his observations, researches and experiments procures knowledge for men".
J.M. Smithson

Aan mijn ouders

CONTENTS

CHAPTER 1 GENERAL INTRODUCTION.

1.1 ^{4}He II and ^{3}He–^{4}He II mixtures. 1

1.2 Basic results of previous work and a preview for experiments to do. 7

CHAPTER 2 PHENOMENOLOGICAL DESCRIPTION.

2.1 Thermohydrodynamic equations in their simplified form, mechanical-vacuum approximation. 13

2.2 Including mutual friction phenomenologically in ^{3}He–^{4}He II mixtures. 17

CHAPTER 3 EXPERIMENTAL SETUP AND MEASURING TECHNIQUES.

3.1 Experimental setup. 23

  3.1.1 The low temperature part of the flow system. 23

  3.1.2 The flow system in detail. 25

3.2 Measuring techniques. 27

  3.2.1 Thermometry. 27

  3.2.2 ^{3}He-concentration. 27

  3.2.3 Pressure measurement. 29

  3.2.4 ^{4}He-chemical potential. 31

3.3 The measuring procedure. 32

CHAPTER 4 STEADY STATE EXPERIMENTS AND RESULTS.

4.1 Introduction. 37

4.2 Designing a flow channel for intermediate flow velocities. 37

4.3 The first setup and the first results. 40

4.4 The flow impedances. 41

4.5 Temperature differences. 44

4.6 Concentration differences. 48

4.7 Pressure differences. 51

4.8 T^2-x diagrams. 55

4.9 The chemical–potential difference. 58

4.10 Conclusion. 61

CHAPTER 5 THE OBSERVATION OF THE CRITICAL VELOCITY AND VORTEX LINE DENSITIES.

5.1 Introduction. 63
5.2 The transition. 64
  5.2.1 Circular tubes. 64
  5.2.2 Measurements with annular channels. 66
5.3 Vortex line densities. 68
5.4 The Vinen model and its application. 71
  5.4.1 The model. 71
  5.4.2 Comparison of our data with the Vinen model. 77
5.5 The value of the critical velocity. 82
  5.5.1 Diameter dependence for circular tubes. 82
  5.5.2 Annular tubes, a different criterion. 84
  5.5.3 Temperature dependence. 85
5.6 A survey concerning related work and the critical velocity. 86
  5.6.1 Some considerations concerning vortices and the critical velocity. 86
  5.6.2 The effect of ^{3}He on ^{4}He vortices. 88
  5.6.3 Related work in mixtures. 89
5.7 Comparison of mutual friction in pure ^{4}He II with mutual friction in mixtures. 90
  5.7.1 Parameters and vortex line densities. 90
  5.7.2 Circular flow channels. 91
  5.7.3 Annular flow channels. 92
5.8 Conclusion. 93

CHAPTER 6 FLUCTUATION EXPERIMENTS.

6.1 Introduction. 95
6.2 Transient effects. 96
  6.2.1 Time constants of the detectors. 96
  6.2.2 The relaxation phenomenon. 97
  6.2.3 The pressure fluctuations. 100
  6.2.4 The fluctuation spectra. 101

6.3 The steady state behaviour. 102
6.4 The fluctuations. 107
  6.4.1 Fourier spectra; influence of a superleak. 107
  6.4.2 Some additional experiments. 113
6.5 Discussion and conclusion. 114

CHAPTER 7 VISCOSITY MEASUREMENTS.

7.1 Introduction. 117
7.2 Theory of the vibrating wire viscometer. 118
7.3 A summary of the results obtained in pure ^{4}He II. 122
7.4 Measurements in the dilution refrigerator. 125
  7.4.1 Experimental setup. 125
  7.4.2 Measurement of the viscosity. 126
7.5 The viscosity of the ^{3}He-^{4}He mixture along the phase separation line. 127
  7.5.1 The results. 127
  7.5.2 Comparison with related work. 130
7.6 Conclusion. 131
Appendix A A summary of viscosity measurements in the helium liquids. 133
Appendix B Vibrating wire specifications. 137

CHAPTER 8 GENERAL CONCLUSIONS AND SUGGESTIONS FOR FUTURE STUDIES.

8.1 General conclusions. 141
8.2 Suggestions for future research. 143

REFERENCES. 147
LIST OF SYMBOLS. 161
SAMENVATTING. 163
SUMMARY. 165
NAWOORD. 167
CURRICULUM VITAE. 168

CHAPTER 1

GENERAL INTRODUCTION

1.1 ^{4}He II AND ^{3}He–^{4}He MIXTURES.

Under atmospheric pressure ^{4}He and ^{3}He condense into the liquid state at 4.2 K and 3.2 K respectively. At low pressures both isotopes remain in the liquid phase down to zero kelvin. At saturated vapour pressure ^{4}He becomes superfluid (^{4}He II) at a temperature $T_\lambda = 2.17$ K (the lambda point). Below the λ-point liquid ^{4}He behaves as if it is composed of two intermingling fluids, one of which can be considered as an ordinary viscous liquid while the other has a viscosity which is equal to zero and carries no entropy. These components are called the normal and superfluid component and are described with the two-fluid model introduced by Landau, see Landau and Lifshitz (1959).

The phase diagram of ^{4}He is shown in figure 1. The region ^{4}He I represents the phase in which ^{4}He is an ordinary liquid. The region ^{4}He II represents the phase in which two-fluid hydrodynamics holds. The boundary between these areas is called the lambda (λ)-line. When the temperature of ^{4}He II is decreased the normal fluid fraction decreases and the superfluid fraction increases, (Tilley (1986))*.

The flow experiments with mixtures of ^{3}He and ^{4}He which will be described in this thesis are related to experiments carried out in pure ^{4}He II. Therefore a short description of flow experiments in pure ^{4}He will be given.

In the temperature region between 1 K and T_λ flow experiments with ^{4}He II show the special properties of the two-fluid behaviour. In such experiments the velocities of the normal and superfluid components can be varied independently. The flow impedance of for instance a circular tube, strongly depends on the values of the normal fluid velocity ($\vec{v}_n$) and the superfluid velocity ($\vec{v}_s$) or their relative motion $\vec{v}_n$-$\vec{v}_s$ and

---

* In most cases only the first author will be mentioned. The reference list gives the complete information.

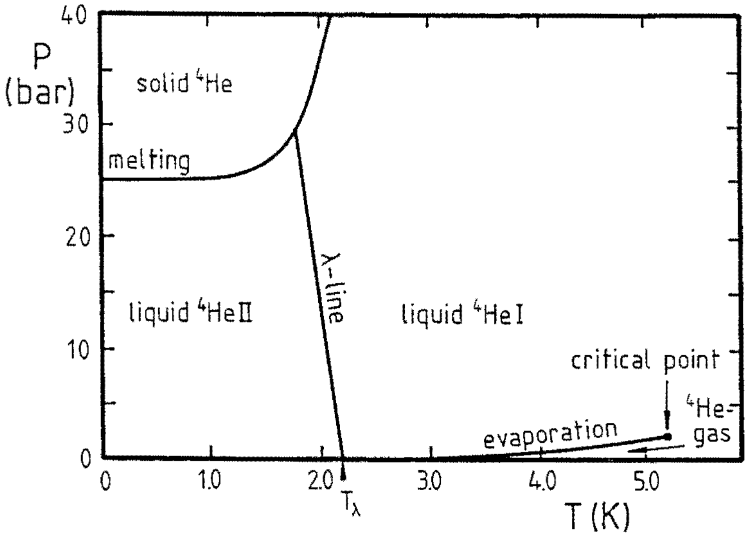

Fig.1 Phase diagram of pure ^{4}He.

has been studied for many years, see the review given by Tough (1982).

In case the flow velocities are very small the flow state is laminar. In that situation the motion of the liquid is described by the two fluid equations derived by Khalatnikov (1965).

At a certain critical velocity, dependent on the directions of $\vec{v}_n$ and $\vec{v}_s$, a change occurs in the flow state of the superfluid and turbulence develops in the superfluid component. This is called superfluid turbulence. It is attributed to the appearance of quantized vortices in the superfluid.

Vortices play a key role in fluid dynamics in general. In superfluid ^{4}He the vortices have some special properties. The ideas concerning these properties are due to Onsager (1949) and Feynman (1955). The superfluid circulation around any closed contour in the liquid defined as:

$$\oint \vec{v}_s \cdot d\vec{l} \tag{1.1}$$

is quantized, in units:

$$\kappa = h/m_4 = 1.0 \cdot 10^{-7}\ m^2/s, \tag{1.2}$$

where h = Planck's constant ($6.6 \cdot 10^{-34}$ Js)
m_4 = mass of a helium-4 atom ($6.7 \cdot 10^{-27}$ kg).

The diameter of the core of the vortices is about 0.5 Å. The superfluid velocity at a distance r from the core of a single straight line vortex is given by the relation for potential curl free flow:

$$v_s = \kappa/2\pi r \ . \tag{1.3}$$

Near the center of the vortex the superfluid thus circulates with an extremely high velocity.

The superfluid accelerates under the influence of a gradient of the molar ^{4}He chemical potential (μ_4) according to:

$$M_4 \frac{d\vec{v}_s}{dt} = -\vec{\nabla}\mu_4 \ , \tag{1.4}$$

where M_4 = the ^{4}He molar weight.

During steady turbulent flow, the difference $\Delta\mu_4$ of the molar ^{4}He chemical potential between two points in the fluid satisfies the relationship:

$$\frac{\Delta\mu_4}{M_4} = \nu\kappa \tag{1.5}$$

where ν is the average number of vortex lines, which in one second crosses any connection between the two points. A nonzero chemical-potential difference is thus intimately connected with the motion of vortex lines in the superfluid, see for instance Anderson (1966).

Hall (1957a,b) and Vinen (1957a,b,c,d) investigated the influence of the presence of quantized vortices on the hydrodynamic properties of ^{4}He II. In Hall's experiments an ordered array of vortices was set up by rotating a bucket of liquid helium-4 below the lambda point. Second sound waves were generated in the bucket and their additional attenuation due to the presence of the vortex arrays was determined. Vinen carried out flow experiments in a channel and he used second sound to probe the flow state in thermal counterflow of ^{4}He II as a function of the counterflow velocity. For velocities above the critical velocity the second sound appeared to be strongly attenuated. Based on a suggestion of Feynman (1955), Vinen proposed that above the critical velocity superfluid vortices were generated and formed a homogeneous vortex tangle nowadays known as superfluid turbulence as mentioned above. Vinen introduced a model which described the dynamics of the vortex tangle. This model will be discussed in chapter 5.

Apart from the quantum turbulence in the superfluid component, classical turbulence can develop in the normal fluid at high velocities. One should not confuse the two types of turbulence. A discussion of the differences and similarities of quantum turbulence with classical turbulence can be found in Donnelly (1986) and Hansen (1986).

The motion of the superfluid vortices relative to the normal fluid leads to an interaction by which dissipation occurs. This interaction is called mutual friction. The dissipative force density ($\vec{F}_{ns}$) can be written in the form:

$$\vec{F}_{ns} = -\frac{B\rho_s\rho_n\kappa}{2\rho}\frac{2}{3}L\vec{v}_{ns} \tag{1.6}$$

where $\vec{F}_{ns}$ = the force density exerted by the normal component
B = Hall-Vinen parameter
L = vortex-line density of the isotropic vortex tangle
ρ = total density
ρ_n = normal fluid density
ρ_s = superfluid density
$\vec{v}_{ns}$ = $\vec{v}_n - \vec{v}_s$.

The vortex line density is the total line length per unit of volume, or when the tangle is isotropic the number of lines intersecting a plane of unit area. This mutual-friction force has to be added to the equations of motion. In a macroscopically steady state the following important result follows:

$$\vec{\nabla}\mu_4 = -\frac{V_4^0\rho}{\rho_s}\vec{F}_{ns} \tag{1.7}$$

where V_4^0 = molar ^{4}He volume.

The vortex line density (L) is in general a complicated function of both the normal and superfluid velocity. But in thermal counterflow the dependence of L on the velocity is found to be rather simple. For this reason, but also for historical reasons, and because of the relation with our experiment it is of importance to discuss briefly this typical counterflow experiment in ^{4}He II.

A basic setup for counterflow in ^{4}He II is shown in figure 2. The system consists of two cells connected by a flow channel filled with pure ^{4}He below T_λ. When in the left cell a constant heating power is supplied, the normal component, which carries the entropy flows from the heat source to the sink and superfluid flows in the reverse direction. At the heater superfluid is converted to normal fluid and at the heat sink vice versa. In this way a so called counterflow develops.

Along the flow channel a temperature and pressure gradient proportional to the

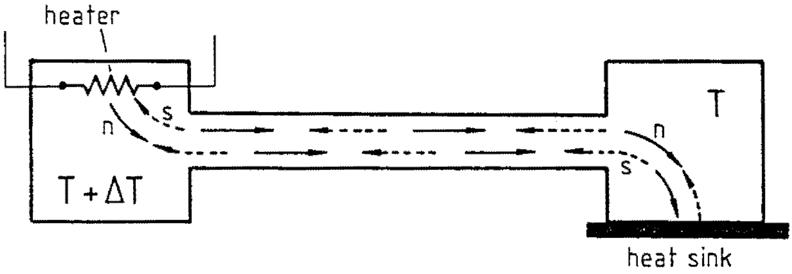

Fig.2 *Counterflow experiment in ⁴He II. Dotted arrows represent the superfluid flow. The full arrows represent the normal flow.*

heat input develop, in agreement with the two fluid model for velocities v_{ns} smaller than the critical velocity. In case the velocity v_{ns} is well above the critical velocity, the temperature gradient was found to increase with the cube of v_{ns}; whereas was affected very little. The steady chemical-potential difference thus results in a mutual-friction force:

$$\vec{F}_{ns} = -A\rho_s\rho_n v_{ns}^2\vec{v}_{ns} \tag{1.8}$$

where A = Gorter-Mellink constant.
Now use equation (1.6) leads to:

$$L \sim v_{ns}^2. \tag{1.9}$$

On phenomenological grounds equation (1.8) was suggested by Gorter and Mellink (1949). They introduced the term mutual friction. It is therefore that A is still called the Gorter-Mellink constant. Although Gorter and Mellink were the first who added this term to the two fluid equations of motion, Hall and Vinen discovered and described in detail the association of mutual friction with vortices. Since Gorter and Mellink's and Hall and Vinen's work an enormous amount of flow experiments has been carried out, mainly in the region 1.2 K$<T<T_\lambda$. In these experiments the critical velocity region and the dependence of the critical velocity on the flow field and geometry was studied for instance. This is described in Tough (1982) and Marees (1987). In subsequent chapters we will come back to this.

In the foregoing the behaviour of pure ⁴He below 2.17 K has been described. Now a closer look will be taken at ³He-⁴He mixtures. The phase diagram is shown in figure 3. The diagram consists of three parts. In area I the liquid behaves as an ordinary mixture

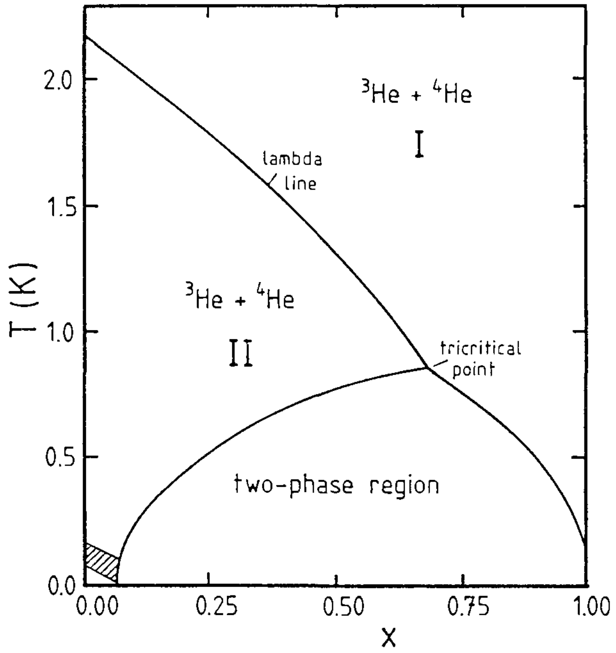

Fig.3 *The phase diagram of liquid ^{3}He-^{4}He mixtures at saturated vapour pressure. The molar ^{3}He concentration x is plotted horizontally and the temperature T vertically. The shaded area represents the region where the experiments were carried out.*

and on the left hand side (II) the mixture has a superfluid component. These regions are separated by the lambda line. At temperatures above 867 mK the mixture is stable for all ^{3}He concentrations. Below 867 mK ^{3}He and ^{4}He cannot be mixed in all concentrations. If the ^{3}He concentration x is chosen in the two-phase region the mixture separates in a ^{3}He rich phase (the right branch) which is called the concentrated phase, and a ^{3}He poor phase (the left branch) called the dilute phase. Due to its lower density the concentrated phase floats on top of the dilute phase. For T<100 mK the concentrated phase consists of nearly 100 % ^{3}He, (Nakamura (1988)). The low temperature limit of the solubility of the ^{3}He at the diluted side is 6.6 %, (Abraham (1969)). The shaded region indicated in figure 3 is the region where the experiments described in this thesis are carried out.

In area II, the ^{4}He component is superfluid as in pure ^{4}He. A two fluid description can still be used since above 1 K the excitations in the ^{4}He interact intimately with the

^{3}He particles so that the ^{3}He particles are incorporated in the normal component. Therefore the ^{3}He drifts with the normal fluid. In a thermal counterflow experiment this leads to the growth of concentration gradients in the flow system, which remain after the flow is stopped being balanced by temperature gradients. This is called the heat flush effect. It played a complicating role in the counterflow experiments as carried out in Leiden by Mudde (1987, 1989, 1990).

At low temperatures ($T < 0.5$ K) the ^{4}He consists almost completely of superfluid and the number of excitations is very small. The analysis of the flow experiments is simplified enormously.

Experiments at low temperatures with mixtures are of importance for the understanding of the diluted side of a dilution refrigerator. Here the ^{3}He flow is imposed and the superfluid ^{4}He II is at rest and there is a well defined flow state. In pure ^{4}He II at temperatures below 1.5 K, the normal fluid fraction is rather small. This means that in the case of counterflow the normal fluid velocity is much larger than the superfluid velocity, which is nearly zero. So this type of flow resembles the flow state in the dilution refrigerator. This resemblance will become more evident in section 1.2 and chapter 2.

1.2 BASIC RESULTS OF PREVIOUS WORK AND A PREVIEW FOR EXPERIMENTS TO DO.

The ^{3}He circulating dilution refrigerator is pre-eminently suitable for studying the hydrodynamics of a mixture of ^{3}He and ^{4}He II. In this thesis only ^{3}He circulating dilution refrigerators will be discussed.

Following a suggestion of London (1951, 1962), the development of these refrigerators started in the sixties. The disclosure of the millikelvin regime made diverse new research areas accessible. Today the dilution refrigerator is a common tool in low temperature laboratories. The main feature of these refrigerators is that they are able to cool below 1 K in continuous operation down to about 2 mK. Many aspects of the dilution refrigerator have been studied in the past. Reference may be made to Wheatley (1968a,b, 1971), Lounasmaa (1974), Frossati (1977), Betts (1976, 1989) and Richardson (1988).

Khalatnikov (1965) derived the basic set of equations for the description of the thermohydrodynamics of superfluid helium mixtures. Wheatley developed a simplified model from these equations for low temperatures and applied it to dilution refrigeration. He treated the ^{4}He II as a background, which is in many aspects equivalent to a vacuum. This model which is called the mechanical-vacuum model will be discussed in chapter 2. He tested this model by measuring the viscous heating in case ^{3}He flowed through ^{4}He II at low flow rates (<60 μmol/s). The theoretical results were in agreement with measurements.

During the seventies refrigerators were built with a ^{3}He circulation rate above 100 μmol/s. In 1978 a dilution refrigerator was built at the low temperature group at the Eindhoven University of Technology with circulation rates up to 2.5 mmol/s. Experiments were carried out with this machine to investigate a multiple mixing chamber technique, see Coops (1979, 1981). In these experiments it was found that the ^{3}He flow is strongly impeded by the ^{4}He II in many cases. In addition to the viscous friction an extra friction force had to be introduced in the hydrodynamic equations (Coops (1982)). Stimulated by these results further experiments at temperatures below 150 mK were carried out by Castelijns (1985, 1986) in the dilute phase of the mixing chamber as is schematically illustrated in figure 4. In this flow experiment the steady ^{3}He flow rate was varied. The presence of phase separation in the mixing chamber implies a fixed relationship between the temperature and the ^{3}He concentration at the tube entrance.

Temperature and concentration changes were measured in different flow channels Z mounted inside the mixing chamber. One of the main results of this investigation was that for the ^{3}He flow rates which were used (150 μmol/s < $\dot{n}_3$ < 1000 μmol/s) the mechanical-vacuum model did not describe the observed large temperature and concentration differences. Besides, nonzero ^{4}He chemical-potential differences were observed. Castelijns gave a phenomenological description of the extra dissipation occurring if ^{3}He flows through ^{4}He II in tubes with a diameter smaller than 2 mm, which resembled the mutual friction caused by superfluid turbulence that occurs in pure ^{4}He counterflow experiments. He also observed pressure differences over flow channels consisting of one single tube but these were too small to be measured accurately. If, however, more tubes were placed in parallel (Kuerten (1985b)), measurable pressure differences were obtained. This result, which is strongly related with the dependence of the viscosity on temperature, will be discussed in more detail later on.

The experiments by Castelijns and the analysis of Kuerten (1985a, 1986a,b, 1987a,b) led to a new description of the flow properties of ^{3}He-^{4}He II mixtures, which we call the mutual-friction model. This model can also be used to calculate the low temperature limits of the refrigerator if certain assumptions are made.

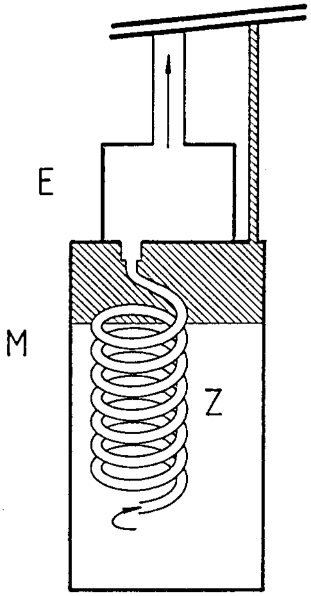

Fig.4 *Schematic representation of the experimental situation used by Castelijns. The mixing chamber (M) is shown with experimental space (E) on top of it, connected by a flow channel Z. The shaded part represents the concentrated phase.*

So in 1986 two different models were known. In case of low ^{3}He velocities the mechanical-vacuum model described the behaviour correctly. For high velocities the behaviour was purely mutual frictional, with high dissipation rates. No studies were made of the intermediate velocity range and it was not known whether a well defined critical velocity would exist.

This led to the investigations described in this thesis. Experiments were performed to determine whether at some well-defined critical value of the velocity mutual friction appears as is suggested by counterflow experiments in ^{4}He II. As the flow rate of our dilution refrigerator was in many cases too large we had to place many tubes in parallel ($\approx$100) in order to reach the intermediate velocity region. Accurate measurements of the temperature, concentration and pressure differences across the flow channels as functions of the ^{3}He flow rate were carried out at constant mixing chamber temperature, in roughly the same setup as used by Castelijns (1985, 1986). With these quantities the mutual-friction force and all quantities which determine the physics of the flow system, can be obtained.

Preliminary results were presented in Kyoto during the 18th Conference on Low Temperature Physics (Zeegers (1987)) and in Smolenice at the International Conference on Macroscopic Quantum Phenomena (Zeegers (1989)).

It was observed that at the critical velocity a change occurred in the amplitude of the fluctuations of the pressure. So a special study was made of these fluctuations using spectral analysis.

Furthermore, in the course of the flow experiments, it turned out that the value for the shear viscosity of the mixtures which is used normally, was not accurately in agreement with the viscosity derived from pressure measurements. Therefore the viscosity was measured in a separate experiment using a vibrating wire viscometer.

Summarized the contents of this thesis are:

Chapter 2 gives a phenomenological description of the thermohydrodynamics of the experiments. The basic equations resulting from the mechanical-vacuum model are treated. Expressions for the temperature, pressure and concentration changes are given. Then the mutual-friction model for mixtures is considered and basic consequences of it are discussed.

Chapter 3 describes the experimental setup and measuring techniques. The experimental setup is described in the first section including preliminary and definitive flow systems. The second section treats the techniques which were used to measure temperature, ^{3}He concentration and pressure differences and how from these quantities the chemical-potential gradient was calculated. In the third section details of the measurement procedure are treated.

Chapter 4 describes the experiments and results regarding the time averaged quantities. The design procedure for the flow channels is treated and a survey of all the measurements is given. The next sections describe, for a few setups, the measured quantities as temperature, concentration and pressure. Results are also presented in the form of T^2-x diagrams showing that the flow was adiabatic. The ^{4}He chemical-potential difference is presented as a function of the velocity showing that there is a definite value of the flow velocity where mutual friction appears. This is called the critical velocity.

Chapter 5 discusses the phenomena characterizing the critical velocity. The effects observed in our experiments are compared with those occurring in ^{4}He II counterflow. Different aspects of the flow phenomena occurring in circular and annular tubes are described. As the mutual friction is due to the motion of vortices in the superfluid, vortex-line densities are computed and compared with values obtained in ^{4}He II counterflow experiments.

Chapter 6 treats the measurements carried out with large tubes and discusses time dependent signals. During stationary flow it was observed that in the critical velocity region the amplitude of the fluctuations in the pressure signal was strongly flow dependent. The fluctuations were analyzed using a spectral method. This technique supplied additional evidence of the presence of a second critical velocity in the measurements in addition to the critical velocity discussed above.

Chapter 7 discusses the measurements of the viscosity coefficient of the mixture using a vibrating wire viscometer. In a special setup the viscometer was used to measure the viscosity of pure ^{4}He II. Furthermore, correct conditions were probed and different aspects of the viscometer were analyzed. Finally the viscosity of the mixture was measured. The measurements are compared with results of other workers and are applied to the flow measurements.

Chapter 8 concludes this thesis and gives some suggestions for future work.

CHAPTER 2

PHENOMENOLOGICAL DESCRIPTION

2.1 THERMOHYDRODYNAMIC EQUATIONS IN THEIR SIMPLIFIED FORM; MECHANICAL-VACUUM APPROXIMATION.

The derivation of the thermohydrodynamic equations of superfluid ^{3}He-^{4}He mixtures was given by Khalatnikov (1965). For temperatures below 1 K aspects concerning the thermodynamics were studied in particular by Radebaugh (1967) and Ebner (1971) and more recently by Kuerten (1985, 1987a). Aspects concerning the hydrodynamics were studied by a.o. Wheatley (1968a,b, 1971) and Van Haeringen (1979a,b) and also by Kuerten (1987a). A general review on the thermohydrodynamics was given by De Waele (1990).

In the mechanical-vacuum model the ^{4}He is considered as non-interacting with the ^{3}He quasiparticles and may be considered as a vacuum. Wheatley applied this model to describe the flow of mixtures at low temperatures, introducing low temperature approximations for the various quantities. In Van Haeringen's work the model was applied to dilution refrigeration to compute e.g. cooling powers and temperature distributions along tubes.

In our experiments two volumes M (mixing chamber) and E (experimental space) were connected by a flow impedance consisting of N flow channels in parallel. These flow channels were either circular tubes or annular tubes as is shown in figure 5. The length of the tubes is ℓ. The circular tubes are characterized by their diameter (d), the annular tubes are characterized by the annular spacing (d) and the annular diameter (D), whereas $d \ll D$. The factor ζ, which we will call the impedance factor, was also used by Wheatley (1968b, 1971). This geometric factor relates the pressure gradient in laminar flow with the volume flow rate. Application of the Poiseuille law for the pressure drop leads for a circular tube to $\zeta = 128/\pi d^4$ and for an annular tube $\zeta = 12/\pi D d^3$, (Bird (1960)).

We consider the situation where ^{3}He flows adiabatically from M to E. The parameter characterizing the distance along the tube will be named z. The temperature (T), molar ^{3}He concentration (x), pressure (p), molar ^{3}He chemical potential (μ_3) and molar ^{4}He chemical potential (μ_4) on the left side in the figure get a lower index m, for "mixing chamber". The quantities in the experimental space have the index e *.

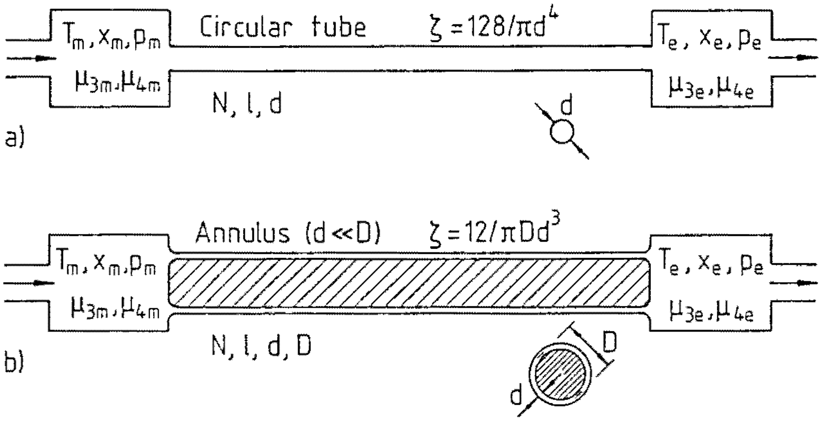

Fig.5a,b Flow channels used in the experiments. Details are explained in the text.

In the case of laminar flow there is only an axial velocity component and the quantities x, T and p only depend on z. We will consider stationary flow states in which the net ^{4}He flow can be neglected.

Conservation of energy can be formulated as follows:

$$\frac{d}{dz}\left[H_3^{os}\dot{n}_3 - NA\kappa\frac{dT}{dz}\right] = 0 \tag{2.1}$$

where H_3^{os} = osmotic enthalpy per mole ^{3}He
A = area of cross section of one flow channel
κ = thermal conductivity
$\dot{n}_3$ = molar ^{3}He flow rate.

The osmotic enthalpy is defined as (Ebner (1971), Kuerten (1985, 1987a)):

$$H_3^{os} = \mu_3 + \frac{TS_m}{x} \tag{2.2}$$

---

*In some cases the index m will also be used to indicate a quantity per mole. Sometimes the same symbol is used for two different quantities like d for tube diameter and annular slit space, κ as quantity of circulation and thermal conduction coefficient and A for Gorter–Mellink constant and tube area. We will always indicate the proper meaning if confusion could occur.

where S_m = entropy per mole mixture.

If the thermal conductivity of the liquid is neglected it follows from equation (2.1) that:

$$H_3^{os} = \text{constant} \tag{2.3}$$

in the tube. In the low temperature limit (T<100 mK) the ^{4}He contribution to the osmotic enthalpy can be neglected. In that situation H_3^{os} at zero pressure is given by (Kuerten (1985, 1987a)):

$$H_3^{os} = 17.58(x-x_0) + 84.06T^2 , \tag{2.4}$$

where $x_0 = 0.066$, which is the concentration along the phase separation line at zero temperature.

In Kuerten (1987a) it was shown that, when the pressure differences are as small as in our experiments (<100 Pa), the pressure contribution to H_3^{os} can be neglected.
From equations (2.3) and (2.4) it follows that:

$$T^2-T_m^2 \simeq -b(x-x_m) \tag{2.5}$$

where $b \simeq 0.20$ K^2.

The relation with the pressure variation along the tube can be obtained from the Gibbs-Duhem equation, reading as:

$$x d\mu_3 + (1-x)d\mu_4 = -S_m dT + V_m dp \tag{2.6}$$

in which V_m is the molar volume of the mixture. Combining equations (2.2), (2.3) and (2.6) yields for the mechanical vacuum model in which the chemical potential μ_4 is constant along the tube:

$$V_3\frac{dp}{dz} + T\frac{d(S_m/x)}{dz} = 0 . \tag{2.7}$$

In (2.7), V_3 is the volume of one mole of ^{3}He in the mixture, which is related to the molar volume V_m by:

$$\frac{V_m}{x} = V_3 . \tag{2.8}$$

In our approximation $V_m/x=V_3$ is taken to be a constant ($V_3 \simeq V_{3d}=415\cdot 10^{-6}$ m^3/mol). This is justified when only very small concentration changes with respect to x_0 are considered. For the application in this thesis concentration differences are always small and the approximation made above is satisfied in the measurements.
In the low temperature limit,

$$\frac{S_m}{x} = C_0 T \tag{2.9}$$

where $C_0 = 104.3$ Jmol^{-1}K^{-2}.

On integrating (2.7) and using (2.9), it follows that for any flow impedance:

$$p - p_m = -\frac{C_0}{2V_3}(T^2 - T_m^2)\,. \tag{2.10}$$

The relations (2.5) and (2.10) are consistent with the condition:

$$p - \Pi = \text{constant}, \tag{2.11}$$

if the low temperature approximation for the osmotic pressure Π is substituted (Kuerten (1985)).

Up to now we did not use Poiseuille's law for the pressure drop:

$$\frac{dp}{dz} = -\frac{\eta \zeta \dot{n}_3 V_3}{N} \tag{2.12}$$

where η = ^{3}He coefficient of viscosity.
If this equation is used to eliminate the pressure from (2.7) and if we use the low temperature approximation:

$$\eta = \frac{\eta_0}{T^2} \tag{2.13}$$

where $\eta_0 = 5 \cdot 10^{-8}$ PasK^2, we obtain the temperature profile along the flow channel:

$$T^4 - T_m^4 = \frac{4\eta_0 \zeta \dot{n}_3 V_3^2}{N C_0}\, z\,. \tag{2.14}$$

Finally, when equations (2.5), (2.10) and (2.14) are combined and applied to flow channels with length ℓ, it follows that the temperature, pressure and concentration differences between the experimental space and the mixing chamber, depend on the flow rate $\dot{n}_3$ as:

$$T_e = T_m \left[1 + \frac{\zeta \ell 4 V_3^2 \eta_0}{N C_0 T_m^4}\, \dot{n}_3\right]^{\frac{1}{4}} \tag{2.15}$$

$$p_e = p_m - \frac{C_0}{2V_3} T_m^2 \left[\left[1 + \frac{\zeta \ell 4 V_3^2 \eta_0}{N C_0 T_m^4}\, \dot{n}_3\right]^{\frac{1}{2}} - 1\right] \tag{2.16}$$

$$x_e = x_m - \frac{T_m^2}{b} \left[\left[1 + \frac{\zeta \ell 4 V_3^2 \eta_0}{N C_0 T_m^4}\, \dot{n}_3\right]^{\frac{1}{2}} - 1\right]\,. \tag{2.17}$$

These equations will be used to interpret the experimental data in the mechanical-vacuum approximation.

2.2 INCLUDING MUTUAL FRICTION PHENOMENOLOGICALLY IN ^{3}He-^{4}He II MIXTURES.

Wheatley (1971) tested the mechanical-vacuum model by studying temperature changes caused by the viscous heating of the liquid in the flow of ^{3}He through a slit. His results were in agreement with the model. Later, however, Niinikoski (1971) measured large osmotic pressure differences between mixing chamber and still and Frossati (1977) observed an anomalous behaviour of the circulation rate $\dot{n}_3$ as a function of $\dot{Q}_S$, the heat supply to the still. These results were not in agreement with the mechanical-vacuum model. The investigations of the Low Temperature group at the Eindhoven University of Technology (Coops (1981, 1982), Castelijns (1985,1986)) showed that mutual friction plays an important role in the flow of ^{3}He through ^{4}He II. This leads to a behaviour which is quite different from what was expected from the mechanical-vacuum model. Differences in pressure, temperature and ^{3}He concentration during a steady flow of ^{3}He in the dilute mixture through various tubes were measured and the following empirical relations were obtained for a wide range of flow velocities:

$$T_e^2 = T_m^2 + a\gamma'' \ell j_3^3 \tag{2.18}$$

where $a = 0.20\ \mathrm{K}^2$, $\gamma'' = 14\cdot10^{-9}\ \mathrm{s}\ ^3\mathrm{m}^5\mathrm{mol}^{-3}$ and the molar ^{3}He flux $j_3 = \dot{n}_3/NA$

$$x_e = x_m - \gamma'' \ell j_3^3 \tag{2.19}$$

$$p_m \simeq p_e\ . \tag{2.20}$$

From the measured quantities Castelijns calculated the ^{4}He chemical potential using thermodynamic data on $\mu_4(p,T,x)$ from literature (Kuerten (1985)) and he established that:

$$\mu_{4e} = \mu_{4m} + \chi \ell j_3^3, \tag{2.21}$$

where $\chi = 11\cdot10^{-9}\ \mathrm{kgsm}^7\mathrm{mol}^{-4}$. The various numerical factors were found to be independent of the flow tube.

Moreover, for the osmotic pressure the inequality was found:

$$p-\Pi \neq \text{constant}. \tag{2.22}$$

So in contrast with the mechanical vacuum approximation there is now a nonzero chemical potential difference. This was attributed to mutual friction because of the resemblance with mutual friction in ^{4}He II counterflow experiments. The equations (2.18)-(2.22) were therefore called the mutual friction model. We will discuss this analogy in somewhat more detail at the end of this section.

First we will demonstrate, however, that the empirical relations (2.18)-(2.20) of the mutual friction model can be derived with the procedure of section 2.1, when some simplifying assumptions are made. The equations (2.1)-(2.3) should remain valid in the presence of mutual friction. So, in the low temperature approximation, the relation between T and x is still given by equation (2.5). A comparison of (2.18) with equation (2.19) shows that this is indeed the case. The heat conduction will be neglected. We like to remark that Kuerten (1987a,b) has included the heat conduction term and calculated the different solutions of this equation in situations without (see also van Haeringen (1979a,b, 1980)) and with mutual friction in the high flow rate regime. The analysis including mutual friction at intermediate flow rates is more complicated as the $\chi j_3{}^3$ approximation to the mutual friction in this flow range is presumably not correct.

Instead of equation (2.7) we find from equation (2.3) due to the nonzero chemical-potential gradient:

$$V_3\frac{dp}{dz} + T\frac{d(S_m/x)}{dz} - \frac{1-x}{x}\frac{d\mu_4}{dz} = 0 \,. \tag{2.23}$$

If we now make the simplifying assumptions that the pressure gradient still obeys Poiseuille's law (2.12)[†] and that besides,

$$\frac{1-x}{x}\frac{d\mu_4}{dz} \simeq \frac{1-x_0}{x_0}\chi j_3{}^3 \,, \tag{2.24}$$

then the low temperature approximation leads to:

$$\frac{dT^2}{dz} - \frac{2\eta_0\zeta\dot{n}_3V_3{}^2}{NC_0}\frac{1}{T^2} - 2\frac{1-x_0}{x_0}\frac{\chi}{C_0}j_3{}^3 = 0 \,, \tag{2.25}$$

where the variation $V_3(z)$ is again neglected.[‡] Now we define:

[†] In the case of thermal counterflow in pure ^{4}He II, mutual friction itself is known to have only a very small direct effect on the pressure difference. This is called the Allen and Reekie rule, see Tough (1982) and Donnelly (1986).

[‡] Since at the higher flow rates the concentration difference across the tubes becomes appreciable, the latter assumption becomes dubious. For a proper treatment one should then also take the variation of η with x into account, however, making the calculations very tedious.

$$c_1 \equiv \frac{2\eta_0 \zeta \dot{n}_3 V_3^2}{N C_0} \tag{2.26}$$

$$c_2 \equiv 2\frac{1-x_0}{x_0} \frac{\chi}{C_0} j_3^3 \, . \tag{2.27}$$

The differential equation (2.25) can be integrated yielding the solution:

$$T^2 - T_m^2 - \frac{c_1}{c_2} \ln\left[\frac{c_1+c_2T^2}{c_1+c_2T_m^2}\right] = c_2 z \, . \tag{2.28}$$

In the limit of zero mutual friction ($\chi \rightarrow 0$ which implies $c_2 \rightarrow 0$) this equation leads to the profile of (2.14). In the limit of highly turbulent flow ($c_2 T_m^2 \gg c_1$) the logarithmic term becomes negligible so that the temperature profile approaches:

$$T^2 = T_m^2 + c_2 z \, . \tag{2.29}$$

If use is made of equation (2.5) the concentration profile can be found. Substitution of $z=\ell$ shows that (2.29) is indeed quantitatively identical to the empirical relation (2.18).

The pressure profile can also be calculated. If in Poiseuille's law equation (2.12), the low temperature approximations are inserted we find:

$$\frac{dp}{dz} = - \frac{C_0}{2V_3} \frac{c_1}{T^2} \, . \tag{2.30}$$

Elimination of z by means of:

$$\frac{dp}{dz} = \frac{dp}{dT^2} \frac{dT^2}{dz} \, . \tag{2.31}$$

and dT^2/dz substituted from equation (2.25) in combination with equation (2.30) yields:

$$\frac{dp}{dT^2}\left[\frac{c_1}{T^2}+c_2\right] = - \frac{C_0}{2V_3} \frac{c_1}{T^2} \, . \tag{2.32}$$

So:

$$p-p_m = - \frac{C_0}{2V_3} \frac{c_1}{c_2} \ln\left[\frac{c_1+c_2T^2}{c_1+c_2T_m^2}\right] \tag{2.33}$$

By replacing the logarithmic term by means of (2.28) this can also be written as:

$$p-p_m = -\frac{C_0}{2V_3}\left[T^2-T_m^2-c_2 z\right] \, . \tag{2.34}$$

For $z=\ell$ equation (2.34) can be compared with equation (2.10). The extra term ($-c_2\ell$) leads indeed, for the same T_e, to a smaller pressure difference in comparison with the mechanical-vacuum approximation. How for a given flow rate equation (2.34) compares with the mechanical-vacuum approximation, however, is less straightforward to see as T is now given by the implicit equation (2.28). In the limit of highly turbulent flow ($c_1/c_2 \ll T_m^2$) equation (2.33) leads to:

$$p_e - p_m = -\frac{C_0}{V_3}\frac{c_1}{c_2}\ln\left[\frac{T_e}{T_m}\right] , \tag{2.35}$$

which, owing to the factor c_1/c_2, even decreases for increasing circulation rate, in accordance with the inequality (2.20) of the mutual friction model. This feature is, of course, a direct consequence of the fact that due to mutual friction a much larger temperature rise occurs in the tube leading to a decrease in viscosity according to equation (2.13) thus resulting in much smaller pressure differences.

The mutual friction model used for the description of the flow of ^{3}He through ^{4}He II at high flow velocities has a strong resemblance with the situation of ^{4}He II counterflow. From equations (1.7) and (1.8) it follows that in thermal counterflow in pure ^{4}He II:

$$\Delta\mu_4 \sim v_{ns}^3. \tag{2.36}$$

In the case of ^{3}He moving in ^{4}He II which is macroscopically at rest it followed from the mutual friction behaviour:

$$\frac{d\mu_4}{dz} = \chi j_3^3. \tag{2.37}$$

If an equation of the type of (1.7) also holds for mixtures, one obtains the following result:

$$\vec{F}_{34} = -(\rho_s/\rho V_4^0)\chi j_3^3 \equiv -A_{34}(\rho-\rho_n)\rho_n|\vec{v}_3|^2\vec{v}_3 \tag{2.38}$$

where $\vec{F}_{34}$ = mutual friction force density exerted on the normal fluid component
A_{34} = Gorter-Mellink type of constant
ρ_n = density of ^{3}He component.

and where v_3 is the average ^{3}He velocity given by:

$$v_3 = V_3 j_3. \tag{2.39}$$

Now the Gorter-Mellink constant equals:

$$A_{34} = \chi/\rho\rho_n V_4^0 V_3^3 . \tag{2.40}$$

We like to remark that this parameter depends on the concentration but it shows indeed the similarity between ^{4}He II and ^{3}He-^{4}He II flows. We will need this argument later on for the computation of vortex line densities in chapter 5.

CHAPTER 3

EXPERIMENTAL SETUP AND MEASURING TECHNIQUES

3.1 EXPERIMENTAL SETUP.

3.1.1 THE LOW TEMPERATURE PART OF THE FLOW SYSTEM.

The experiments were carried out in a dilution refrigerator, with a flow rate adjustable between 0.06 mmol/s and 2.5 mmol/s. A detailed description is given by Coops (1981, 1982) and Castelijns (1985, 1986). The basic setup is shown in figure 6.

^{3}He is pumped from the diluted phase in the still and is recondensed, via the gas handling system outside the cryostat, at the 1K plate. Further precooling of the concentrated inflow is realized with the still and by 7-10 step heat exchangers. In the mixing chamber concentrated and diluted phase are in a steady state and separated by the phase boundary, see section 1.1. Via a flow channel ^{3}He flows through the background of ^{4}He II to the experimental space on top of the mixing chamber. The mixing chamber and the experimental space connected by the flow channel are the most relevant parts of the experiments which are the subject of this thesis. The ^{3}He flows back to the diluted side of the heat exchangers through a wide tube and onwards to the still.

At the still a heater is mounted which can supply a power of up to 70 mW by which it controls the ^{3}He flow rate ($\dot{n}_3$). The flow rate is measured in the room temperature part of the flow system. Due to the low temperature and therefore the low vapour pressure of the ^{4}He in the still the circulated gas contains only 3% of ^{4}He. This will be neglected in the analysis of the experimental data presented in this thesis. It is discussed briefly in section 3.3.

The dilution refrigerator is suspended from a concrete block with a weight of 6 ton mounted on air springs and is vibration isolated. The lowest temperature reached is 7 mK.

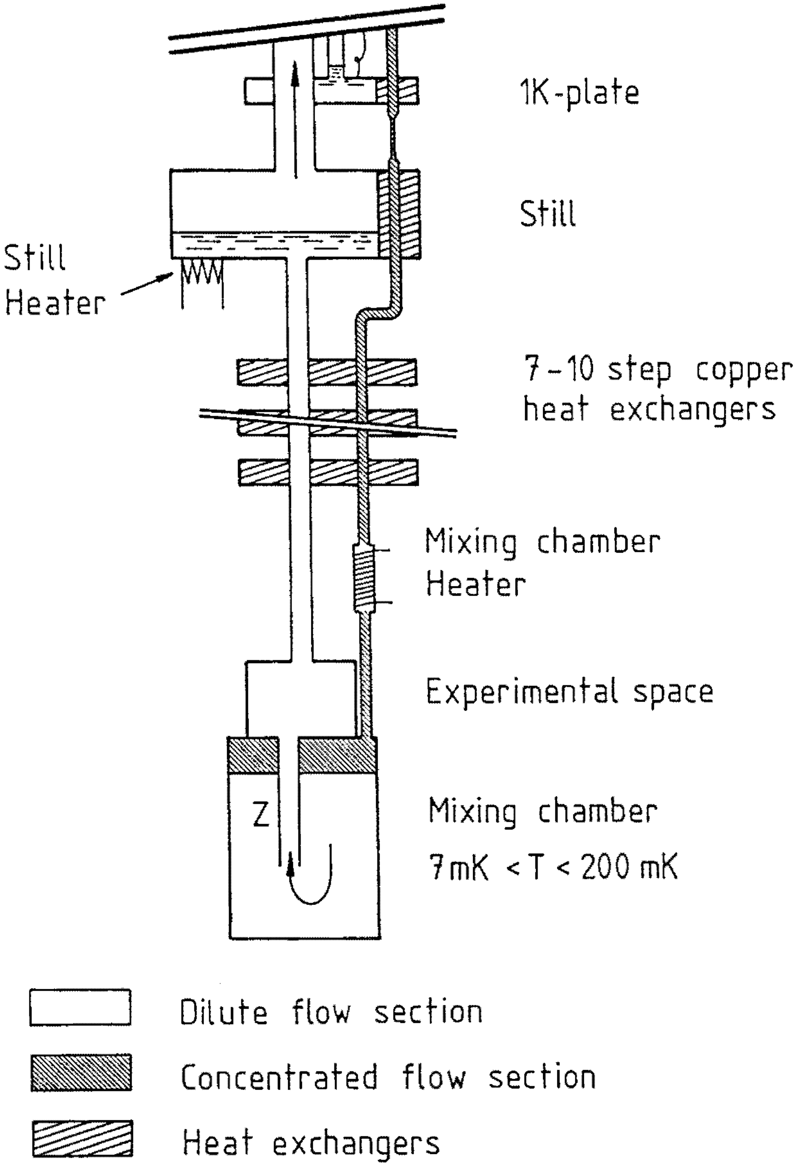
1K-plate
Still
Still Heater
7-10 step copper heat exchangers
Mixing chamber Heater
Experimental space
Z
Mixing chamber
7mK < T < 200 mK
Dilute flow section
Concentrated flow section
Heat exchangers

Fig.6 Low temperature part of the flow system, schematically. The part shown is situated in the vacuum chamber of the dilution refrigerator. The experiment is carried out in the tube Z connecting mixing chamber and experimental space.

3.1.2 THE FLOW SYSTEM IN DETAIL.

In figure 7 the three different flow systems used in this research are shown. The concentrated ^{3}He entering the mixing chamber can be warmed using a heater, the mixing chamber heater, placed between the concentrated side of the last heat exchanger and the mixing chamber. It is also present but not shown in the situations of figure 7b and c. With this heater T_m can be controlled between 10 and 200 mK using a heating power up to 1 mW for given rates of circulation $\dot{n}_3$.

At various locations thermometers are installed: T_i measures the temperature of the concentrated ^{3}He entering the mixing chamber, T_m the mixing chamber temperature of the dilute phase, T_e the temperature in the experimental space and T_d the temperature downstream of the flow impedance (Z) in the first setup. The temperature T_h is the temperature of the concentrated ^{3}He leaving the last heat exchanger, which is not measured.

In system 7a the mixing chamber and experimental space are connected by a wide tube so that the viscous or mutual frictional heating inside it is negligibly small and $T_m=T_e$. In this setup, the flow resistance under investigation is installed between the experimental space (E) and the diluted side of the last heat exchanger and so the temperature T_d is measured at constant T_e as a function of the ^{3}He flow velocity. This flow impedance consists of N tubes with diameter d and length ℓ. In setup 7a only temperatures are measured.

In the second system, (figure 7b) the mixing chamber is constructed with an extra tail. In this way flow channels with a total length of 380 mm can be installed between M and E. With this setup also concentration and pressure differences over the flow impedance are measured.

In the third flow system (figure 7c) the flow channel is installed between M and E via connections inside the vacuum space surrounding both chambers. In this way there is no limit to the length of the tube. Tubes with inner diameter up to 7.40 mm and length 6 m were sometimes mounted in a coil in this setup.

In addition the mixing chamber and experimental space can be equipped with different measuring devices e.g. extra pressure cells, thermometers, shunting tubes and superleaks, vibrating wire viscometers, capacitors for concentration measurement etc.

The determination of the flow characteristics of a particular flow channel usually took one week. The system had to be warmed up to room temperature and opened for replacing the flow channel. During this investigation this was done about 140 times. The experimental setup proved to be highly reliable.

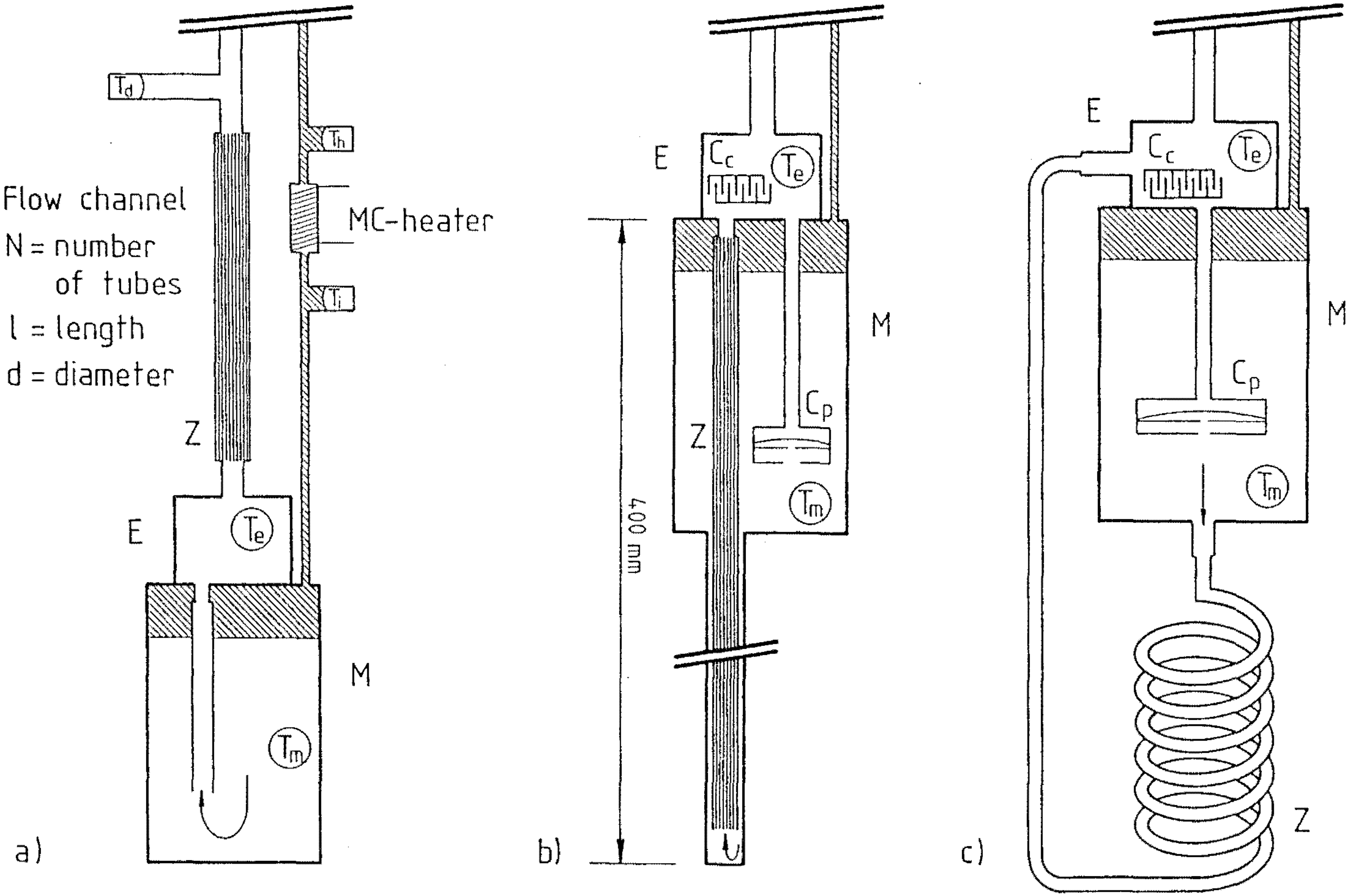
Flow channel
N = number of tubes
l = length
d = diameter
Td
Th
MC-heater
Ti
Z
E
Te
M
Tm
a)
E
Cc
Te
400 mm
M
Cp
Z
Tm
b)
E
Cc
Te
M
Cp
Tm
Z
c)

Fig.7a–c Flow systems in detail, schematically. Z = flow impedance; M = mixing chamber; E = experimental space; C_c *= concentration capacitor;* C_p *= pressure cell;* T_u*,* T_m*,* T_e*,* T_d *= Speer resistance thermometers. Shaded area represents the concentrated* ^3He.

3.2 MEASURING TECHNIQUES.

3.2.1 THERMOMETRY.

At several locations the temperature is measured with 220Ω Speer carbon resistance thermometers, (Hudson (1975), Anderson (1972)), using a resistance bridge (IT-VS2). They were calibrated in zero magnetic field using CMN-thermometry (cerium magnesium nitrate, Hudson (1975)) in combination with two superconducting fixed point devices: SRM 767 with five transition points between 7.6 K and 515 mK and SRM 768 with five transition points between 205 mK and 15 mK, (Schooley (1972), Soulen (1979)). The calibration was carried out with both the two SRM devices as well as the CMN-thermometer installed in the mixing chamber, (Castelijns (1986)). In the 20-200 mK range the calibration has an accuracy of about 0.2 mK. We have observed that the calibration can change if a particular thermometer is heated during soldering. When this is avoided the calibration remains correct within 2 mK over a year. Below 15 mK resistance thermometry was not used because r.f. heating affected the resistance value. In these cases a CMN-thermometer was used, which was calibrated with the resistance thermometers in the higher temperature range and by extrapolation to about 7 mK.

3.2.2 ^{3}He CONCENTRATION.

The ^{3}He concentration measurement is based on the concentration dependence of the dielectric constant of liquid ^{3}He-^{4}He mixtures (Kierstead (1976)). In the experimental space a parallel plate air capacitor* is placed, as shown in figures 6 and

---

* An asterisk * indicates that the word or product name (in this case air capacitors) appears in the reference list.

7. The capacitance is measured using a capacitance bridge (General Radio 1615-A) in combination with a lock-in amplifier (PAR 124A). One can in principle calculate dC/dx with Kiersteads' (1976) formula for the dielectric constant ϵ_r as a function of the ^{3}He concentration x:

$$\epsilon_r = 1.0572 - 0.0166\,x. \tag{3.1}$$

However, the effect of parasitic capacitances of the connecting wires complicates the analysis of the measurement. So it was necessary to calibrate the capacitor. Two methods were used:

1) Measurement of the temperature dependence of the capacitance along the phase separation line. The values of the derivative dx/dT^2 as used by Kuerten (1985) and Abraham (1969) differ slightly, which introduces some uncertainty in the calibration.
2) Measurement of capacitance at 20 mK where the ^{3}He concentration is accurately known to be 6.645% and subsequently removing all ^{3}He from the system so that only pure ^{4}He remains (x = 0).

During the calibration the mixing chamber and experimental space were connected by a short and wide tube so that there was no concentration difference between the two chambers. The calibrations were consistent within 0.15 fF/% for setup 7b and the following sensitivity was obtained:

$$\frac{dC}{dx} = -\ 5.53\ \ (\pm\ 0.15)\ \mathrm{fF}/\%. \tag{3.2}$$

The nominal value of the capacitor was about 34 pF, wire capacitance not included. For the mixing chamber in figure 7c only procedure 1 was carried out yielding:

$$\frac{dC}{dx} = -10.2\ \ (\pm\ 0.1)\ \mathrm{fF}/\%. \tag{3.3}$$

The nominal value of the capacitor is 62.5 pF in this case, not taking into account the wire capacitance. The error in formula (3.3) is due to the uncertainty in the measurement of the phase separation line of Abraham. We decided to take their calibration as the correct one for our determination of the sensitivity. The error in our data is much smaller and does not contribute to the final error.

In combination with a Capacitance Bridge (General Radio 1615-A) we used a home made external reference capacitor with a value of 100 aF. In this way fast ^{3}He concentration changes of in principle 0.002% and 0.001% can be determined in the two setups respectively.

The calibration data of setup 7c are shown in figure 8. The discontinuity at about

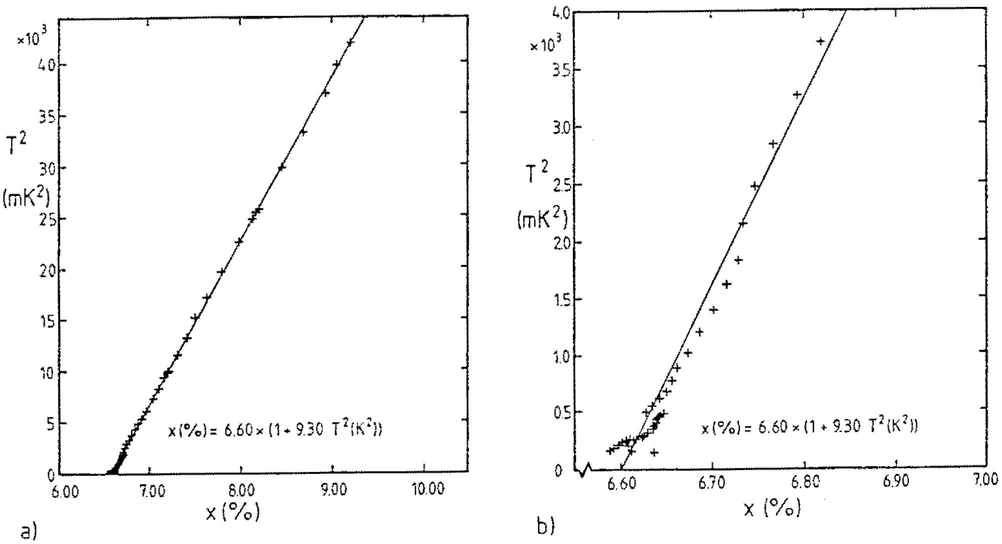

Fig.8 *Phase separation line in a T^2-x diagram.*
a) T^2 as a function of x in the temperature range 12–200 mK.
b) T^2 as a function of x in the temperature range 12–40 mK, expanded scale.
The straight line is a least squares fit to the results.

500 mK^2 is due to day to day changes of the capacitance which are not well understood. The points below $0.5 \cdot 10^3$ (mK)^2 were measured in one day.

3.2.3 PRESSURE MEASUREMENT.

Pressure measurements are carried out with a similar type of device as described in Castelijns (1986). However, the transducer used by Castelijns was made of an Araldite* housing and a flexible foil of Kapton*. Due to the much lower thermal expansion of Kapton than of Araldite the foil bulged out and behaved as a click clack. Based on the literature (Greywall (1980), Griffioen (1985), Collaudin (1986), Landau (1970)) a new prototype was developed using a metal housing. Finally three transducers were built based on the experience with this prototype, see figure 9. It consists of a housing made of stainless steel, a set screw, a connecting tube, a fixed capacitor plate with two small holes in it and a flexible plate. Some parts are electrically insulated. Instead of Kapton, an aluminized Mylar* foil with a thickness of 7 μm or 2 μm is used as flexible plate.

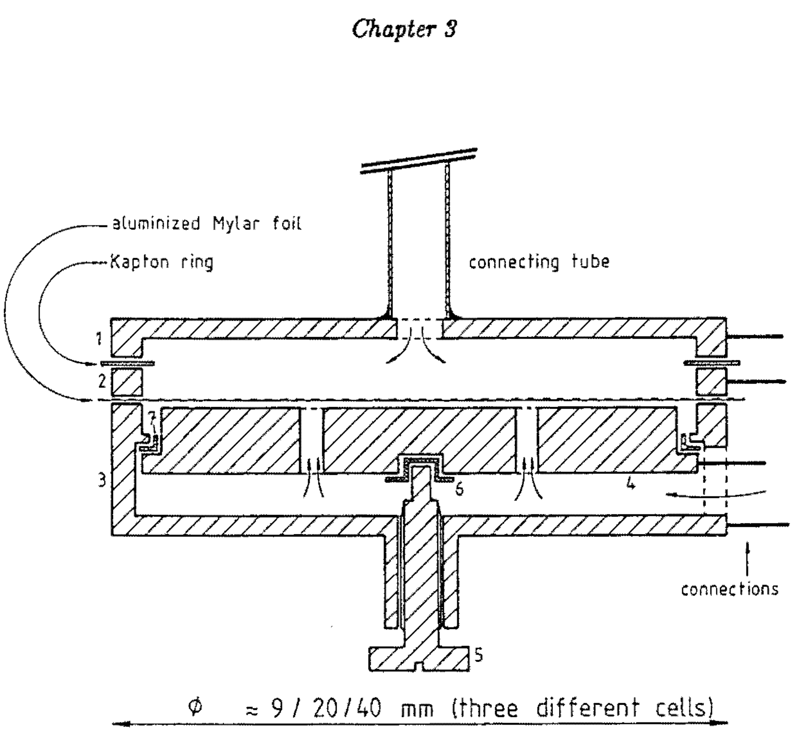

Fig.9 *Stainless steel pressure transducer. 1,2,3 Housing; 4 Fixed capacitor plate; 5 Set screw; 6 Insulating Celoron* button; 7 Insulating Araldite* ring. All parts are glued together with Stycast 1266*. Part 4 is insulated from the housing 3 by the ring 7 and spacer 6. Part 2 is insulated from part 1 and 3 by a Kapton ring and the Mylar foil and is used for electrical connection. Parts 1 and 3 are connected forming the electrical mass, which has a function as electrical shielding. The set-screw is adjusted finger tight. Pressure communication occurs through the holes as indicated by the arrows.*

The aluminized part of the Mylar foil is glued to the housing under tension in a special setup, where the foil is stretched evenly in all directions using a cylindrical stretcher. If the foil is glued to part 2 electrical contact remains between it and the foil. To get the correct sensitivity some trial and error is needed. As the stainless steel has a much lower thermal expansion than the Mylar foil the problems of shrinking are overcome. Furthermore, the metal housing provides effective electrical shielding. There is no interference with the resistance thermometers.

The transducer was calibrated in a special setup, in which a pressure difference could be created by means of a liquid ^{4}He II column.

The important parameters of the transducers are compiled in table 1. The foil of transducer 1 was damaged and a new foil was mounted, so it is indicated twice (1a, b) in the table. If the foil is damaged a new foil can be mounted. The system can be

Table 1 *Specifications of the pressure transducer which are described in the text. Distance means the distance between foil and plate, diameter is the diameter of the capacitor plate.*

No.	Capacity (pF)	Diam. (mm)	Distance (μm)	Sensitivity (fF/Pa)	Resol. (mPa)	Range (Pa)
1a	25.8	14	60	-11.7	5	300
1b	50.6	14	30	-38.5	2	300
2	852	34	10	-3170	0.1	150
3	2.38	4	10	-0.32	400	400

reassembled in one day. One negative aspect of the transducers is that the capacitance value at zero flow ($C_{p=0}$) never returns to the same value in different measuring runs. This value may change by a few percent. So pressure changes can be measured accurately but the absolute value of the pressure may be in error within about 5%. We corrected this by assuming that the change in $C_{p=0}$ is caused by a small alteration of the distance between the capacitor plates and that no changes in foil elasticity occur. If the value of the capacitance at calibration is called C_{old} and the zero value during measurement $C_{p=0}$, is called C_{new}, then the change can be taken into account using the following relation:

$$\frac{dC}{dp}_{new} = \frac{dC}{dp}_{old}\left[\frac{C_{new}}{C_{old}}\right]^2 . \tag{3.4}$$

When there is a linear p dependent term in the calibration it is possible to carry out a higher order correction. Using the method of Collaudin (1986) and carrying out a Taylor expansion these effects can be corrected for. With transducer 1 it was observed that the calibration contained such a linear term.

3.2.4 ^{4}He-CHEMICAL POTENTIAL.

The chemical potential is calculated from the basic variables T, x and p, (Kuerten (1985)). At low temperatures the following equation holds:

$$\mu_4(0,T,x) = -0.06092-1.242(x-0.0660)-2.253\ T^2 . \tag{3.5}$$

The effect of the pressure can also be calculated using the expansion:

$$\mu_4(p,T,x) = \mu_4(0,T,x) + V_4(0,T,x)p + \frac{1}{2}\frac{\partial V_4}{\partial p}\bigg|_{p=0} p^2 + ------ \qquad (3.6)$$

where V_4 = partial volume of the ^{4}He component, Kuerten (1987a).
The second and higher order terms are negligible for the analysis of our measurements. Equation (3.6) thus yields for low temperatures:

$$\mu_4(p,T,x) = \mu_4(0,T,x) + 27.58 \cdot 10^{-6} \cdot p\ . \qquad (3.7)$$

In this way for pressures up to 10^4 Pa, μ_4 and $\Delta\mu_4$ can be calculated from the experimental results.

3.3 THE MEASURING PROCEDURE.

The measurements which are described in the next chapters were carried out at constant mixing chamber temperature. The mixing chamber heater was used to control the mixing chamber temperature. The still heater mainly determines the flow. In figure 10 an illustration is shown where the mixing chamber heating power $\dot{Q}_m$ is plotted as a function of the still heating power $\dot{Q}_s$ at constant T_m when the flow channel Z_B was installed. To understand the procedure which was used to control the temperature T_m, we will treat the relationship between $\dot{Q}_s$, $\dot{Q}_m$ and the flow rate. We apply the enthalpy balance to a "black box" enclosing the low temperature part (main impedance, still, heat exchangers, flow impedance and mixing chamber) of the dilution refrigerator, crossing just above the still and just below the condenser (1 K plate), cf. figure 6. As usual we assume that pure ^{3}He is circulating. The enthalpy balance reads:

$$\dot{n}_3 H_{m,l}(p_{1K},T_{1K}) + \dot{Q} = \dot{n}_3 H_{m,g}(T_S)\ . \qquad (3.8)$$

In this equation $H_{m,l}(p_{1K},T_{1K})$ and $H_{m,g}(T_S)$ represent the molar enthalpies of the incoming ^{3}He liquid from the 1 K plate and the outgoing ^{3}He gas at the still respectively and $\dot{Q}$ represents the sum of the heatloads to the black box. We like to remark that the molar gas enthalpy is independent of the pressure in this temperature region. The term $H_{m,g}$ can be written as a sum of $H_{m,l}$, representing the liquid ^{3}He enthalpy at the still temperature and L_3, representing the latent heat at the same

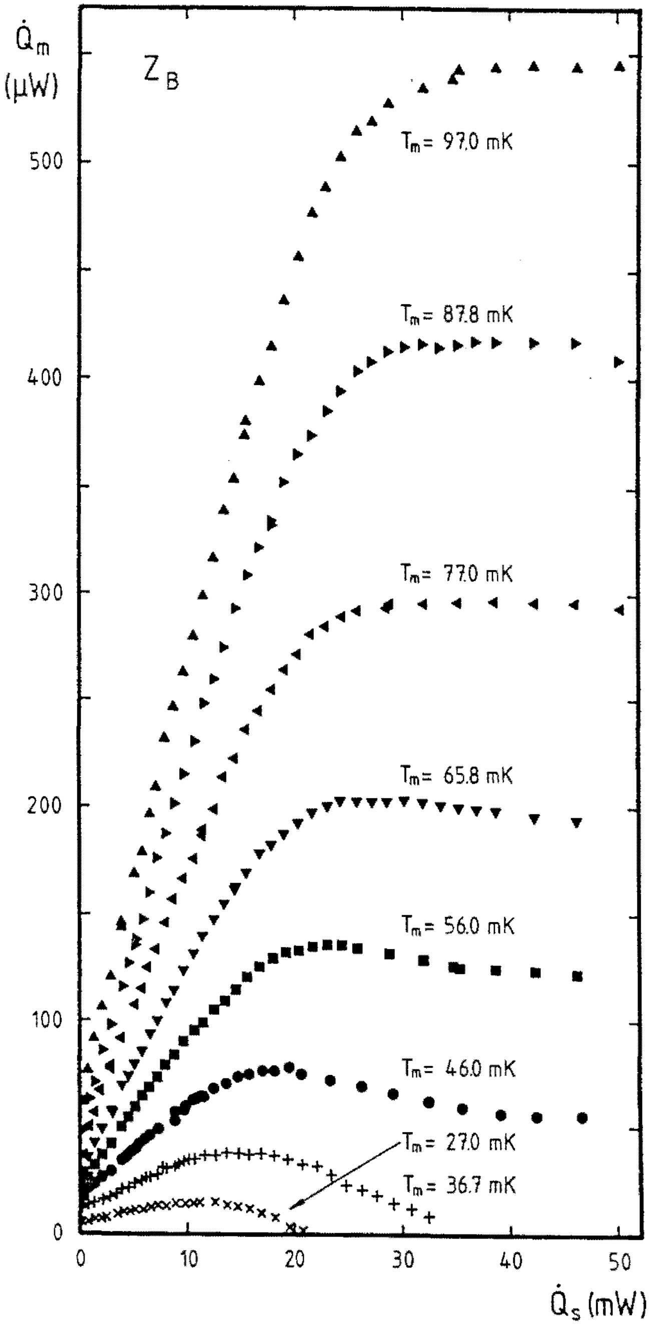

Fig. 10 $\dot{Q}_m$ *as a function of* $\dot{Q}_s$ *for a flow impedance* Z_B *(see chapter 4) at different mixing chamber temperatures.*

temperature. The term $\dot{Q}$ consists of the heating powers $\dot{Q}_s$, $\dot{Q}_m$ and heat leaks which are mainly the constant heat leak from the 1 K bath via the tubing to the still $\dot{Q}_{s0}$. Consequently:

$$\dot{n}_3\left[H_{m,l}(p_s,T_s) - H_{m,l}(p_{1K},T_{1K})\right] + \dot{n}_3L_3(T_s) = \dot{Q}_s + \dot{Q}_m + \dot{Q}_{s0}\ . \tag{3.9}$$

At low flow rates ($\dot{n}_3$<0.25 mmol/s) the temperatures of the 1 K plate and the still are approximately constant and the enthalpy variations corresponding to the pressure variations are smaller than 0.5 J/mol and can be neglected (Lounasmaa (1974)). The enthalpy difference of the liquid at T_{1K} and T_s is of the order 1.5 J/mol. The latent heat is of the order 34 J/mol. So we can write:

$$\dot{n}_3L_{3eff} = \dot{Q}_s + \dot{Q}_{s0} + \dot{Q}_m \tag{3.10}$$

and L_{3eff} is an effective latent heat of approximately 32.5 J/mol. This equation shows that at zero applied heat load ($\dot{Q}_s+\dot{Q}_m = 0$) there is a nonzero ^{3}He flow due to the heat leak ($\dot{Q}_{s0}$), furthermore it shows the expected linearity between $\dot{n}_3$ and $\dot{Q}_s$ for fixed $\dot{Q}_m$.

In the low temperature limit the cooling power of the dilution process in the mixing chamber which is consumed by the heater is given by:

$$\dot{Q}_m = \dot{n}_3(93T_m^2-11.4T_h^2)\ \mathrm{J/molK^2}\ , \tag{3.11}$$

which is found by the analysis of the enthalpy balance of the mixing chamber. T_h is the temperature of the concentrated ^{3}He leaving the last heat exchanger (cf. figure 7a).

As the concentrated ^{3}He leaving the last heat exchanger is cooled by the dilute ^{3}He entering the heat exchanger at T_e (or T_d) it follows that $T_e<T_h$. In our system at temperatures above 40 mK we can write (Castelijns (1986)):

$$T_h = vT_e\ , \tag{3.12}$$

where v >1. When the viscous or mutual frictional heating in the flow channel is negligible as we will assume, then

$$T_e \simeq T_m\ . \tag{3.13}$$

Inserting this dependency in (3.12) and then (3.12) in (3.11) and eliminating $\dot{n}_3$ with equations (3.10) and assuming that in general $\dot{Q}_m \ll \dot{Q}_s$ and neglecting it in equation (3.10) yields:

$$\dot{Q}_m = \frac{\dot{Q}_s+\dot{Q}_{s0}}{L_{3\ eff}}(93-11.4v^2)T_m^2\ \mathrm{J/molK^2}\ . \tag{3.14}$$

This equation shows two effects. First at constant $\dot{Q}_s$, the value of $\dot{Q}_m$ rises quadratically with T_m. Second, at constant T_m, $\dot{Q}_m$ rises linearly with $\dot{Q}_s$.

From figure 10 it is evident that for low $\dot{Q}_s$ and constant T_m the linear relationship between $\dot{Q}_s$ and $\dot{Q}_m$ holds. The curves extrapolate to one point at the $\dot{Q}_s$ axis, which is about -3 mW and the modulus represents the heat leak $\dot{Q}_{s0}$. The curves of 27 mK and 36.7 mK do not extrapolate to the same value as there is already a significant viscous temperature rise in the flow channel (see chapter 4, figure 13e), so equation (3.12) is not correct anymore.

From figure 10 we can determine that $(1/T_m^2)(d\dot{Q}_m/d\dot{Q}_s) = 2.17 \pm 0.04\ K^2$ and we find $\upsilon \simeq 1.4$, for pure ^{3}He circulation. If we assume that about 3% ^{4}He circulates then we estimate $\upsilon \simeq 1.3$, which can be compared with the value for perfect heat exchangers where $\upsilon = 1$.

For still heating powers above 8 mW, T_e rises due to mutual friction. Equation (3.13) is not satisfied anymore and T_h rises too so the $\dot{Q}_s$-$\dot{Q}_m$ curves become non-linear (Castelijns (1986)). At very high heat loads ($\dot{Q}_s > 20$ mW) the ^{3}He flow rate does not increase anymore but instead the ^{4}He flow rate, which does not contribute to the cooling power, increases. The slope of the curves decreases and finally $\dot{Q}_m$ becomes approximately constant for constant T_m.

In general different flow impedances yield a different $\dot{Q}_m$-$\dot{Q}_s$ dependence for flow rates where the geometry dependent effects of dissipation become important. Control of T_m is carried out manually. In principle T_m can be adjusted within 0.1 mK depending on patience and skill of the experimentalist. Nearly all measurements were carried out starting at high flow rates and then decreasing it. This was done because the time constant of the system is smallest at high flow rates and besides controlling at low flow rates is best achieved if there is already some guidance by a part of the $\dot{Q}_m$-$\dot{Q}_s$-graph. Time constants of the flow system are on the order of a few minutes for high flow rates (1 mmol/s) and up to half an hour at low flow rates (0.1 mmol/s). In general adjustment of the next measuring point takes at least four times this time constant. All measurements were carried out after a stationary situation was established. A complete measurement over the total flow range in about 40 steps takes about fifty hours and can just be carried out within one week.

The diagrams in the next chapter will be presented not as a function of the ^{3}He flow rate but as a function of the effective ^{3}He velocity in the flow channel, defined as:

$$v \equiv \frac{\dot{n} V_3}{NA}, \tag{3.15}$$

with $\dot{n} = \dot{n}_3 + \dot{n}_4$ the measured gas flow rate.

In general the $\dot{n}_4$ contribution is very small (<4%) as was discussed by Castelijns (1986) and in that case v actually represents the ^{3}He flow velocity. However, when the flow velocity becomes large the ^{4}He flow rate increases and v no longer represents the ^{3}He flow velocity. This can be seen in the diagrams which are presented in chapter 4. Where necessary a dotted vertical line will indicate the value of v above which too much ^{4}He is circulated. Only values of v smaller than this value were taken into account in the analysis of the data.

CHAPTER 4

STEADY STATE EXPERIMENTS AND RESULTS

4.1 INTRODUCTION.

This chapter describes in detail the steady flow experiments that concern the critical velocities.

In section 4.2 the design features of our flow channels will be discussed. Section 4.3 summarizes the experimental procedure. In the next four sections 4.4–4.7 the typical results from T, x and p measurements are presented for some flow impedances. T^2–x diagrams and chemical potential difference ($\Delta\mu_4$) graphs are discussed in the sections 4.8 and 4.9. Results will be compared with the phenomenological description in all sections. Section 4.10 concludes this chapter.

4.2 DESIGNING A FLOW CHANNEL FOR INTERMEDIATE FLOW VELOCITIES.

In ^{4}He II flow velocities are observed at which mutual friction first appears (section 1.1). At the time when this work was started there were no measurements of such critical velocities in ^{3}He–^{4}He II mixtures. In order to choose the flow channel suitable for the detection of a critical velocity we used the following design considerations:

Firstly it was assumed that the relation between the critical velocity (v_c) and the tube diameter (d) resembles the relation which holds approximately in ^{4}He II counterflow (Tough (1982)). The critical velocity was thus estimated at:

$$v_c d = W_c \tag{4.1}$$

where $W_c \simeq 10\ \mathrm{mm}^2/\mathrm{s}$.

The ^{3}He flow rate of the dilution refrigerator can be varied between a lower limit $\dot{n}_{3\mathrm{min}}$ and an upper limit $\dot{n}_{3\mathrm{max}}$ where $\dot{n}_{3\mathrm{min}} = 0.064$ mmol/s in principle but in practice 0.15 mmol/s and $\dot{n}_{3\mathrm{max}} = 1$ mmol/s. So we require that the ^{3}He flow rate $\dot{n}_{3c}$, which corresponds with the critical velocity, satisfies the condition:

$$\dot{n}_{3\mathrm{min}} < \dot{n}_{3c} < \dot{n}_{3\mathrm{max}} \,. \tag{4.2}$$

By chosing $\dot{n}_{3c} = 0.5\ \dot{n}_{3\mathrm{max}}$ the critical velocity appears at the centre of the circulation range of our dilution refrigerator. With N flow channels in parallel,

$$v_c = \frac{4\dot{n}_{3c}V_3}{N\pi d^2} \tag{4.3}$$

and with equation (4.1) we thus obtain:

$$N = \frac{2\dot{n}_{3\mathrm{max}}V_3}{W_c \pi d} \,. \tag{4.4}$$

With the values of $\dot{n}_{3\mathrm{max}}$, $V_3 \simeq V_{3d} = 415 \cdot 10^{-6}\ \mathrm{m}^3/\mathrm{mol}$ and W_c mentioned earlier we get in engineering terms $N \simeq 27$ (mm/d), so e.g. when d = 0.3 mm about 100 capillaries have to be placed in parallel.

To choose the length of the tubes we can leave it undecided whether this critical velocity in mixtures shows up by a discontinuous temperature rise due to the appearance of mutual friction, or by a continuous but steep change of the temperature T_e.

The expected temperature difference ΔT_c between M and E when mutual friction occurs at $v = v_c$ can be estimated from equation (2.18), which for small ΔT_c can be approximated as:

$$\Delta T_c = \frac{a\gamma'' \ell}{2T}(v_c/V_{3d})^3. \tag{4.5}$$

In order to determine v_c accurately ΔT at the critical velocity should be larger than a certain minimum value ΔT_{min}:

$$\Delta T_c \geq \Delta T_{\mathrm{min}}. \tag{4.6}$$

Conditions (4.5-6) can be transformed into:

$$\left[\frac{\ell}{\mathrm{mm}}\right] \geq 1700 \left[\frac{T}{30\ \mathrm{mK}}\right]\left[\frac{\Delta T_{\mathrm{min}}}{\mathrm{mK}}\right]\left[\frac{d}{\mathrm{mm}}\right]^3 . \tag{4.7}$$

For $T = 30$ mK, $\Delta T_{min} = 1$ mK and $d = 0.3$ mm it follows that $\ell \geq 46$ mm.

The design conditions can be represented graphically. They are shown in figure 11.

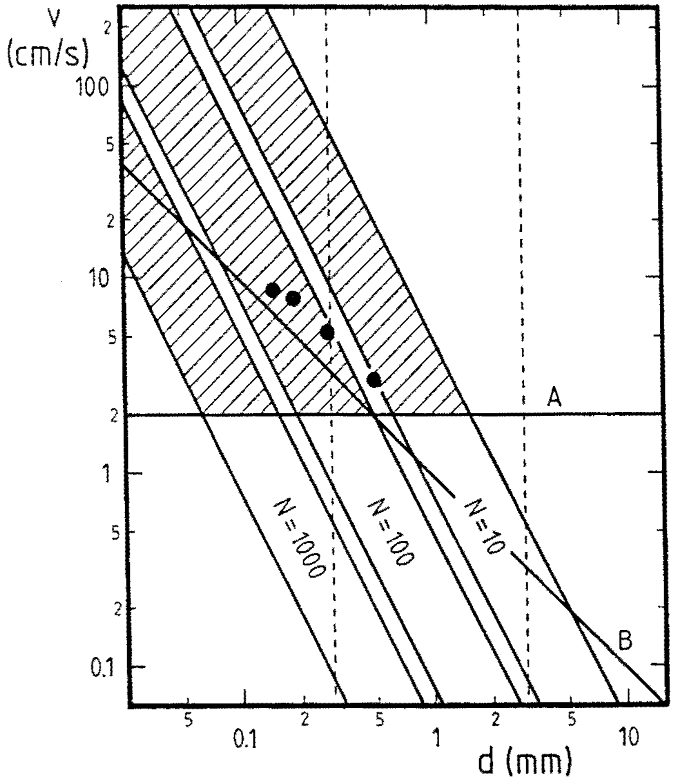

Fig.11 *v–d plot used in the design of the initial flow channels. Line A represents equation (4.5), line B equation (4.1). The regions N = 10–1000 represent the criterion (4.2). The dots correspond to critical velocities which were measured during the first five trials, see next section.*

Line A represents the relation (4.5) where $\Delta T_c = 1$ mK, $T = 30$ mK and $\ell = 200$ mm. The value 200 mm is about the maximum length possible in the setup of figure 7a. The region with $\Delta T > 1$ mK is the half plane above line A for this case. Line B represents equation (4.1). Several regions are drawn for different numbers of tubes representing the range (4.2). A tube diameter of about 0.3 mm leads according to line B to a v_c of about 3 cm/s. This is above line A and it lies in the region where 100 tubes need to be placed in parallel to reach v_c and to be able to detect it. Taking d=3 mm results in a v_c value of about 0.3 cm/s. As this point lies below line A it is impossible to determine v_c.

Tube lengths much larger than 200 mm will be necessary to bring ΔT in the desired region. This graph formed the basis for the choice of the first tube systems for the study of the velocity range intermediate between the laminar flow states and the states of well developed turbulence, described by the mutual friction model.

4.3 THE FIRST SETUP AND THE FIRST RESULTS.

Based on the arguments described in the previous section the setup of figure 7a was constructed. First 113 (Z_C), and later 60 (Z_D) capillaries were placed in parallel. Their length was l=198 mm and 177 mm respectively, their diameter was 0.30 mm. Using the

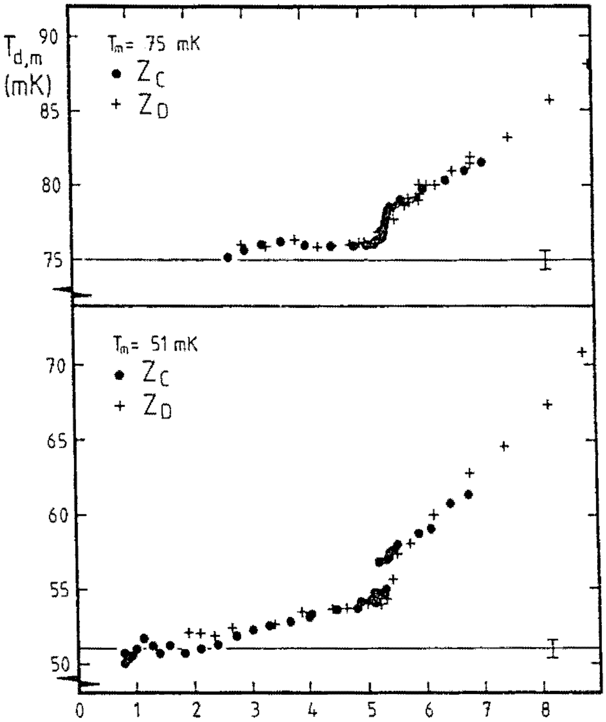

Fig.12 *T_d as a function of the ^3He flow velocity for two tube systems, see table 2, and two mixing chamber temperatures. The horizontal line represents the value of T_m at which the data were taken.*

technique described in section 3.3 the downstream temperature T_d was measured as a function of $\dot{n}_3$ at constant mixing chamber temperature. In figure 12 the first results are presented.

The temperature T_d is plotted as function of the flow velocity v for mixing chamber temperatures of 75 mK and 51 mK. For low velocities T_d increases gradually. This can be accounted for by viscous heating. At a critical velocity of about 5.5 cm/s there is a rather discontinuous temperature rise. For higher flow velocities the increase of temperature with velocity is steeper than in the low velocity range. This is typically the mutual friction behaviour. It can be noticed that the critical velocity for the two series of data almost coincide. The difference in length of the two impedances does not show up in the measurements, because these differences are too small to be detected.

In the setup of figure 7a measurements were carried out with five different flow impedances with channel diameters d = 0.155, 0.19, 0.30 and 0.50 mm (Z_L, Z_A, Z_C, Z_D and Z_F). In all flow channels the same sort of behaviour occurred near v_c. These critical velocities are shown in figure 11 by dots. In retrospect these results confirm the estimates based on the design criteria of section 4.2.

In the setup of figure 7a neither pressure nor concentration differences could be measured. This is the reason why this setup was modified in a way shown in figures 7b or c. In the next sections the experiments with these devices will be described and we will compare the results of the measurements with the equations of the mechanical-vacuum and the mutual-friction model.

4.4 THE FLOW IMPEDANCES.

In table 2 a survey is given of all the circular flow channels used in our experiments. The first column gives the label used to identify the flow impedance. The second, third and fourth column show the number of tubes, length and diameter respectively. In the fifth column the tube material is indicated. The columns six, seven and eight display the critical flow rate, critical flow velocity and product of critical flow velocity and diameter respectively. The last column gives the mixing chamber temperatures at which the measurements were carried out.

The uncertainties in the last digit of the different parameters are indicated by numbers between brackets. The tube diameters of the small diameter circular flow channels were determined by taking a photograph using a microscope and measuring

Table 2 *A survey of all the circular flow channels investigated in this research. Numbers in between brackets indicate the error in the parameter. CN means cupronickel, St means stainless steel, Gl means glass.*

No.	N	ℓ (mm)	d (mm)	Mat	$\dot{n}_{3c}$ (mmol/s)	v_c (cm/s)	$v_c d$ (mm^2/s)	T_m (mK)
Z_A	70	30.0(1)	0.19(1)	CN	0.300(25)	6.5(1)	12(2)	27.2/46.0
Z_B	28	23.0(1)	0.261(5)	CN	0.245(5)	7.0(4)	18.3(7)	27.0/36.7/46.0 56.0/65.8/77.0 87.8/97.0/37.0
Z_C	113	198.0(1)	0.30(1)	CN	1.00(2)	5.3(1)	15.9(3)	51/75
Z_D	60	177.0(1)	0.30(1)	CN	0.52(2)	5.2(4)	15.6(7)	27.2/46
Z_E	19	82.4(1)	0.40(1)	CN	0.275(10)	5.0(2)	19.8(6)	46.0
Z_F	34	199.0(5)	0.50(1)	CN	0.505(10)	3.3(2)	16.3(6)	27.2/46.0
Z_G	15	322.7(1)	0.65(1)	CN	0.29(1)	2.47(7)	16.1(5)	46.0
Z_H	13	380.1(1)	0.81(1)	CN	0.34(1)	2.2(1)	17.7(5)	27.2/46.0
Z_I	1	10.45(5)	1.20(5)	CN	?	?	?	37.1/56.0
Z_J	3	209.8(1)	1.80(2)	CN	0.21(2)	1.2(1)	21(4)	33.9
Z_K	3	1876(2)	1.80(2)	CN	0.215(10)	1.17(6)	21(1)	33.0
Z_L	85	59.2(1)	0.155(10)	St	0.36(1)	10(1)	15(1)	36.2/46.0
Z_M	1	5973(5)	4.36(3)	St	0.225(15)	0.63(5)	27(2)	38.1
Z_N	1	2571(4)	7.40(25)	St	0.490(25)	0.47(4)	35(3)	34.9
Z_O	222	5.6(1)	0.054(10)	Gl	0.14(1)	12(5)	6(2)	46.0
Z_P	243	25.0(1)	0.12(1)	Gl	0.550(5)	9(2)	11(1)	46.0
Z_Q	120	79.7(1)	0.160(5)	Gl	0.445(5)	7.9(5)	12.7(5)	46.0
Z_R	96	70.1(1)	0.22(1)	Gl	0.490(5)	5.8(6)	12.7(5)	46.0
Z_S	54	178.4(1)	0.29(1)	Gl	0.415(10)	5.0(4)	14.5(8)	27.4/46.0/27.4

Table 3 *A survey of all the annular flow channels investigated in this research. Numbers in between brackets indicate the error in the parameter. GS means german silver, St means steel, Br means brass, Cu means copper.*

No.	N	ℓ (mm)	D (mm)	d (μm)	Mat	$\dot{n}_{3ca}$ (mmol/s)	v_{ca} (cm/s)	$v_{ca}d$ (mm^2/s)	T_m (mK)
Z_T	1	20.0(1)	10.325	50(1)	GS	0.23(3)	5.8(5)	2.9(3)	46.0
Z_U	1	60.0(1)	7.857	101(1)	GS	0.20(3)	3.4(4)	3.4(4)	46.0
Z_V	1	60.0(1)	7.92	100(10)	GS	0.25(5)	4.2(1)	4.2(1)	32.2/45.2/46.0
Z_W	1	180.0(1)	7.37	150(10)	St	0.27(5)	3.3(7)	5(1)	32.2/46.0
Z_X	1	310.5(1)	7.31	210(10)	St	0.25(2)	2.2(2)	4.4(4)	46.0
Z_Y	3	300.0(1)	7.890	100(3)	Br	0.30(5)	1.7(2)	1.7(2)	39.7
Z_Z	1	100.0(1)	26.027	1000(1)	Cu	>1	>0.5	>5	33.0

Table 4 *A selection of the geometric data of the flow channels which will be discussed in the sections below.*

No.	N	ℓ (mm)	D (mm)	d (mm)	Mat.	Fig.
Z_I	1	10.45	–	1.20	CN	a
Z_D	60	177.0	–	0.30	CN	b
Z_S	54	178.4	–	0.29	Gl	c
Z_U	1	60.0	7.857	0.101	GS	d
Z_B	28	23.0	–	0.261	CN	e

the diameter on the photograph using a marking gauge. The diameter of the wider tubes was determined using a set of calibrated rods or measuring it directly. In some cases the data provided by the factory were used which were found to be highly reliable.

All flow channels were, if necessary, cleaned by first pulling a wire through them and then rinsing them with alcohol-toluene followed by drying. For Z_A and Z_O there is an uncertainty in the number of tubes of 2 and 5 respectively.

The error in the critical flow rate was estimated from the curves of the measured parameters as functions of the flow.

In table 3 the annular flow channels and their properties are presented. This table has the same structure as table 2. However, there is one extra column containing D (the annular tube diameter). In this table d is the slit spacing and the "apparent" critical velocity is indicated as will be discussed in the next sections. An extra index a is used to distinguish the apparent critical velocity from the true critical velocity v_c. The annular flow channels were made on a precision lathe with an accuracy of 1 μm.

It is no use to present the results of all the measurements in this thesis since this would mean that over 175 graphs would have to be shown. In the next sections a selection of typical results is presented for the flow impedances Z_I, Z_D, Z_S, Z_U and Z_B. They are represented by the figure numbers a, b, c, d and e respectively. For easy reference the geometries of these five flow channels are collected in table 4 in aid of the discussion in the next sections. In all figures measurements are compared with the mutual-friction model (MF) in the limit of highly (quantum) turbulent flow, represented by the empirical equations (2.18)-(2.22) and with the mechanical-vacuum model (MV), represented by equations (2.15)-(2.17).

4.5 TEMPERATURE DIFFERENCES.

The temperature T_e is plotted as a function of v, in the figures 13a-e. Figure 13a shows the results obtained with tube Z_I. Because of the high velocities in the single tube, even at the lowest circulation rate mutual friction dominates in this case. As turned out later the critical velocity for this system is about 1.5 cm/s which is well outside the range of the measurements. Moreover, it would be impossible to detect v_c because of the short length and corresponding small temperature difference (equation (4.7)). There is good agreement with the mutual-friction model.

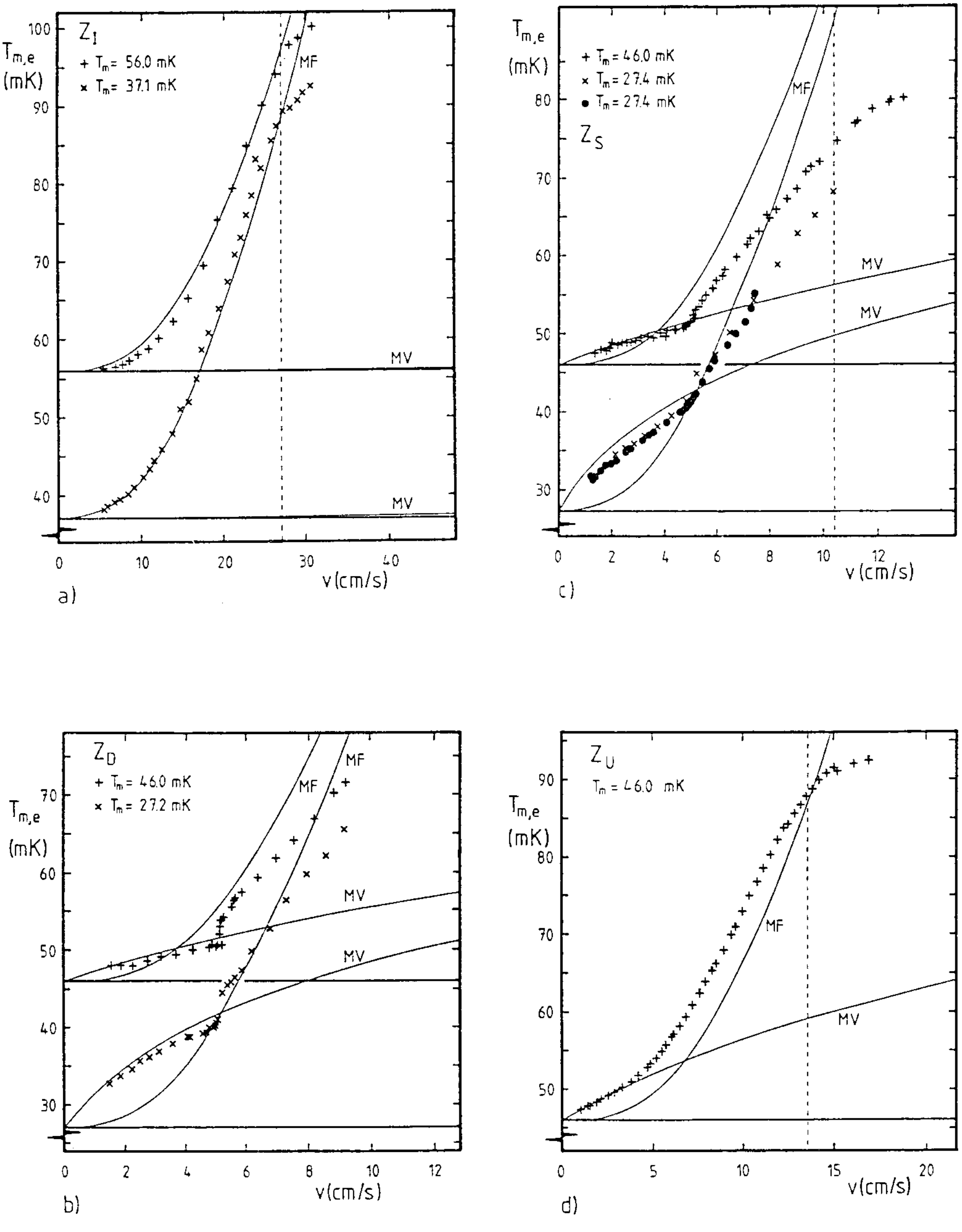
Z_I
+ T_m = 56.0 mK
× T_m = 37.1 mK
$T_{m,e}$ (mK)
MF
MV
MV
v(cm/s)
a)
Z_S
+ T_m = 46.0 mK
× T_m = 27.4 mK
● T_m = 27.4 mK
$T_{m,e}$ (mK)
MF
MV
MV
v(cm/s)
c)
Z_D
+ T_m = 46.0 mK
× T_m = 27.2 mK
$T_{m,e}$ (mK)
MF
MF
MV
MV
v(cm/s)
b)
Z_U
T_m = 46.0 mK
$T_{m,e}$ (mK)
MF
MV
v(cm/s)
d)

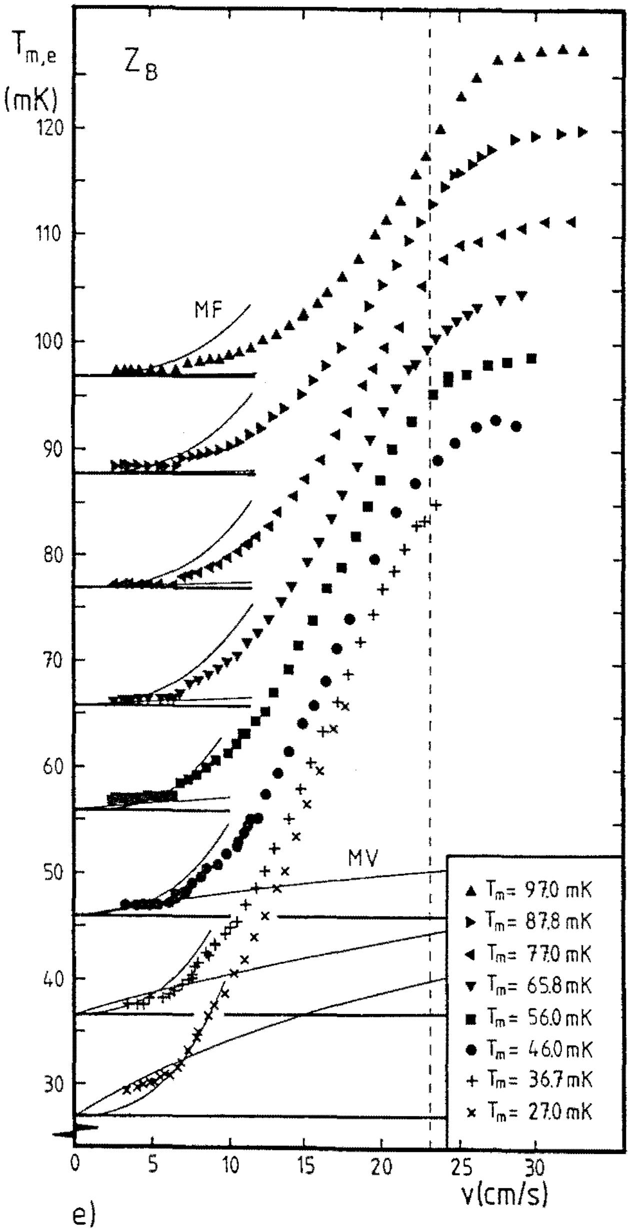

Fig.13a–e *Temperature (T_e) measured as a function of the flow velocity for the five impedances and different T_m. The values of T_m are represented by horizontal lines. MV and MF represent the temperature T_e calculated with equations (2.15) and (2.18) respectively, without any adjustable parameters. Only values of the velocity below the vertical line are of significance.*

In figure 13b the result with Z_D is shown. With this metal tube the critical velocity is very distinct and equal to 5.2 cm/s (cf. figure 12). For low velocities the mechanical-vacuum model (MV) is in reasonable agreement with the measurements. Differences can mainly be attributed to measuring accuracy and to an incorrect viscosity approximation, $\eta = 5 \cdot 10^{-8}/T^2$ and V_3 dependency on x. The latter will be discussed in chapter 7. Above the critical velocity the measured T_e is not in agreement with the mutual-friction model. This is not surprising because just above the critical velocity the mutual-friction model indeed does not apply. It is remarkable that the discrepancy clearly tends to increase with increasing velocity. We will come back to this in the next chapter.

Figure 13c represents a measurement with glass tubes of similar dimensions as the metal tubes of 0.30 mm diameter. It resembles figure 13b rather closely though with glass the transition at v_c is more gradual.

In Figure 13d a measurement of an annular flow channel with a slit of 101 μm is presented. There is reasonable agreement with the mechanical vacuum approximation in the low velocity part of the figure. Here, one cannot observe a sharply defined critical velocity as in the circular tube experiments. In none of the annular impedances a critical velocity has been observed. More discussion of this important observation is presented in the next chapter.

Figure 13e represents measurements of the T_e-v dependence at eight different mixing chamber temperatures. These measurements were carried out as accurately as possible. Even though the tubes are very short one still can observe a critical velocity at 7 cm/s. Although the mixing chamber temperature ranged from 27 mK up to 97 mK there are no indications that the critical velocity changes. In chapter 5 we will show that at still higher temperatures the critical velocity generally has a tendency to decrease.

An important consequence of the measurements with flow channel Z_B at eight different temperatures is that it proves that the critical velocity is indeed not due to classical turbulence in the ^{3}He. The Reynolds number for pipe flow can be defined by:

$$\mathrm{Re} = vd\rho_n/\eta = vd\rho_n T^2/\eta_0. \tag{4.8}$$

There can be some discussion about the use of ρ_n in the definition, but this does not change the conclusion. The Reynolds number calculated for $v = v_c$ varies from 8 at low temperatures to about 80 at high temperatures. In case ρ is used instead of ρ_n it yields $80 < \mathrm{Re} < 800$. So Re changes about a factor 10 while v_c is constant. Thus it can safely be concluded that v_c is not determined by viscous instability effects as appear in ordinary liquids. In addition, the value of Re is much smaller than the critical value of about 2000 which is observed in experiments with ordinary liquids (Tritton (1988), Landau and Lifshitz (1959)). As the transition is not in the ^{3}He, the critical velocity is strong evidence for the appearance of quantum turbulence in ^{4}He.

In some measurements it was observed that at a value above the critical velocity a sudden upward kink in the curves, cf. figure 13e, occurred. We consider this as an indication of a second critical velocity. This will be shown in more detail in chapter 6.

At the high flow-velocity part of the figures it can be seen that the temperature becomes constant. This was discussed in section 3.3. It is the same effect as is described in Castelijns' thesis (1986) i.e. extra heat input in the still heater eventually increases only the ^{4}He flow rate.

4.6 CONCENTRATION DIFFERENCES.

In figure 14a-e the concentration differences are displayed. The mixing chamber concentration is assumed to be given by Kuerten's (1985a) polynomial fit for the phase separation curve,

$$x_m = 0.066+0.506T_m^2-0.249T_m^3+18.2T_m^4-74.2T_m^5. \tag{4.9}$$

It is not possible to stop the circulation in order to measure the zero flow value of the capacitance (C_c) which would represent the situation $x_e=x_m\simeq0.066$. The best way to obtain the capacitance value belonging to the saturated solution is by extrapolation of the data measured down to the lowest possible flow rate, using the mechanical-vacuum approximation as a guide. We therefore carried out the measurements down to the lowest possible circulation rate. Because the viscosity is not correctly known this method can lead to an error in x of about 0.03 %.

The measurements clearly show the change of behaviour at the critical velocity. Figure 14a shows that the mutual-friction model at high flow velocities again gives a fair description. In the other graphs there is merely reasonable agreement with the mechanical vacuum behaviour at low velocities. Again saturation can be seen in all graphs near the high flow limit.

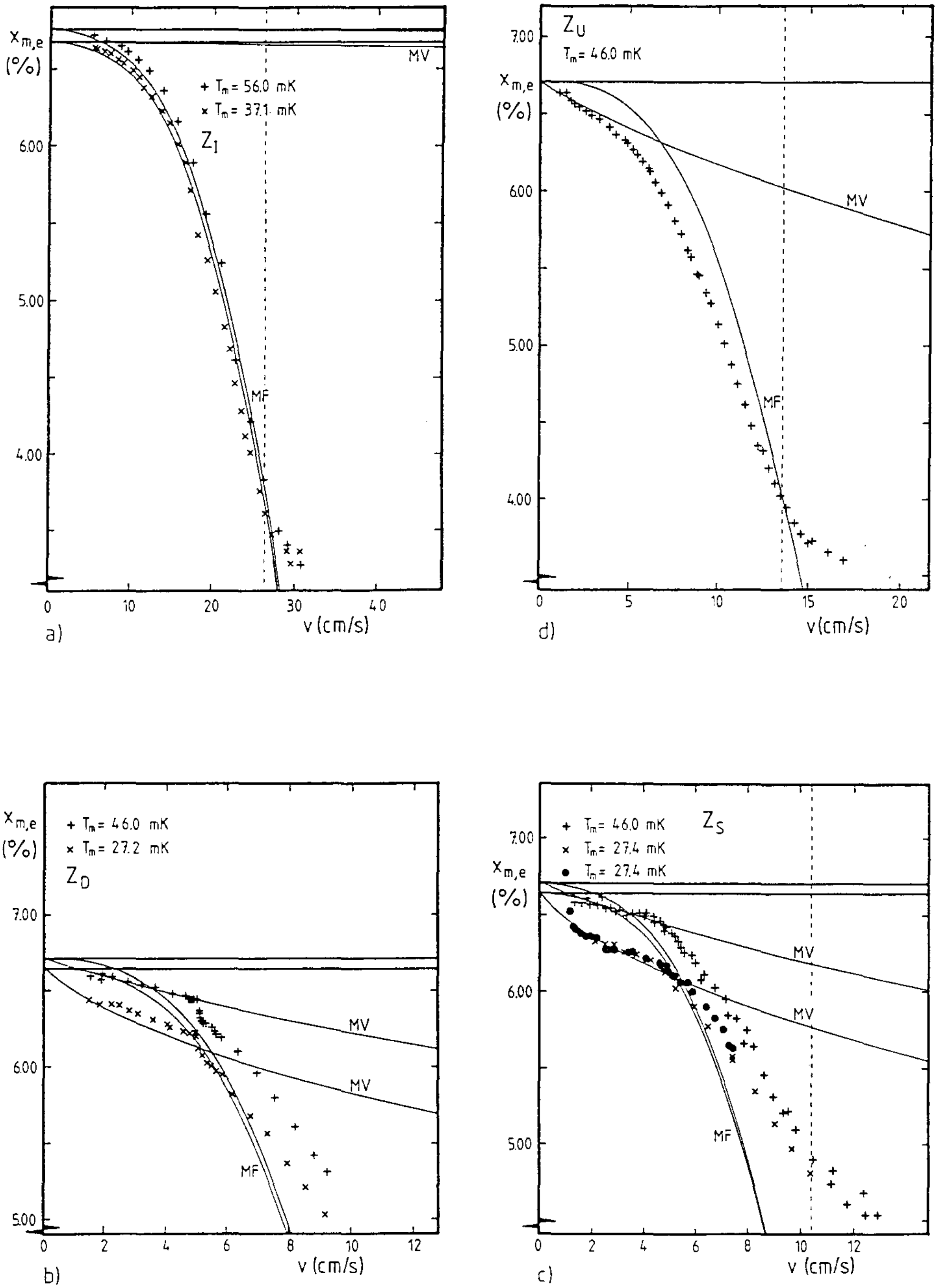
$x_{m,e}$
(%)
MV
+ T_m= 56.0 mK
× T_m= 37.1 mK
Z_I
6.00
5.00
4.00
MF
0
10
20
30
40
v (cm/s)
a)
Z_U
T_m= 46.0 mK
7.00
$x_{m,e}$
(%)
6.00
MV
5.00
MF
4.00
0
5
10
15
20
v(cm/s)
d)
$x_{m,e}$
(%)
+ T_m= 46.0 mK
× T_m= 27.2 mK
Z_D
7.00
6.00
MV
MV
MF
5.00
0
2
4
6
8
10
12
v (cm/s)
b)
7.00
$x_{m,e}$
(%)
+ T_m= 46.0 mK
× T_m= 27.4 mK
● T_m= 27.4 mK
Z_S
MV
6.00
MV
MF
5.00
0
2
4
6
8
10
12
v (cm/s)
c)

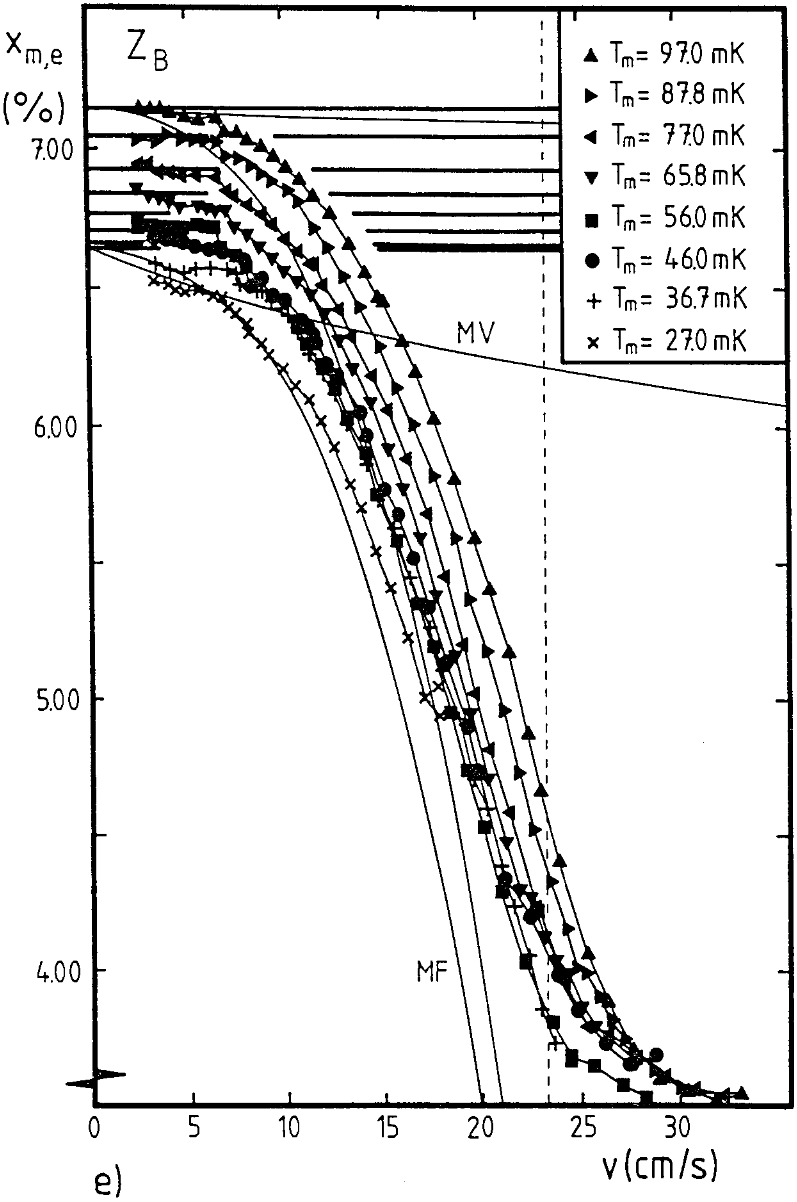

Fig.14a-e *Concentration differences measured with the same flow systems as mentioned in figure 13. The values of x_m are represented by horizontal lines. MV and MF represent the concentration x_e calculated with equations (2.17) and (2.19) respectively. In figure 14e the model curves have only been drawn for the two extreme T_m-values.*

4.7 PRESSURE DIFFERENCES.

With impedance Z_I no pressure differences were measured so figure 15a is missing. Maximum pressure differences of about 15 Pa across Z_I would be expected on the bases of the mechanical vacuum approximation. This flow channel is similar to the impedances used by Castelijns (1986) and the expected Δp are even much lower than 15 Pa due to the large temperature increase caused by mutual friction (equations (2.20) and (2.35)).

In the figures 15b-e the pressure differences over the other flow channels are shown as functions of v. In principle the zero flow value of the pressure gauge could be measured by stopping pumping at the still at the end of a measuring run and observing the relaxation of the pressure transducer capacitance. Unfortunately this technique appeared to be unreliable and was therefore not used. So in all cases the zero flow value was again obtained by extrapolating the C-$\dot{n}_3$ curve to zero flow rate.

The measurements shown in figure 15b were carried out with the prototype transducer, which showed discontinuous jumps in its $C_{p=0}$ value. Therefore the reliability of the calibration is not so high. Nevertheless, we consider the overall pressure flow dependence to be correct. Why this is so is most clearly demonstrated with the measurement at 46.0 mK. For v smaller than 5.22 cm/s the mechanical-vacuum model can be applied and shows reasonable agreement with the measurements. At the critical velocity at 27.2 mK a transition to lower pressure is observed which is enlarged in figure 16c. This difference is more than 10 times the resolution so it is real. In the measurement at 46.0 mK this effect was not observed presumably due to an unstable flow and a lower viscosity, but the scatter in the data near v_c gives an indication for a transition in this region.

Enlargements of the flow behaviour of Z_D in the critical region are presented in figure 16. At the transition mutual friction appears and the temperature increases as is seen in figure 13b and 16a. Due to this increase in T the mean viscosity decreases thus Δp decreases at the same flow velocity (see also chapter 2). The magnitude of the effect depends on the steepness of the transition. At high velocities both Δp-curves level off due to the decreasing viscosity. The transition occurring in the figures 16b,c is rather sudden and occurs in a very small velocity range.

Figure 15c shows the pressure measurement in the glass tubes Z_S. The experiment at 27.4 mK was carried out twice in two separate runs between which the system was warmed up to room temperature. This shows that the pressure measurement is quite

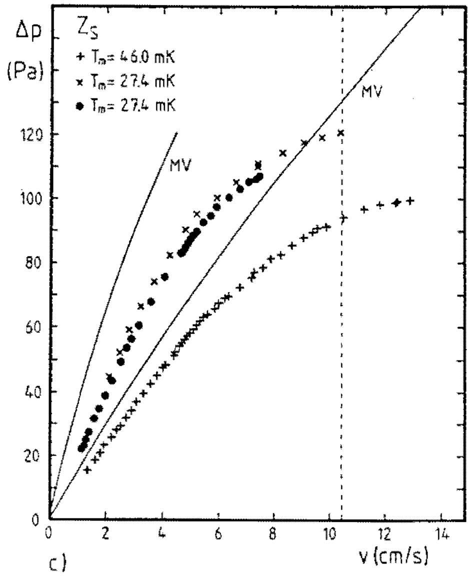
Δp
(Pa)
Z_S
+ T_m= 46.0 mK
× T_m= 27.4 mK
● T_m= 27.4 mK
MV
MV
0
20
40
60
80
100
120
0
2
4
6
8
10
12
14
v (cm/s)
c)

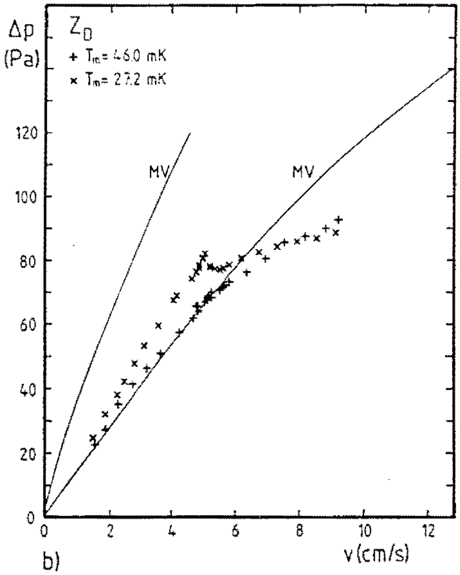
Δp
(Pa)
Z_D
+ T_m= 46.0 mK
× T_m= 27.2 mK
MV
MV
0
20
40
60
80
100
120
0
2
4
6
8
10
12
v (cm/s)
b)

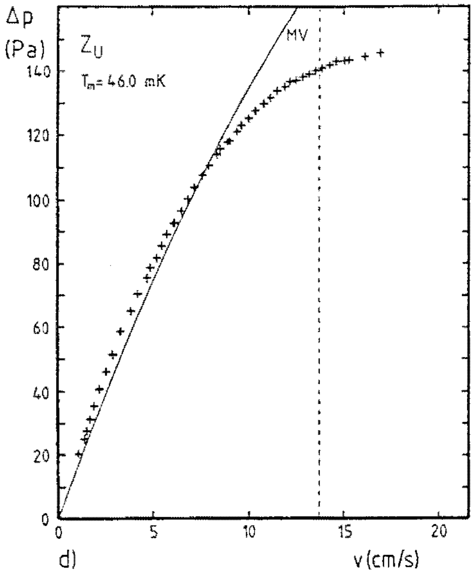
Δp
(Pa)
Z_U
T_m= 46.0 mK
MV
0
20
40
60
80
100
120
140
0
5
10
15
20
v (cm/s)
d)

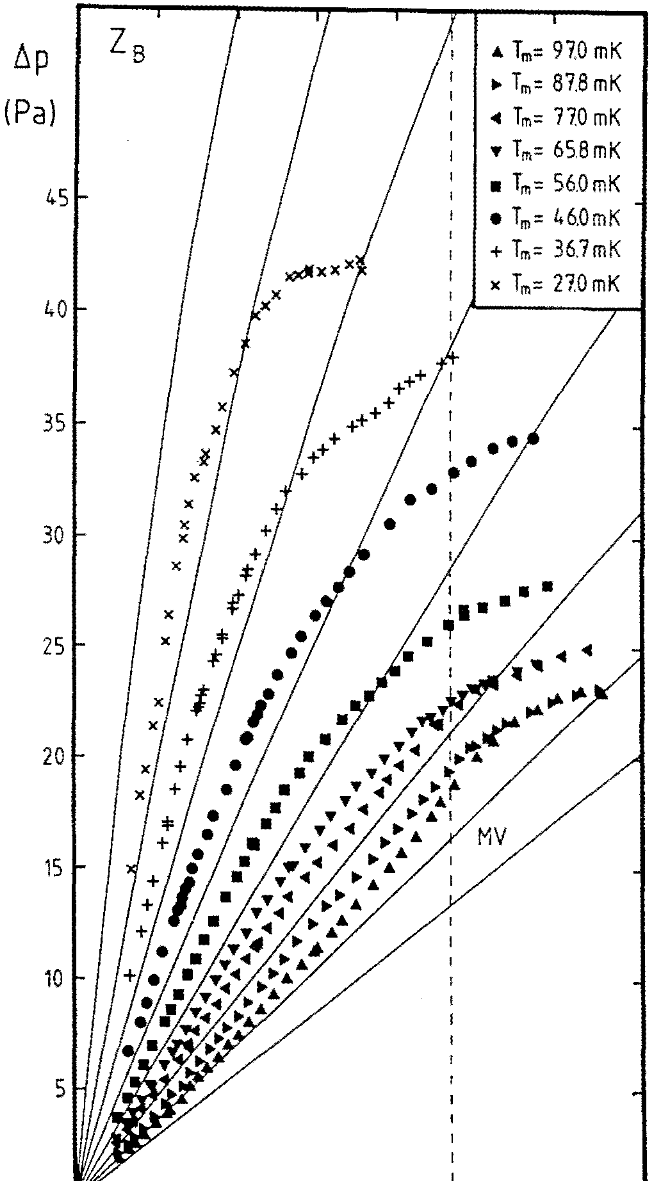

Fig.15b-e *Pressure difference measurements as a function of flow velocity. The mechanical-vacuum model behaviour is shown as calculated with equation (2.16). Mutual friction behaviour is not calculated.*

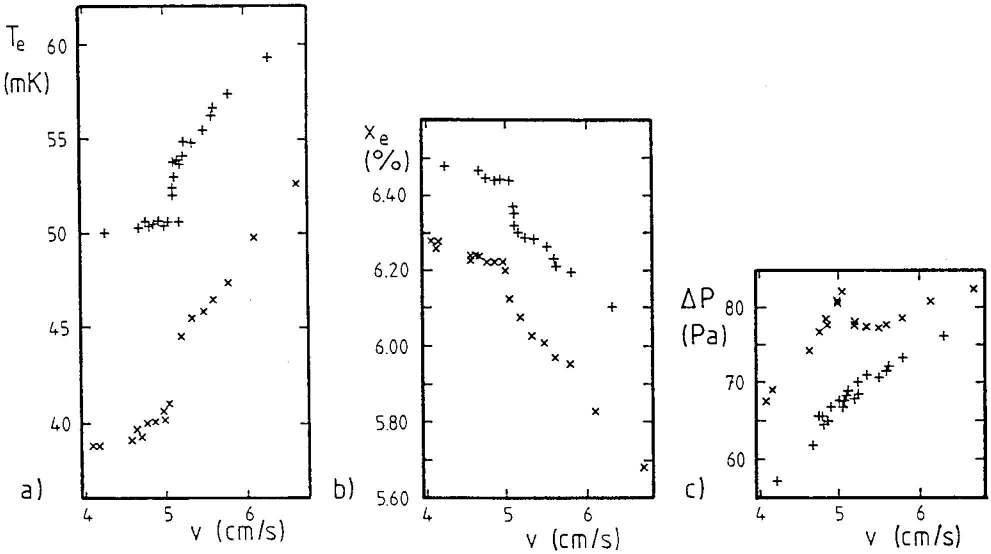

Fig.16a-c *Enlargement of temperature-, concentration and pressure difference at the transition in Fig.13b, 14b and 15b.*

reproducible. As the temperature does not change steeply at v_c no decrease of pressure can be observed here.

In figure 15d again the slit experiment is shown. As noted before there is no v_c in the sense observed in the circular tube experiments. This point will be discussed in more detail in chapter 5.

Figure 15e represents the measurements carried out at different temperatures T_m with flow impedance Z_B. At low temperatures the mechanical-vacuum model predicts a too high pressure drop and at high temperatures the reverse is the case. It is our general impression, also from the other measurements, that at about 70 mK the measurements agree accurately with the mechanical-vacuum approximation (equations (2.16-2.17)) but then at lower temperatures the pressure drops predicted by the model are too high. At higher temperatures the predicted pressure is too low. In section 7.5 this feature will be discussed.

In ^{4}He II counterflow experiments there is only a small effect on the pressure observed as the mutual friction sets in. This was first noticed by Allen and Reekie (1939) who observed the continuation of the linearity between pressure and heating power beyond the power where mutual friction sets in. The small extra pressure difference is mostly interpreted as an effect due to the superfluid turbulence. Then the excess pressure is related to the vortex line density, (Tough (1982)). Yamauchi (1985) estimated the effect theoretically taking the force between the vortex lines and the tube wall into account. He found that the excess pressure depends on the square root of the vortex line density which was in agreement with some measurements.

The existence of an excess pressure is difficult to establish in our measurements, as the viscosity, and so the pressure, depends strongly on the temperature. However, at temperatures above 80 mK the viscosity-temperature dependency becomes smaller (chapter 7). In figure 15e nearly all the curves show a decrease in slope above about 7 cm/s. However, the curves at T_m = 77 mK but especially the T_m = 87.8 mK and 97.0 mK indicate an increase in slope above v_c. This may be an indication of the superfluid turbulence excess pressure.

If the effect is to be estimated correctly from the measurements at all temperatures, the dependence of for instance the viscosity, the specific heat and V_3 on T and x has to be known accurately. Then from the measured temperature dependence the normal fluid contribution to the pressure drop can be calculated via equation (2.34) provided that a correct numerical estimation for the ^{4}He chemical potential variation can be found in the intermediate flow range. If the measured pressure difference above v_c is larger than the one calculated there is evidence for an excess pressure. The effects are small, otherwise it should have been visible in the measurements below 70 mK. It is an interesting aspect for further studies.

4.8 T^2-x DIAGRAMS

The heat exchange through the walls of the flow tube and the heat conduction through the liquid in the flow direction is negligible, and thus the flow is adiabatic. This is confirmed by a comparison of the measurements carried out in setup 7a with those of 7b which showed no differences. In figure 17a-e T_e^2 is plotted as a function of the concentration x_e. The measurements of the different flow channels are indicated and can be compared with the isenthalps, $T^2+0.20x$ = constant, equation (2.5). If the osmotic enthalpy is constant, which should be the case in these adiabatic measurements, this equation holds. In all diagrams the isenthalps with $H_3^{os} = 0$ and 0.2 J/mol are drawn according to Kuerten (1985a, 1987a). In figure 17e also the isenthalps of H_3^{os} = 0.4, 0.6 and 0.8 J/mol are shown. In figure 17e the dotted line indicates the "high dissipation limit" as mentioned by Castelijns (1986).

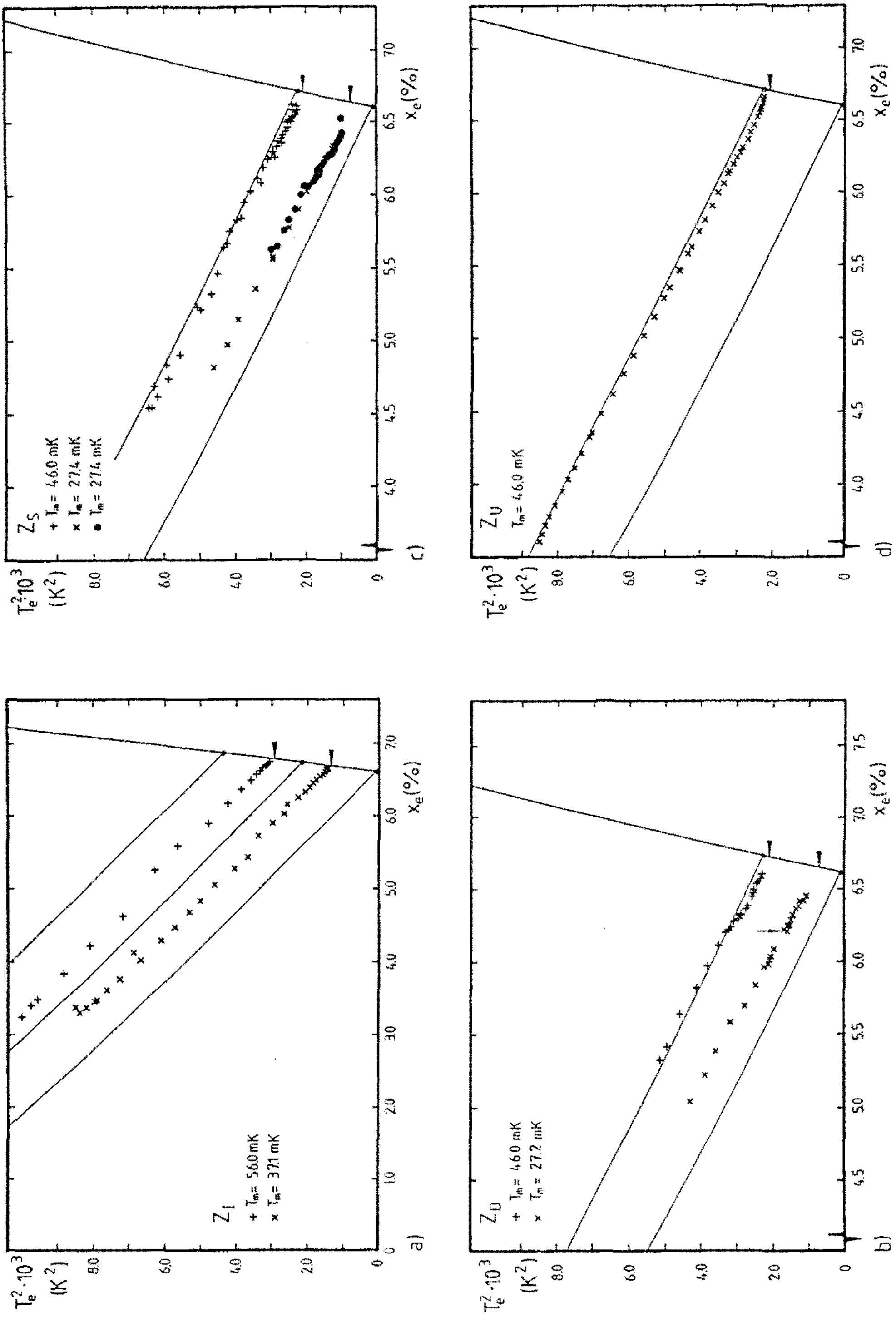
a)
Z_I
+ T_m = 56.0 mK
× T_m = 37.1 mK
T_e^2·10^3 (K^2)
x_e(%)
0
2.0
4.0
6.0
8.0
1.0
2.0
3.0
4.0
5.0
6.0
7.0
b)
Z_D
+ T_m = 46.0 mK
× T_m = 27.2 mK
T_e^2·10^3 (K^2)
x_e(%)
4.5
5.0
5.5
6.0
6.5
7.0
7.5
c)
Z_S
+ T_m = 46.0 mK
× T_m = 27.4 mK
● T_m = 27.4 mK
T_e^2·10^3 (K^2)
x_e(%)
4.0
4.5
5.0
5.5
6.0
6.5
7.0
d)
Z_U
T_m = 46.0 mK
T_e^2·10^3 (K^2)
x_e(%)

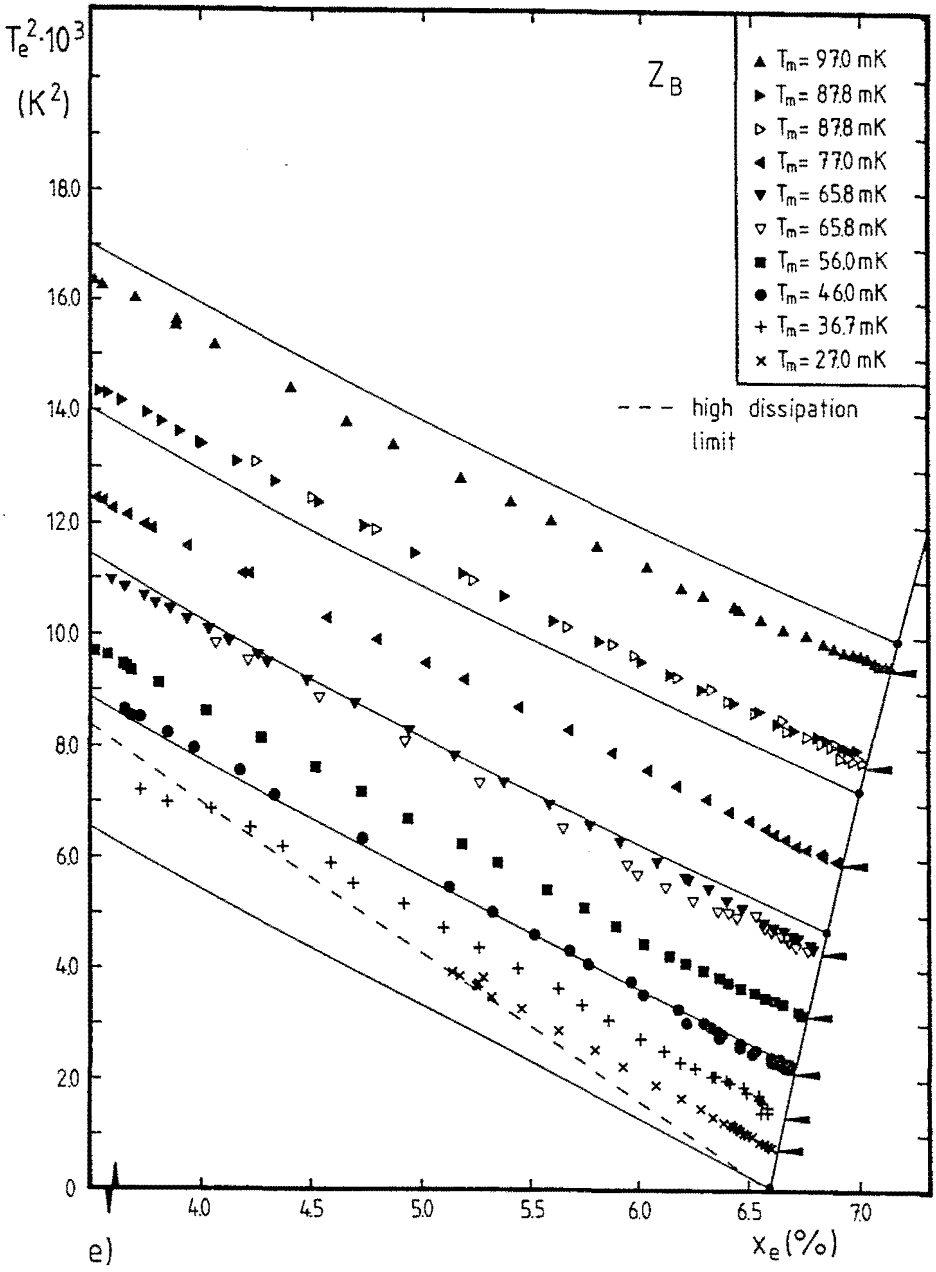

Fig.17a–e *T^2–x diagrams of the measurements as presented in the figures 13–15. Curves of constant enthalpy are also drawn. The line on the right hand side of the diagrams represents the phase separation line. The arrows indicate T_m^2 at the phase separation line.*

Within experimental error the measurements are in agreement with equation (2.5) whether mutual friction plays a role or not. At v_c -in figure 17b indicated by an arrow- a jump occurs along the isenthalp. The measurements give no indication of deviation from the isenthalp. They confirm that adiabatic conditions hold below and above the transition. Figure 17e shows that this is also valid at higher temperatures.

4.9 THE ^{4}He CHEMICAL-POTENTIAL DIFFERENCE.

Figure 18a shows the ^{4}He chemical-potential difference calculated as described in section 3.2.4 for the data of impedance Z_I. The third-power dependence of the mutual friction according to equation (2.21) is also shown. No pressure difference was measured in this experiment. The chemical potential was calculated assuming $\Delta p=0$. The effect of the pressure is rather small (Kuerten (1985a, 1987a)). The model is in good agreement with the measurements.

Figure 18b shows $\Delta\mu_4$ in the critical velocity region. For 0<v<5.22 cm/s, $\Delta\mu_4 = 0$ within the experimental error. The finite values of $\Delta\mu_4$ at $v<v_c$ are caused presumably by the inaccuracy in the determination of the concentration. An uncertainty of 0.05 % leads to an error of about 0.5 mJ/mol. At about 5.22 cm/s a rather steep increase occurs. As can be expected the agreement with equation (2.21) is rather poor because this equation only holds in the high velocity regime.

Figure 18c shows the more gradual behaviour as found with the glass capillaries. Again a non-zero offset appears for low velocities.

In figure 18d the measurement with the annular flow channel is shown. There is a good correspondence with the mutual-friction model. Referring to figure 18a, the good agreement with the mutual-friction model could be seen as an argument that the critical velocity lies well below the detection limit. This tentative conclusion will be discussed in chapter 5.

Figure 18e shows the measurement at the different T_m values. For clarity the data points corresponding with the different mixing chamber temperatures have been shifted by 2 mJ/mol. If the measurements are not shifted then they coincide within error which means that $\Delta\mu_4$ is independent of T_m.

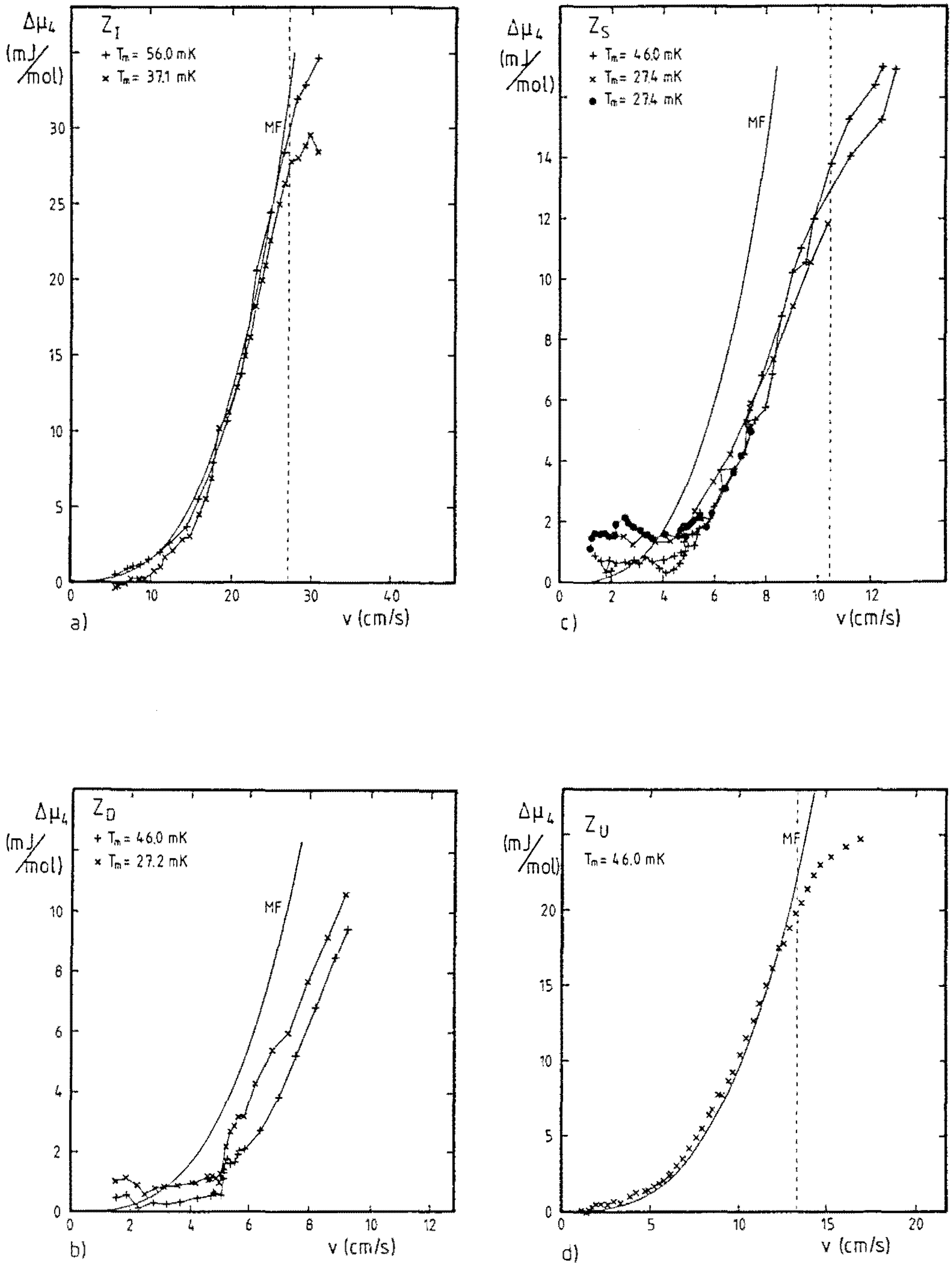
Δμ₄ (mJ/mol)
Z_I
+ Tₘ = 56.0 mK
× Tₘ = 37.1 mK
MF
0 5 10 15 20 25 30
0 10 20 30 40
a)
v (cm/s)
Δμ₄ (mJ/mol)
Z_S
+ Tₘ = 46.0 mK
× Tₘ = 27.4 mK
● Tₘ = 27.4 mK
MF
0 2 4 6 8 10 12 14
0 2 4 6 8 10 12
c)
v (cm/s)
Δμ₄ (mJ/mol)
Z_D
+ Tₘ = 46.0 mK
× Tₘ = 27.2 mK
MF
0 2 4 6 8 10
0 2 4 6 8 10 12
b)
v (cm/s)
Δμ₄ (mJ/mol)
Z_U
Tₘ = 46.0 mK
MF
0 5 10 15 20
0 5 10 15 20
d)
v (cm/s)

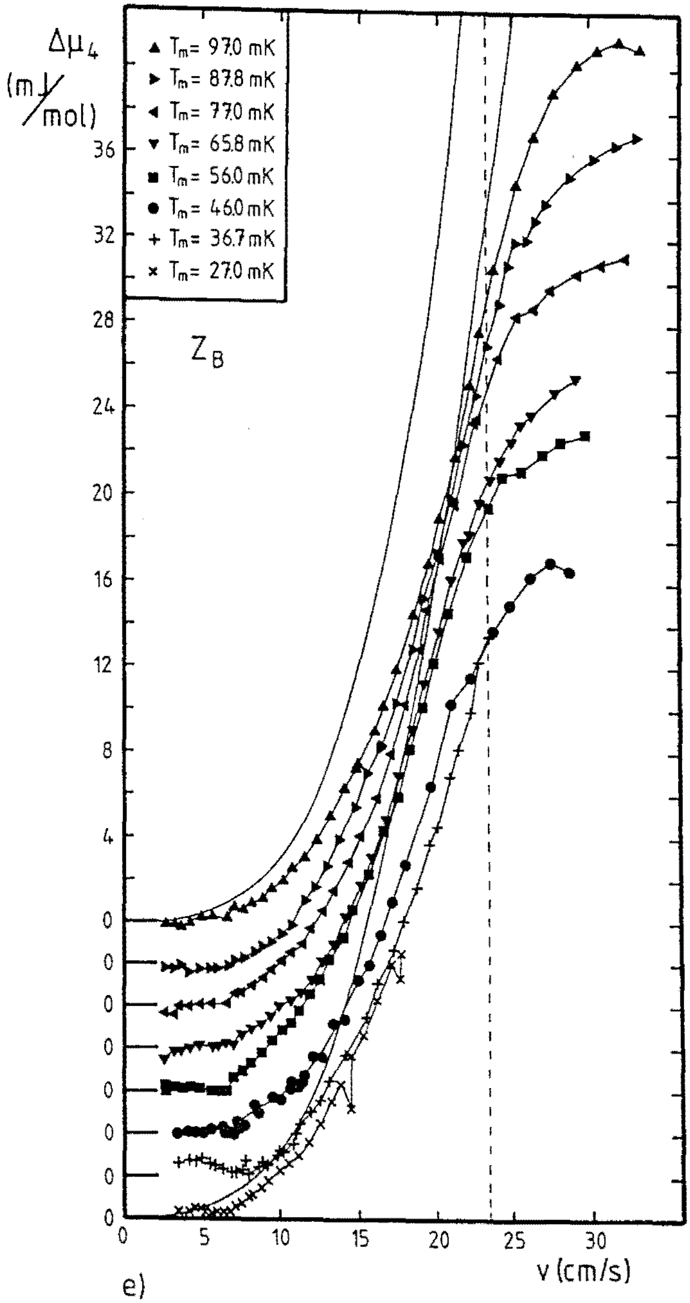

Fig.18a-e *Chemical-potential difference as a function of the flow velocity in the five different flow impedances.* $\Delta\mu_4$ *calculated with equation (2.21) is also shown.*

4.10 CONCLUSION.

There exists a critical velocity above which mutual friction appears. This is clearly shown in all measurements with circular tubes. Experiments with annular tubes do not show an abrupt change of the measured quantities. This behaviour is in general agreement with the observations in counterflow in ^{4}He II.

For low velocities $v<v_c$ the mechanical-vacuum model predicts the correct behaviour apart from deviations of the viscosity coefficient from the assumed $5\cdot10^{-8}/T^2$ dependence and the influence of the dependency of V_3 on the concentration. For high velocities $v \gg v_c$ the mutual-friction model is confirmed by our measurements. For velocities in the intermediate region the simple mutual-friction model is not correct.

The osmotic enthalpy is conserved in the flow channel thus the flow is adiabatic.

The measurements with Z_B show an indication of a second critical velocity which will be confirmed by the measurement of pressure fluctuations and are discussed in chapter 6. A comparison with related work in ^{4}He II, in particular concerning the critical velocity will be given in the next chapter.

CHAPTER 5

THE OBSERVATION OF THE CRITICAL VELOCITY AND VORTEX LINE DENSITIES

5.1 INTRODUCTION.

In this chapter a closer look is taken at the transition region between laminar and turbulent flow. The critical velocities in circular and annular flow channels are compared with each other and with results obtained in pure ^{4}He II. The vortex line density L of the turbulent flow state is calculated under the assumption that the vortex tangles are isentropic. This vortex line density plays an important role in the Vinen model, which describes the generation and decay of vortices in the superfluid component. A comparison of the results from circular and annular tubes with the predictions of the Vinen model is made.

Section 5.2 discusses the transition as it is observed in our measurements in circular flow channels as well as in annular flow channels. The vortex line density is calculated in section 5.3. The Vinen model of generation and decay of a vortex tangle and its application is discussed in section 5.4. In section 5.5 the value of the critical velocity is discussed for the circular and the annular flow channels. In section 5.6 a short survey is presented discussing the different aspects related with critical velocities, effects of ^{3}He on vortices and related work in ^{3}He-^{4}He II mixtures. In section 5.7 a comparison is made of our results on mixtures with results on pure ^{4}He II. Section 5.8 concludes this chapter.

5.2 THE TRANSITION.

5.2.1 CIRCULAR TUBES.

Most of the measurements were carried out decreasing the flow rate from high to low values. During the first experiments with metal tubes the transition region was explored in detail, varying the flow up and down. When the velocity was increased very slowly from below to above v_c, the critical velocity was the same as in case it was decreased from above to below. Only once there was an indication for hysteresis with d=0.15 mm capillaries (impedance Z_L).

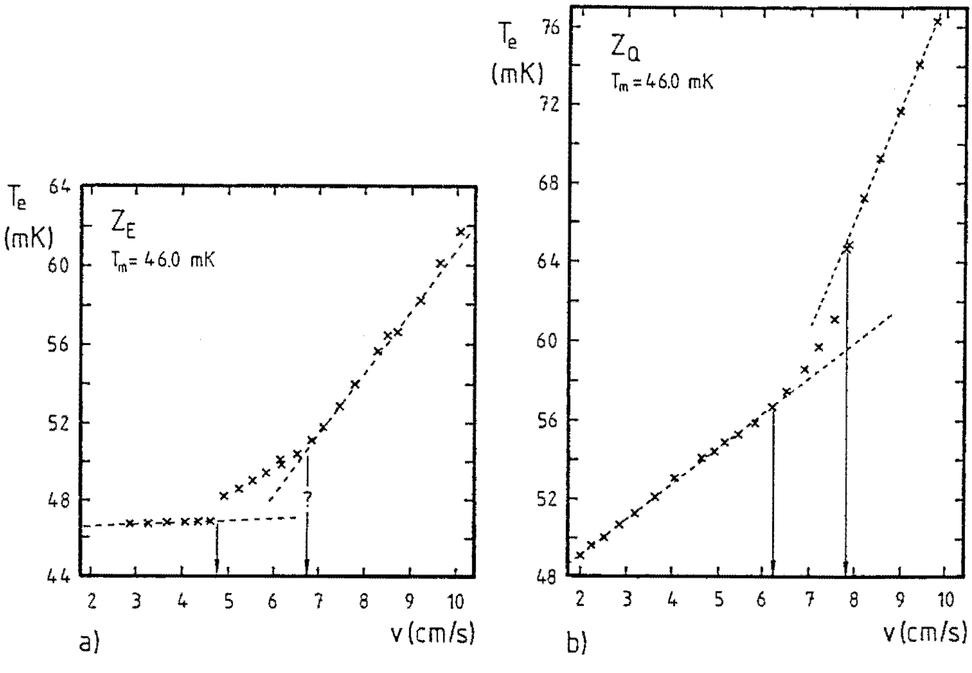

Fig.19 *Typical transitions in the temperature-velocity diagram for two different tubes (only the results of temperature measurements are given) indications of possible* v_{c1} *and* v_{c2} *are given.*
a *Typical transition in metal tubes, e.g.* Z_E.
b *Glass tube,* Z_Q.

In all the measurements with metal tubes the transition showed a discontinuity in the measured quantity (figure 16 and 19a). There are also indications of the presence of a second critical velocity. This is illustrated in figure 19a where, for velocities just above the critical value the temperature rises linearly with v. However, at a velocity of about 6.5 cm/s the temperature rise becomes steeper. This can also be seen in figure 13e, in the low temperature measurements at about 12 cm/s. It is also observed in the pressure and concentration data. However, such an indication does not show up in all measurements and one has to be acquainted with the effect to recognize it. More evidence for a second v_c was obtained from analysis of the pressure fluctuations in wide tubes. We will come back to this in chapter 6.

With glass tubes the situation is slightly different (figure 19b). A typical result is also given in figure 13b. The characteristic jump in temperature is absent. A gradual deviation from the mechanical vacuum model is observed and then at some higher velocity we have the impression that a steep change in temperature occurs.

With the small diameter glass capillaries it was difficult to produce bundles with capillaries of equal diameter. Generally the variations in d amount to 10–15%. For the glass tubes of diameter 0.29 mm the diameter variations are smaller (smaller than 3%).

At first sight, since the critical velocity of a tube depends on its diameter, one may expect a smeared out transition and hysteretic behaviour when a distribution of tube diameters is present in the bundle. On the other hand the transition may be sharp even in the case of a distribution of diameters. We can give an idea of the phenomena which occur when a bundle of capillaries with a diameter distribution becomes "critical". For small flow rates the ^{3}He flow divides itself according to the condition of equal Poiseuille pressure difference:

$$\dot{n}_{3i} = -\frac{\Delta p}{\eta V_3}\frac{1}{\ell_i \zeta_i} = \frac{A_i}{V_3} v_{3i} \,. \tag{5.1}$$

When the critical velocity in one of the capillaries (capillary 1) is reached the ratio of distribution is maintained but in this capillary more and more ^{4}He is dragged along with the ^{3}He, which flows back through the other capillaries with such a velocity that:

$$\oint_{i,j} v_s d\ell = 0 \qquad\qquad i\neq 1,\ j\neq 1 \tag{5.2}$$

but,

$$\oint_{1,k} v_s d\ell = N\kappa \,, \tag{5.3}$$

where N is independent of k. This circulation slips in, quantum after quantum. This leads to discrete changes in the flow state. When the flow rate is increased and the critical velocity in a second capillary (2) is attained, circulation slips into this capillary too. This process will continue until the last capillary has become "critical". If the flow rate is increased any further a nonzero ^{4}He-chemical potential appears due to the continuous generation and decay of a quantized vortex tangle. If a linear critical velocity criterion is assumed to hold in the form:

$$(v_3-v_4)_c d = W_c\ , \tag{5.4}$$

it can be shown straightforwardly that:

$$\dot{n}_{3c}{}^{max} = \sum_i \dot{n}_{3ic}\ . \tag{5.5}$$

So the total critical flow rate through the impedance is equal to the summation of critical flows through the N independent capillaries. This is due to the linearity of equation (5.4). In the case of a nonlinear critical flow rate dependency on the diameter only the final relation (5.5) will have to be revised. Finally the whole flow impedance is critical and as the transitions in the capillaries occur unambiguously no hysteresis is to be expected.

5.2.2 MEASUREMENTS WITH ANNULAR CHANNELS.

In all our measurements with mixtures in annular channels a gradual deviation from the laminar flow regime was observed and v_c was difficult to determine (figure 13d). In order to resolve this behaviour in more detail an experiment was carried out with a flow channel with the same cross section as Z_U but much longer and with three tubes in parallel (Z_Y in table 3).

The results of this experiment are presented in figure 20a-d. At about 2.5 cm/s the difference with the mechanical-vacuum behaviour is observed. In the $\Delta\mu_4$ diagram there is a gradual increase from zero (figure 20d).† It is, however, difficult to speak of a well defined critical velocity. One gets the impression that the real critical velocity can even be much smaller than the velocity where the measured quantities begin to deviate significantly from the MV model. The latter is mainly determined by the resolution of the measurement of the temperature. The difference of v_{ca} between Z_U and Z_Y shows the dependence on measuring accuracy. The apparent critical velocities (v_{ca}) as derived

---

† There is some doubt whether the measured pressure differences for velocities above about 2 cm/s are correct. For these correspondingly high pressure differences the pressure transducer was not calibrated and we suspect that in this range it is not justified to extrapolate the pressure cell calibration. This means that the calculated $\Delta\mu_4$ is too large. However, this does not change our point of view with respect to the apparent critical velocity.

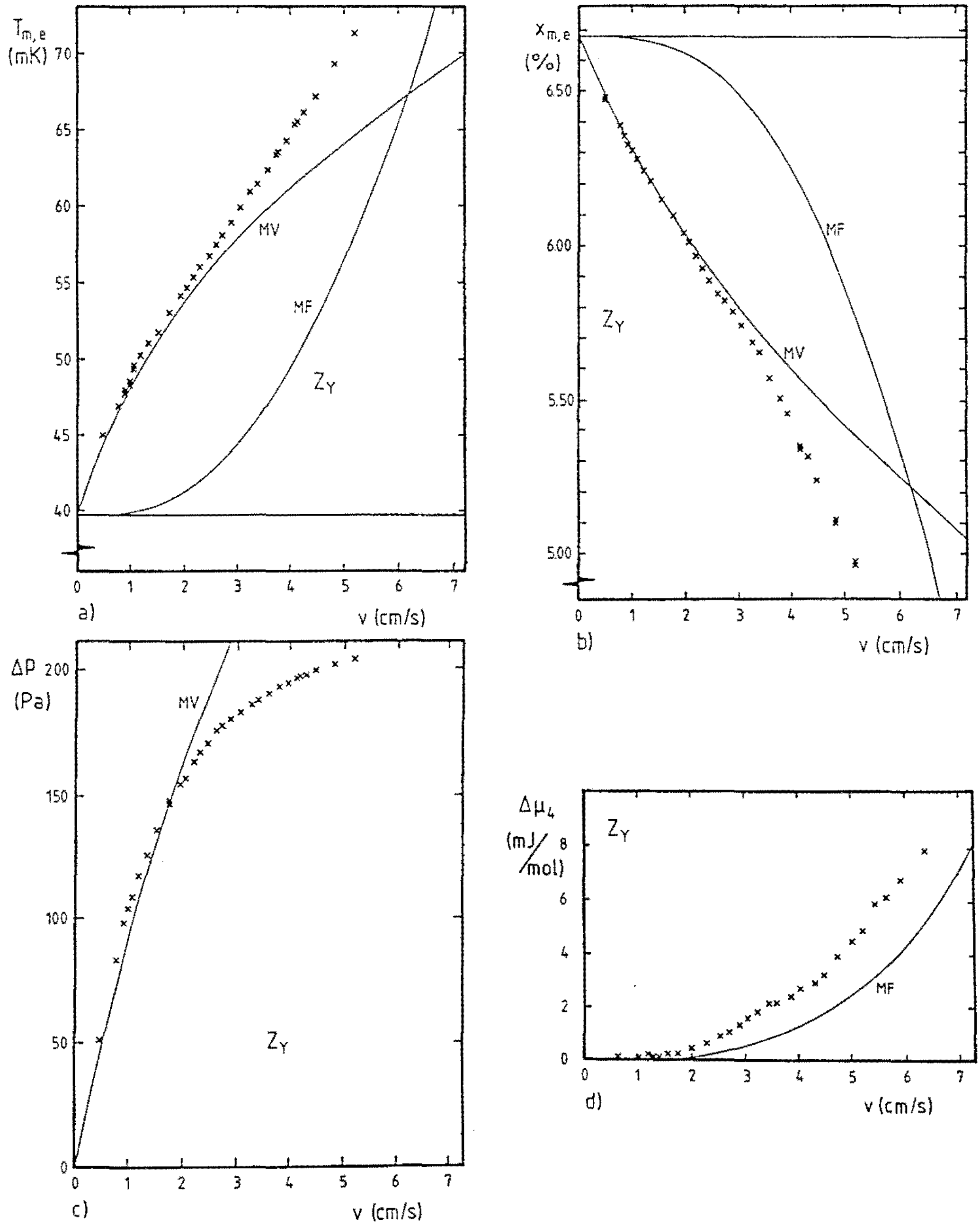

Fig.20 *The flow properties as measured with the flow channel Z_Y. The measurements were carried out at T_m=39.7 mK. The mutual friction (MF) and mechanical vacuum (MV) models are shown.*
a) T_e-v dependence, b) x_e-v dependence, c) Δp-v dependence, d) $\Delta\mu_4$-v dependence.

from the position of deviation from the mechanical vacuum model are indicated between brackets in table 3. At the high velocity range in the graph the data tend to approach asymptotically to the highly turbulent flow solution. A more detailed discussion of the critical velocity of annular channels will be given in section 5.5.2.‡

The difference of the critical velocity in circular and annular tubes can also be shown from pressure fluctuations. In circular tubes there is a change in fluctuation amplitude at v_c; in annular tubes no amplitude change is observed at v_{ca}. This will be discussed in more detail in chapter 6.

5.3 VORTEX LINE DENSITIES.

The vortex line density will now be calculated as a function of the flow velocity from the data by means of the equations (1.6) and (1.7). For ^{4}He II the basic parameters, for instance B, are known from second sound experiments (Tough (1982), Barenghi (1982b, 1983a) and Swanson (1985a,b)). For mixtures the determination of L is not possible as B is not known. Therefore $\sqrt{BL}$ is calculated as a function of the flow velocity using (1.6), (1.7) and the chemical potential data. The following values are used: $\rho = 140$ kg/m^3, $\rho_n = \rho_3 m^*/m_3 \simeq 17.71$ kg/m^3 and $m^*/m_3 = 2.46$ (Kuerten (1985a, 1987a)).

In figure 21a-e results are shown for the five flow impedances also presented by figures 13-18.

Below the critical velocity no data points are of course presented. The measured small values of $\Delta\mu_4$ usually obtained below v_c (figure 18), are attributed to errors in the concentration x. The data were corrected for this error by means of a small zero shift.

Fig.21a shows the results of one short 1.2 mm diameter capillary (Z_I). A high vortex line density was attained. No critical velocity was observed. The critical velocity can be estimated to be about 1.3 cm/s from the relation of $v_c d = 15$ mm^2/s (see figure 25). The straight line starting at the origin (which is shown in all graphs) is drawn

---

‡ Due to the large length of the tubes large concentration differences occur and thus the mechanical-vacuum model under the assumption that V_3 and C_0 are constant, is not correct anymore. If the concentration dependencies in these quantities is taken into account, an analitical expression for the quantities T, x and p can still be given. This leads to a better agreement with the measured quantities, however, the dependence of the viscosity with x needs to be accounted for too.

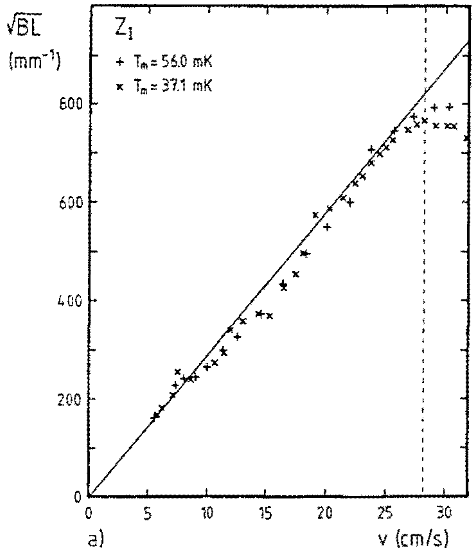
√BL
(mm⁻¹)
Z_I
+ T_m = 56.0 mK
× T_m = 37.1 mK
0
200
400
600
800
0
5
10
15
20
25
30
a)
v (cm/s)

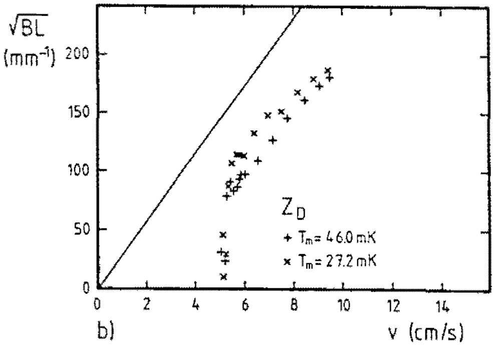
√BL
(mm⁻¹)
Z_D
+ T_m = 46.0 mK
× T_m = 27.2 mK
0
50
100
150
200
0
2
4
6
8
10
12
14
b)
v (cm/s)

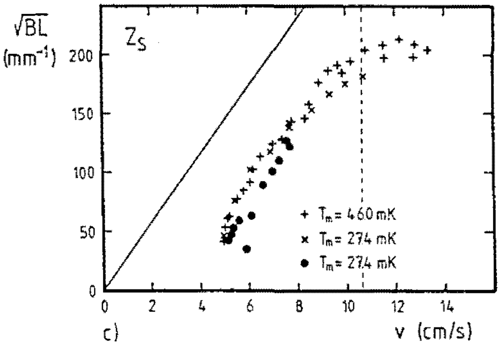
√BL
(mm⁻¹)
Z_S
+ T_m = 46.0 mK
× T_m = 27.4 mK
● T_m = 27.4 mK
0
50
100
150
200
0
2
4
6
8
10
12
14
c)
v (cm/s)

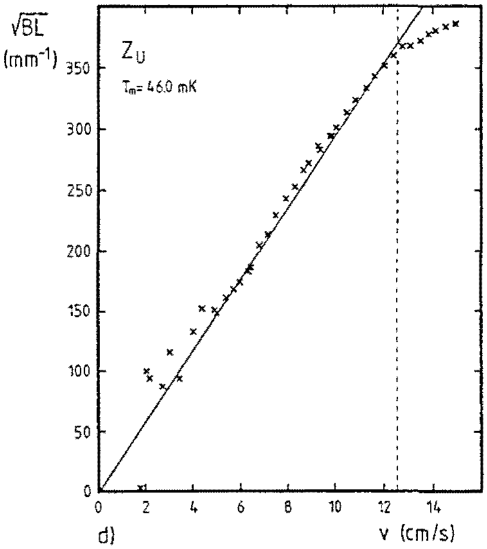
√BL
(mm⁻¹)
Z_U
T_m = 46.0 mK
0
50
100
150
200
250
300
350
0
2
4
6
8
10
12
14
d)
v (cm/s)

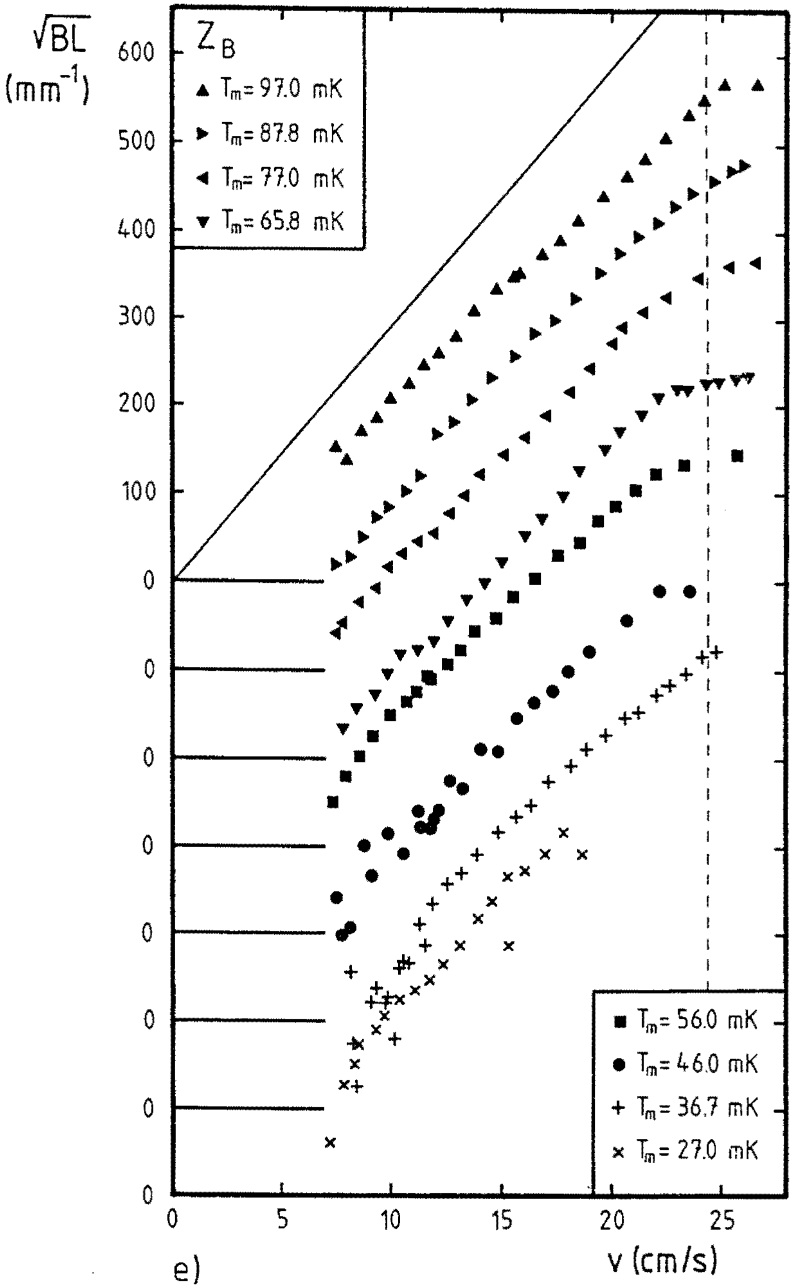

Fig.21a–e *Vortex line densities $\sqrt{BL}$ as a function of the flow velocity. In figure e the different curves have been shifted to get a better representation of the results. The lines through the origin are explained in the text.*

based on the highly turbulent flow solution and is obtained by using equation (1.6) and (1.7) in combination with equation (2.21). There is good agreement with the measurements as would be expected on the basis of chapter 4.

The figures 21b and c show the critical velocity.

In figure 21d all measured points are presented. At low velocities scatter in $\sqrt{BL}$ can be seen due to the small systematic errors as mentioned above. A critical velocity cannot be seen. The resemblance with figure 21a is striking. This strongly suggests that the fluid in the annular tube was in the high vortex line density region ($v \gg v_c$), which is in agreement with results from thermal counterflow experiments in high aspect ratio rectangular channels as carried out by Tough (1982).

From figure 21e it can be seen that the slope of the graphs is the same for all curves. The values of the data at T_m=56 mK are somewhat larger than those measured at the other temperatures. Perhaps this is due to an incorrect zero of the concentration capacitance. An error of 0.01 % gives a difference in $\sqrt{BL}$ of 15 mm^{-1}.

The order of magnitude of $\sqrt{BL}$ is the same as the results of Mudde (1989, 1990), see section 5.6.3.

5.4 THE VINEN MODEL AND ITS APPLICATION.

5.4.1 THE MODEL.

The vortex line density L is the important quantity in the description of mutual friction. Hall (1957a,b) and Vinen (1957a.b,c,d) proposed a model describing the evolution of a vortex tangle as a function of time during the transition to steady thermal counterflow in ^{4}He II. Two terms are important:

1) Average vortex line creation rate per unit of volume:

$$\dot{L}_{cr} = \chi_1' L^{3/2} v (1 - A'/A), \tag{5.6}$$

where the dimensionless parameter χ' is defined as:

$$\chi_1' = \frac{B \rho_n \chi_1}{2\rho} \tag{5.7}$$

and χ_1 = constant of order unity
B = Hall-Vinen parameter
A = cross-sectional area of the flow channel
A' = cross-sectional area of a boundary layer
v = counterflow velocity $|\vec{v}_n - \vec{v}_s|$.

The term between brackets takes into account that in a boundary layer near the wall no vortex line creation occurs. The thickness of this boundary layer is assumed to be of the order of the average vortex spacing, i.e. $\delta/2\sqrt{L}$ with δ a constant of order unity and d is the tube diameter or slit spacing. When the vortex spacing becomes so large that,

$$\sqrt{L} > \delta/d, \tag{5.8}$$

the model becomes meaningless.

2) The annihilation rate of vorticity per unit of volume:

$$\dot{L}_{an} = - \chi_2' L^2 \tag{5.9}$$

where $\chi_2' = \frac{\kappa}{2\pi} \chi_2 \ (m^2 s^{-1})$ (5.10)

and χ_2 = constant of order unity.

The summation of the equations (5.6) and (5.9) leads to the equation describing the evolution of the vortex line length:

$$\dot{L} = (\dot{L}_{cr} + \dot{L}_{an}) = \chi_1' L^{3/2} v(1-A'/A) - \chi_2' L^2 \tag{5.11}$$

Now three situations may be considered:
A Infinite liquid without walls (or high vortex line density situation),
B Parallel plate geometry,
C Circular tube geometry.

A Infinite liquid without walls.

As there are no walls the basic equation is determined by the condition that $A'/A = 0$. In the stationary state $\dot{L} = 0$ this yields L=0 and:

$$L_0 = \gamma^2 v^2. \tag{5.12}$$

where $\gamma = \chi_1'/\chi_2'$. (5.13)

B Parallel plate geometry.

This geometry represents the annular flow channels in this research, as in our situation $d \ll D$. Now equation (5.11) becomes:

$$\dot{L} = \chi_1' L^{3/2}\, v \left[1 - \frac{\delta}{d\sqrt{L}}\right] - \chi_2' L^2 . \tag{5.14}$$

Now one can introduce the dimensionless parameters x, w and τ defined by:

$$x = dL^{1/2}/\delta \tag{5.15}$$

$$w = \gamma v d/\delta. \tag{5.16}$$

$$\tau = \chi_2' \delta^2 t/2d^2 = t/t_0 . \tag{5.17}$$

The parameter $x\delta$ represents the number of vortex spacings in between the plates. The velocity is reduced by $\delta/\gamma d$, a velocity which will turn out to be closely related to the critical velocity of the flow channel. The characteristic time t_0 is determined by the width d of the flow channel.

Using (5.15), (5.16) and (5.17) in (5.14) leads to:

$$\frac{dx}{d\tau} = wx(x-1) - x^3. \tag{5.18}$$

In the stationary situation the solutions for x are:

$$x_1 = 0 \text{ or } x_{2,3} = \frac{w \pm \sqrt{w^2 - 4w}}{2} . \tag{5.19}$$

Nonzero solutions thus only exist for $w \geq 4$, what according to equation (5.16) corresponds to a critical velocity:

$$v_c = \frac{4\delta}{\gamma d} . \tag{5.20}$$

The corresponding critical line density follows as

$$L_c^{1/2} = 2\delta/d . \tag{5.21}$$

C Circular tube geometry.

For a tube of diameter d equation (5.11) leads to:

$$\dot{L} = \chi_1' L^{3/2} v \left[1 - \frac{\delta}{d\sqrt{L}}\right]^2 - \chi_2' L^2 , \tag{5.22}$$

which in the reduced units becomes:

$$\frac{dx}{d\tau} = w(x-1)^2-x^3 \tag{5.23}$$

where $x\delta$ now counts the number of vortex spacings (that fit) on a diameter of the tube. The steady solutions for given w are now the roots of the cubic equation:

$$x^3 - w(x-1)^2 = 0 \ . \tag{5.24}$$

Practical solutions in this case only exist for $w \geq 6.75$, which leads to a critical velocity:

$$v_c = \frac{6.75 \cdot \delta}{\gamma d} \ . \tag{5.25}$$

The corresponding critical solution $x_c = 3$, which leads to a critical vortex line density,

$$L_c^{1/2} = \delta x_c/d = 3\delta/d \ . \tag{5.26}$$

The infinite liquid situation, case A, can also be interpreted in terms of x and w and leads to a solution of the type $x = w$.

Now the different geometries will be discussed by means of a presentation in the form of graphs. In figure 22a and b a diagram is shown where $dx/d\tau$ ($\equiv \dot{x}$) is plotted as a function of x for different constant values of w.

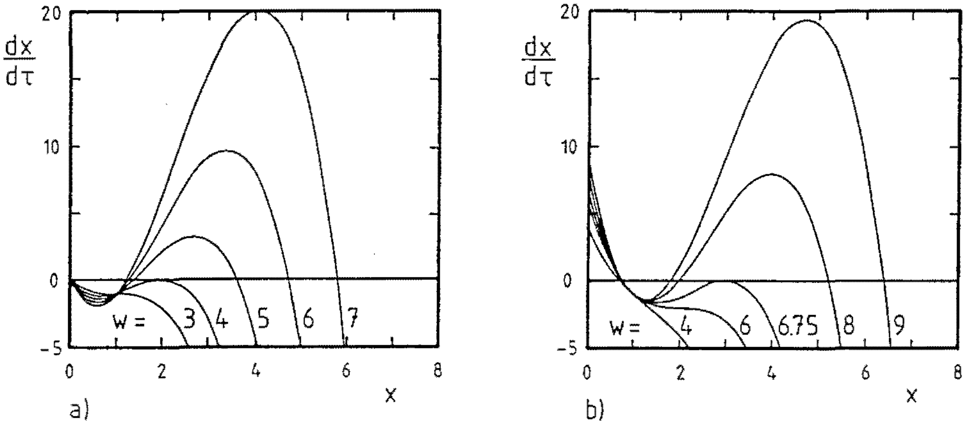

Fig.22 Plots of $\dot{x}$ versus x for different constant w values as indicated in the diagram. a) Annular tube geometry. b) Circular tube geometry.

In case $x<1$ the solutions do not satisfy the condition (5.8) and are therefore physically not of interest, although the stable solution for $x<1$ for circular tubes is drawn in figure 23.

For $x>1$ the figures for an annular or circular tube geometry are qualitatively the

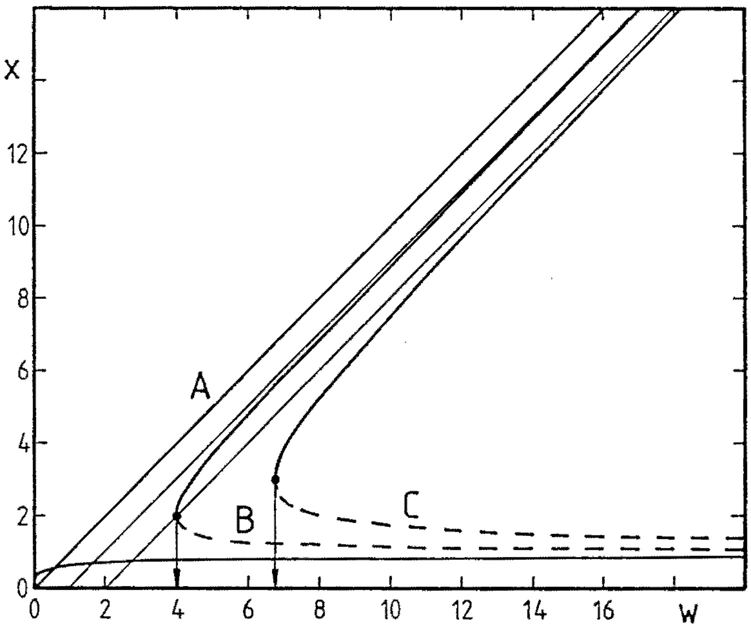

Fig.23 *The three different solutions of Vinen's equation. The parameter x is shown as a function of w. The infinite liquid situation is represented by the straight line through the origin (solution A), the solutions of the parallel plate and circular tube system are shown by B and C respectively. The other two straight lines are their asymptotes. Full curves represent the stable branch of the solutions and the dashed curves the unstable branch.*

same. In the case of the annular tube for w values smaller than 4 and in case of the circular flow tube for w values smaller than 6.75 there are no stable points.

For $w = 4$ and $w = 6.75$ in the annular and circular tube geometry respectively, $\dot{x}$ becomes zero for $x = 2$ and $x = 3$ respectively. These are marginal stable points because $d\dot{x}/dx = 0$. These points represent the critical velocity as was discussed above with cases B and C, as summarized:

Annular tube $\quad x_c = 2 \quad (dL_c^{1/2} = 2\delta)$

$$w_c = 4 \qquad (v_c d = 4\delta/\gamma) \tag{5.27}$$

Circular tube $\quad x_c = 3 \quad (dL_c^{1/2} = 3\delta)$

$$w_c = 6.75 \qquad (v_c d = 6.75\delta/\gamma)\ . \tag{5.28}$$

For $w>w_c$ two intersections occur with the $\dot{x} = 0$ axis. The first crossing occurs with a positive slope. This means that these solutions are unstable. The second crossing occurs with a negative slope. These are the stable solutions. From figure 22 it can be seen that the higher the flow the larger the slope and the more stable the solution is. By linearizing the equation (5.11) without the boundary term on substituting $L = L_0+\Delta L$, where L_0 is the stable solution, a characteristic time τ_0 of the order $(\chi_2' L_0)^{-1}$ is obtained, see De Goeje (1985, 1986). The higher the vortex line density the smaller the characteristic time. Calculation of the slopes of the production rates of equation (5.11) yields for the stable states of the infinite liquid the value $(\chi_2' L_0/2)^{-1}$ which is indeed the intrinsic relaxation time of the vortex tangle.

The solutions of the equations (5.19) and (5.24) are drawn with their asymptotes in figure 23. The full curves are the stable solutions and the unstable solutions correspond with the dashed part of the curve. The critical condition w_c occurs at $dw/dx=0$.

For high velocities all the solutions tend to the same $\dot{L}_0 \sim v_3^2$ behaviour, which occurs always in the infinite liquid situation. This behaviour can also be understood using dimensional analysis in the equation of the motion of the vortex lines. This analysis was carried out in Kuerten (1987a) and Schwarz (1988).

The experimental curves of figure 21 show a remarkable resemblance with the ones of figure 23, suggesting that the Vinen model may also be applicable in our case of mixtures. A more detailed, quantitative comparison will be presented in the next section. Here we like to point out that just beyond the critical velocity the vortex line densities of the Vinen model are very small, the total length of vortex line per unit length of flow tube, $L_c d^2$, being 4m, respectively 9m, for channel types B and C. Consequently the intrinsic relaxation time is of the order of one second. The occurrence of the observed low frequency fluctuations therefore seems plausible. We also like to point out that the Vinen model has a statistical basis and in the critical velocity region vortex line densities are small. Also on these grounds large fluctuations must be expected. This can mean that the statistical Vinen approach is probably not applicable. In this velocity region numerical calculations may give more appropriate information (Schwarz (1990)).

The equation (5.18) is the description according to Vinen (1957c) for the x production rate of plane parallel plates. The same equation was also used at Ohio State University (Childers (1973, 1974, 1976)). However, for circular tubes the equation (5.23) has to be used instead.

Although Vinen's theory is based on dimensional arguments there is more evidence for it. Schwarz (1977, 1978) showed that the model may be derived from his equations of the vortex dynamics. Geurst (1989) showed that Vinen's equation can be derived if one considers the energy and impulse of the vortex lines. He proposes a new interpretation for the production and annihilation terms of the equation based on a "generalized force", μ_1, which is derived from a potential energy.

Vinen assumes isotropy and homogeneity of the vortex tangle. If anisotropy has influence it could mean that for instance in equation (1.6) the term 2/3 has to be modified. If the vortex line density is nonhomogeneous, extra gradient dependent terms appear in the equation (Van Beelen (1988)). In this way also nonuniform flow states can be described.

5.4.2 COMPARISON OF OUR DATA WITH THE VINEN MODEL.

Vinen's model as discussed in the section above will now be applied to our data in terms of the parameters x and w, section 5.4.1. This procedure may be carried out in two ways. The first is a fitting technique and in the second method use is made of the critical velocity. Only the first method will be presented. The second technique will be discussed briefly but will not be applied.

The scale of the parameter x can be calculated if use is made of the equations (1.6), (1.7) and (5.15) and yielding:

$$\mathrm{x} \equiv \mathrm{k}\left[\frac{\Delta\mu}{\ell \mathrm{v}}\right]^{\frac{1}{2}}\mathrm{d}, \tag{5.29}$$

where k is a factor given by the expression:

$$\mathrm{k} \equiv \frac{1}{\delta}\left[\frac{3\rho}{\mathrm{B}\rho_\mathrm{n}\rho_\mathrm{s}\mathrm{V}_4\kappa}\right]^{\frac{1}{2}}. \tag{5.30}$$

In this equation V_4 is the molar ^{4}He volume in the mixture. Now we define:

$$\alpha \equiv \mathrm{k}\delta/\gamma. \tag{5.31}$$

The expressions (5.29) and (5.16) are substituted in the equations (5.19) and (5.24). This yields for the annular tube geometry if we use (5.31):

$$\mathrm{vd} = \alpha\,\frac{\left[\left[\frac{\Delta\mu_4}{\ell \mathrm{v}}\right]^{\frac{1}{2}}\mathrm{d}\right]^2}{\left[\frac{\Delta\mu_4}{\ell \mathrm{v}}\right]^{\frac{1}{2}}\mathrm{d} - \frac{1}{\mathrm{k}}}, \tag{5.32}$$

and for the circular tube geometry:

$$\mathrm{vd} = \alpha \frac{\left[\left[\frac{\Delta\mu_4}{\ell \mathrm{v}}\right]^{\frac{1}{2}} \mathrm{d}\right]^3}{\left[\left[\frac{\Delta\mu_4}{\ell \mathrm{v}}\right]^{\frac{1}{2}} \mathrm{d} - \frac{1}{\mathrm{k}}\right]^2} . \tag{5.33}$$

Now the procedure consists of plotting the experimental data in a graph with abscissa vd and ordinate $\mathrm{d}\sqrt{\Delta\mu_4/\ell \mathrm{v}}$. A fitting procedure is applied in order that the Vinen model corresponds to the best as possible with the measurement. This means that k and α (or γ/δ) are determined. However, γ and δ and thus χ_1, χ_2 and B cannot be determined separately.[†*]

We will now discuss briefly the second technique as was mentioned at the beginning of the discussion. This technique uses equation (5.29) and the Gorter Mellink relationship (2.21). If, furthermore, use is made of equation (5.16), γ/δ can be expressed in terms of k. The second assumption is that we require that at $\mathrm{v_c}$, w=4 holds for the annular tube and w=6.75 for the circular tube. This requirement determines γ/δ and then k can also be found. Although the results yield an exact coincidence with the

Table 5 Fit of the data to the Vinen model.

No.	α	k[molJ^{-1}s^{-1}]	γ/δ[sm^{-2}]
Z_I	0.087	–	–
Z_D	0.106	$5.26\cdot10^4$	$4.96\cdot10^5$
Z_S	0.100	$4.35\cdot10^4$	$4.35\cdot10^5$
Z_U	0.084	–	–
Z_B	0.100	$4.35\cdot10^4$	$4.35\cdot10^5$

[†*] It was suggested by Van Beelen (private communication) that the experimental results can also be analyzed in terms of the parameters $x=(\mathrm{d}/\delta\sqrt{\mathrm{B}})\sqrt{\mathrm{BL}}$ and $w=(\gamma/\delta)\mathrm{vd}$. For the annular tubes the equation (5.32) yields:
$\mathrm{vd} = \frac{1}{\gamma\sqrt{\mathrm{B}}} \frac{(\mathrm{d}\sqrt{\mathrm{BL}})^2}{(\mathrm{d}\sqrt{\mathrm{BL}}-\delta\sqrt{\mathrm{B}})}$ and equation (5.33) yields: $\mathrm{vd} = \frac{1}{\gamma\sqrt{\mathrm{B}}} \frac{(\mathrm{d}\sqrt{\mathrm{BL}})^3}{(\mathrm{d}\sqrt{\mathrm{BL}}-\delta\sqrt{\mathrm{B}})^2}$ for the circular flow channels. From a fitting technique $\gamma\sqrt{\mathrm{B}}$ and $\delta\sqrt{\mathrm{B}}$ must now be determined. In that case comparison with ^{4}He is easier. However these parameters can also be determined using equations (5.30) and (5.31).

critical velocity, general agreement is not so good and we will not discuss it further.

The fitting procedure was carried out for the different measurements. The results are shown in figure 24a-e. In this figure $d\sqrt{\Delta\mu_4/\ell v}\ 10^5$ is plotted as a function of vd. In table 5 the basic parameters are shown. In the graphs the parameters are indicated.

We will first discuss figure 24 b,c and e. Here measurements were carried out in the critical velocity region. The parameters α and k could therefore be determined accurately. The fitting was only carried out for the measurements at 46 mK in figure 24b and c. For figure 24e the average value of the data was taken from which the parameters were determined.

In figure 24b and e it can be seen that the calculated critical velocities as found from the fitting procedure are smaller than those found directly from the measurements. There can be several reasons for this. The first is that at about v_c there are only a few vortex lines present and perhaps in that case the Vinen approximation is not correct. The second reason could be that at around v_c, $d\dot{x}/dx$ is small, see the discussion at figure 21, and stabilization at a different v_c can occur due to small external influences. In the measurement with flow channel Z_B (figure 24e), v_c occured always at the same value so if there is an external influence it is not determined by the temperature.

In figure 24a the measurement with one tube with d = 1.2 mm is presented. Here the critical velocity could not be measured. A least squares straight line fit yields α=0.087. This value is different from that found for the measurements discussed above (estimated uncertainty 2%). This means that the high flow region is not described by the same parameters as just above v_c. This could mean that there is perhaps a second critical velocity at which a change occurs from $\alpha \simeq 0.087$ to $\alpha \simeq 0.100$ related to a similar effect in He II namely the TI→TII transition. The factor k and thus γ/δ cannot be determined accurately for this measurement and are not indicated in table 5.

In figure 24d the results obtained with the annular flow channel are shown. The points can be fitted with a straight line. The least squares fit yields an α of 0.084 which is about the same as that found in the experiment with flow channel Z_I when the fluid was in the high turbulence regime (figure 24a). This might be an indication that TIII, which is a flow state defined by Tough (1982) for slits, is the same as TII for circular flow channels. The critical velocity is much smaller than the velocity range in which the measurements were carried out. This indicates that the measured data lie in the high turbulence regime too.

Our measurements seem to indicate that there are two regions of turbulence. A low velocity region which can be described by $\alpha \simeq 0.10$ and a high velocity region where $\alpha \simeq 0.085$.

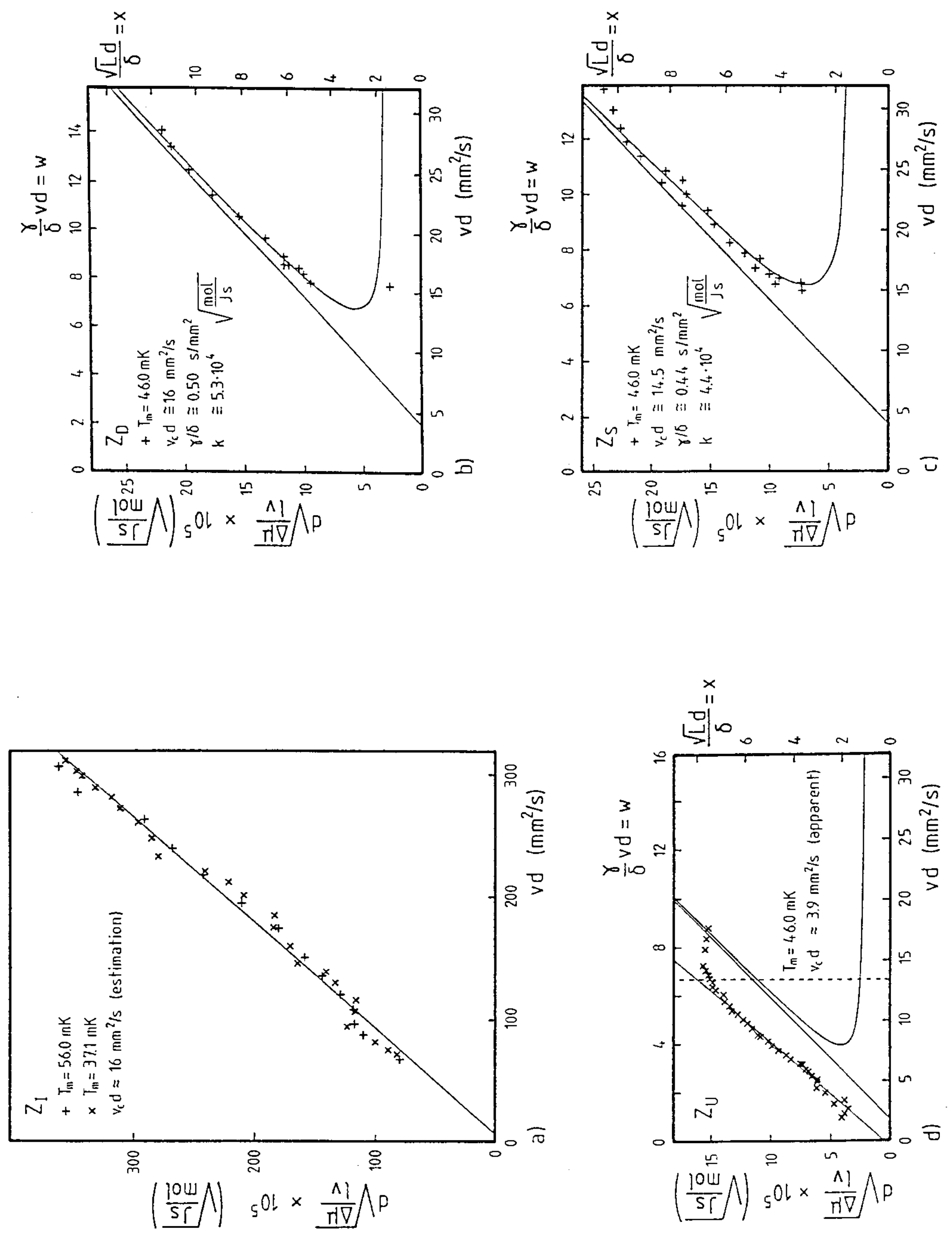
Z_I
$+\ T_m = 56.0$ mK
$\times\ T_m = 37.1$ mK
$v_c d \approx 16$ mm²/s (estimation)
$d\sqrt{\frac{\Delta\mu}{IV}} \times 10^5$ $\left(\sqrt{\frac{Js}{mol}}\right)$
0
100
200
300
vd (mm²/s)
a)
Z_D
$+\ T_m = 46.0$ mK
$v_c d \cong 16$ mm²/s
$\gamma/\delta \cong 0.50$ s/mm²
$k \cong 5.3 \cdot 10^4$ $\sqrt{\frac{mol}{Js}}$
$\frac{\gamma}{\delta} vd = w$
$\frac{\sqrt{Ld}}{\delta} = x$
0
2
4
6
8
10
12
14
5
10
15
20
25
30
vd (mm²/s)
b)
Z_S
$+\ T_m = 46.0$ mK
$v_c d \cong 14.5$ mm²/s
$\gamma/\delta \cong 0.44$ s/mm²
$k \cong 4.4 \cdot 10^4$ $\sqrt{\frac{mol}{Js}}$
$\frac{\gamma}{\delta} vd = w$
$\frac{\sqrt{Ld}}{\delta} = x$
c)
Z_U
$T_m = 46.0$ mK
$v_c d \approx 3.9$ mm²/s (apparent)
$\frac{\gamma}{\delta} vd = w$
$\frac{\sqrt{Ld}}{\delta} = x$
16
vd (mm²/s)
d)

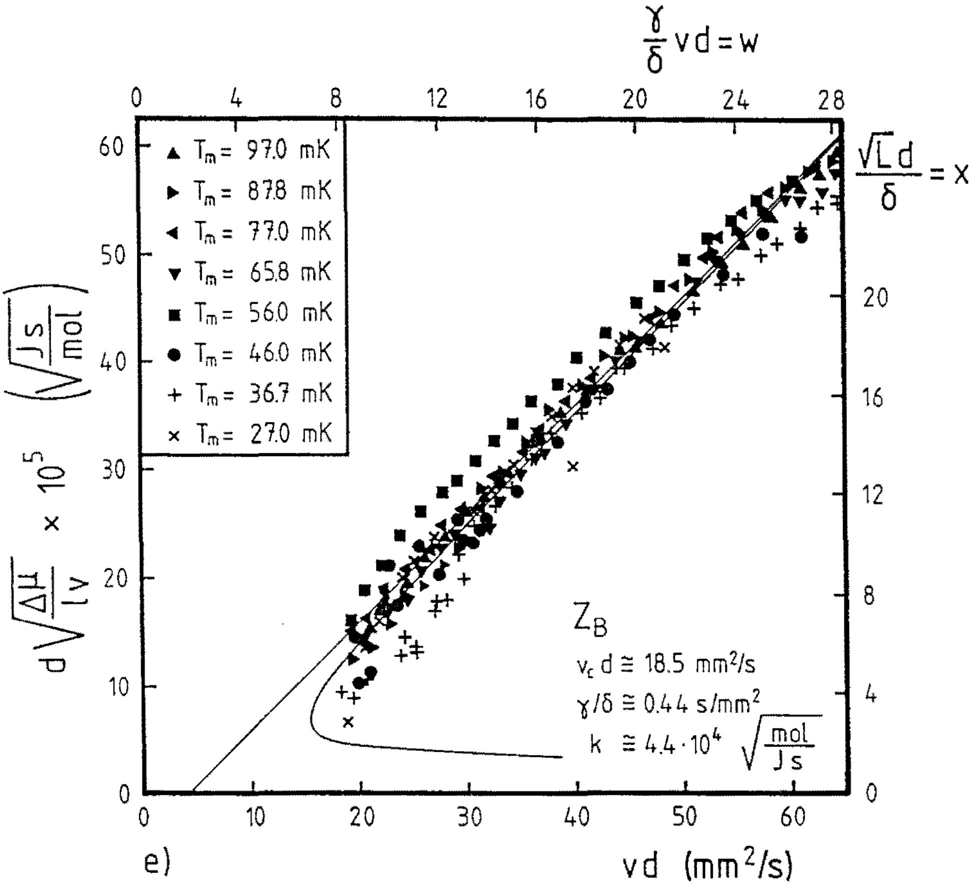

Fig.24a-e *Vinen parameters x and w for the different measurements.*

The parameter α is given by:

$$\alpha = \frac{\chi_2}{\chi_1} \frac{1}{\mathrm{B}\sqrt{\mathrm{B}}} \frac{\rho}{\rho_{\mathrm{n}}} \left[\frac{\rho}{\rho_{\mathrm{n}}\rho_{\mathrm{s}}\mathrm{V}_4}\right]^{\frac{1}{2}} \frac{\sqrt{3\kappa}}{\pi} \tag{5.34}$$

and does not depend on channel type. Perhaps it is not so strange that the α's for both channel types are practically the same in the high velocity region as in that case the wall influence becomes very small. The parameter k depends on δ, which might be channel geometry dependent. If there is such a dependency then this can only be solved by carrying out measurements in the critical velocity region for the annular tubes. However, we can substitute the constants, which were found in the critical velocity region with the circular tubes, in the equations for annular tubes. The result for this is also shown in figure 24d. The scales above and on the right side of the diagram correspond with this choice. It can be seen that of course there is no agreement with the measurement.

We conclude that the Vinen model provides a fair description of the flow in circular capillaries. The results of the experiments with the annular flow channels indicate that the liquid is in the high turbulent state (TII). This observation would be at variance with the Vinen model. More measurements at lower velocities are needed.

5.5 THE VALUE OF THE CRITICAL VELOCITY.

5.5.1 DIAMETER DEPENDENCE FOR CIRCULAR TUBES.

In section 5.6 it will be shown that the product of critical velocity and tube diameter might be an important parameter. The $v_c d$ product is presented as a function of tube diameter in figure 25. Note that the diameter is plotted on a logarithmic scale. There is much scatter in the data which perhaps is due to the different ℓ/d ratio's, or inlet conditions for the different capillaries. For the tubes with diameters 0.11 mm and 0.16 mm two triangles are indicated. The lower one corresponds with the velocity (v_{c1}) where the measurement deviates from the mechanical-vacuum model. The higher with the velocity where a second transition (v_{c2}) seemed to occur (see figure 19b). The measured points roughly follow a straight line corresponding with the equation:

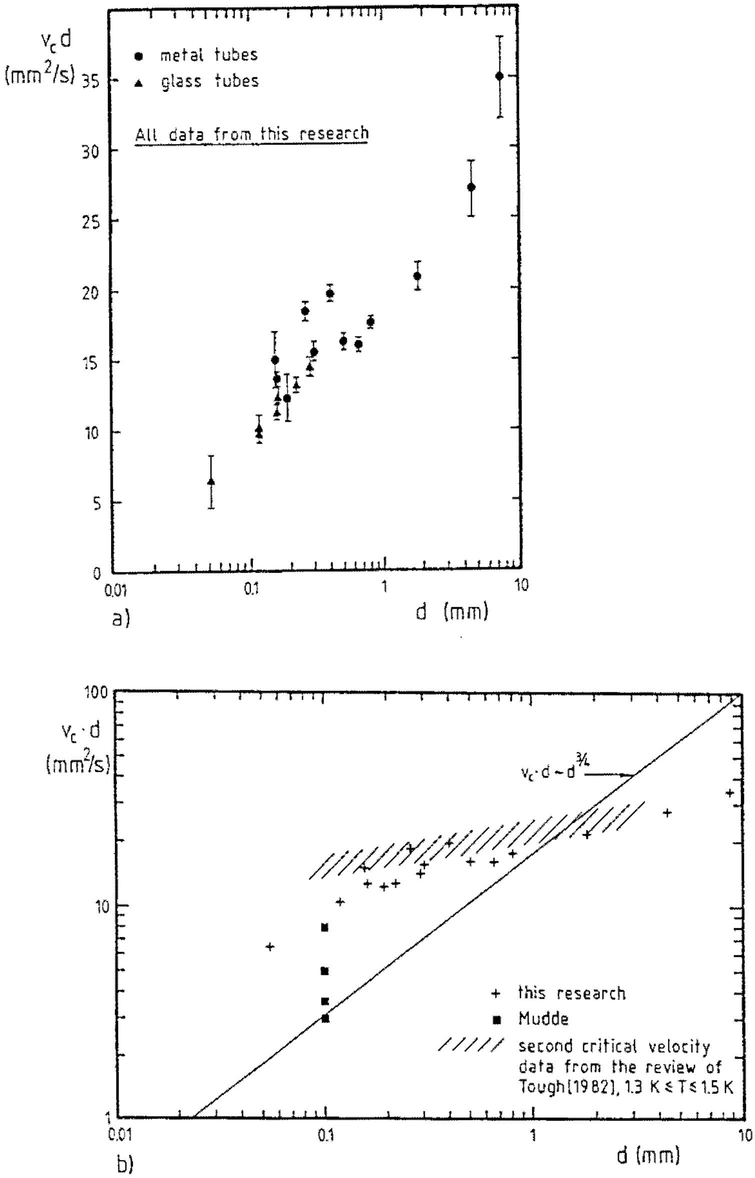

Fig.25a *The product $v_c d$ as a function of the diameter d in a semi-logarithmic plot. Data can be found in Table 3.* ● *metal tubes,* ▲ *glass tubes. Data are for circular tubes only.*

b *$v_c d$ data in a log-log plot. The $d^{3/4}$ behaviour is represented by the straight line.* ■ *Mudde (1987, 1989), averaged values for mixtures of $x=4.6\%$, 7.2% and 11.0% and for different temperatures $T = 1.30$, 1.45, 1.60 and 1.70 K. The highest value represents lowest temperature.*

$$v_c d = 5 \cdot \ln\left[\frac{d}{0.015\text{mm}}\right] \text{ mm}^2\text{s}^{-1} . \tag{5.35}$$

If this logarithmic dependence would be satisfied down to the lowest d values it would imply that $v_c d$ would become zero for about 15 μm. This would mean that no flow of ^{3}He in ^{4}He II would be possible without mutual friction in capillaries of abcut 10 μm or smaller. To draw definite conclusions concerning the zero value of $v_c d$ more experiments are necessary using in particular capillaries with diameters in the 5 μm - 100 μm range. Also entrance conditions, ℓ/d ratio and material properties have to be changed in order to study the dependence of v_c on them.

On purely empirical grounds Van Alphen (1966, 1969) proposed a behaviour for critical superfluid velocities in pure ^{4}He II for zero v_n:

$$v_c d \sim d^{3/4}. \tag{5.36}$$

He considered the superfluid critical velocity v_{sc} if v_n is zero, which is not the case in our situation. In figure 25b equation (5.36) is shown together with our data. It is clear that it does not agree with our results which is maybe not surprising. Data from Mudde (1987, 1989) presented by (▪) in figure 25b will be discussed in section 5.6. The logarithmic behaviour for pure ^{4}He II which was also drawn in Van Alphen's diagram lies a factor 10–100 lower than our data and is not shown.

In our situation the normal fluid component moves and the superfluid is at rest. We like to emphasize that our data can really only be compared with the critical values in pure normal fluid flow in ^{4}He. The critical velocity is strongly influenced by the value of the simultaneously present superfluid velocity as was investigated in Leiden by Marees (1985, 1986) and at Ohio State University by Courts (1988, 1989). Due to the motion of the normal fluid component, classical turbulence can develop. However, this is not the case in our situation as was discussed in section 4.5. If we compare our values of $v_c d$ with those in the review of Tough (1982) measured in counterflow experiments the order of magnitude is the same. Data for T = 1.3 K and 1.4 K are also indicated in figure 25b. for $v = v_{c2}$. The value of the critical velocity we measure is somewhat smaller.

5.5.2 ANNULAR TUBES, A DIFFERENT CRITERION.

In section 5.2.2 and 5.4 it was demonstrated that the critical velocity is not sharply defined in annular tubes. It is perhaps much smaller than our detection limit. The value of the ^{3}He velocity where the measurements deviate from the mechanical-vacuum model, results in an apparent critical velocity v_{ca}, which depends on the measuring accuracy. The larger the length of the tube the lower the v_{ca} one will observe. In table 3 this tendency is shown. In our experiments the tube length was chosen as long as possible, under the requirement that the viscous heating does not become too large. The maximum length, determined by the space in our dilution refrigerator, is about 350 mm.

In annular tubes two length scales can be important: the annular spacing d and the tube diameter D. If the annular spacing $d \simeq 0.1$ mm and if the apparent critical velocity v_{ca} are used to calculate the $v_c d$ product we find $v_c d \simeq 2$ mm²/s. This is much smaller than the corresponding value obtained for the circular tubes ($v_c d = 15$ mm²/s). If instead the annular tube diameter D=7.87 mm is used in the $v_c d$ product and if the value from figure 25 is applied this leads to $v_c D = 35$ mm²/s, and so $v_c \simeq 4$ mm/s. This is too small to be detected with our flow channels.

If this condition holds, then in a single annular tube with $d < 0.1$ mm a critical velocity cannot be measured, because viscous heating is too large according to equation (2.15). With $d \simeq 0.3$ mm and 3 flow channels in parallel the critical velocity may be reached. With the analysis of section 4.2 it is found that for a temperature jump of 1 mK at v_c a length of about 15 meters would be necessary. This will be difficult to realize but it is worth to investigate how the slit width d and the tube diameter D determine the critical velocity. It can solve an interesting aspect of the development and growth of vortices at the wall and it can give further insight into the applicability of the Vinen model.

5.5.3 TEMPERATURE DEPENDENCE.

From figure 13e, it follows that below 100 mK the critical velocity is practically T independent. We examined the v_c-T dependence of impedance Z_B also at higher temperatures sweeping the flow through the critical value and recording the fluctuations in the signal of the pressure transducer when the critical velocity is passed (see chapter 6). The critical flow rate was determined while slowly increasing or decreasing the mixing chamber temperature with the mixing-chamber heater.

The result of this experiment is shown in figure 26. The curved line represents the calculated critical flow rate according to the relation:

$$\dot{n}_{3c} = \frac{v_c A}{V_3} \tag{5.37}$$

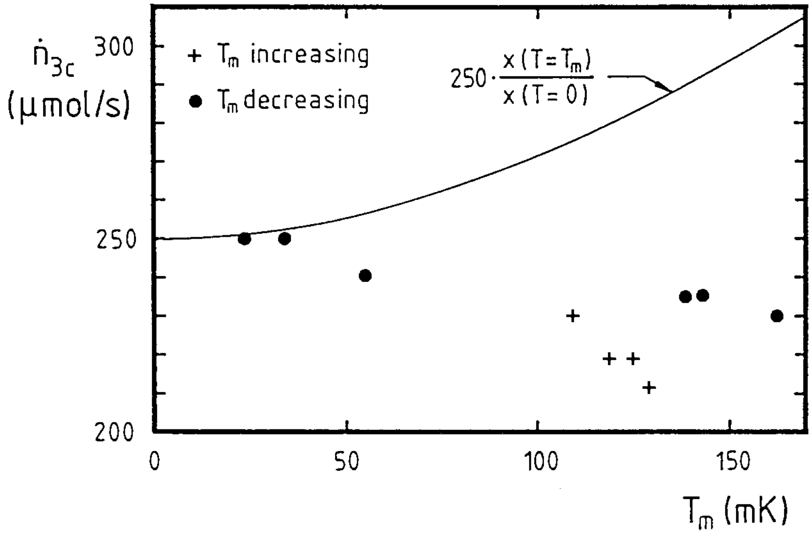

Fig.26 *Critical flow rate* $\dot{n}_c$ *as a function of* T_m *in flow impedance.*

assuming a T independent v_c. The T dependence in the curve is due to the dependence of V_3 on the concentration variation along the phase separation boundary (Kuerten (1987)). The measured points are below these calculated values. This indicates that at higher temperatures v_c slowly starts to decrease with T.

5.6 A SURVEY CONCERNING RELATED WORK AND THE CRITICAL VELOCITY.

5.6.1 SOME CONSIDERATIONS CONCERNING VORTICES AND THE CRITICAL VELOCITY.

Critical velocities play an important role in the motion of ordinary fluids. In general for velocities above a critical velocity nonlinearity, vortex formation and turbulence develop. In liquid helium below the lambda point the problem of critical velocities is more complicated than in ordinary liquids. This is due to the fact that ^{4}He II consists of two different components, which can move relative to each other and the walls. Besides, ^{4}He II is a quantum liquid which has special properties.

The theoretical study of critical velocities in liquid helium II dates back to Landau (1941) who showed that excitations of momentum (P) and energy (E) could only be generated if the superfluid velocity was larger than the minimum of E/P, where E and P are determined by the excitation (phonon-roton) spectrum. This result, nowadays known as Landau's criterion yields for the superfluid critical velocity:

$$v_{sc} = (E/P)_{min} \,. \tag{5.38}$$

The critical velocities occurring in flow experiments– a few centimeters per second – are much smaller than those following from (5.38), which are on the order of 60 m/s and so this equation does not describe the critical velocities as found in experiments.

Onsager (1949) proposed that quantum vortices could be generated in ^{4}He II. Ever since, the formation and evolution of vortices in relation to critical velocities and mutual friction has been the subject of intensive investigations and was first studied by Feynman (1955). He showed that to first order the product $v_c d$ for the flow of a superfluid in a channel with diameter d should be linear in ln(d).

After Vinen (1963) two types of critical velocities can be proposed. The first type is called "ideal" and is associated with the formation of vorticity starting from nothing. The second type is called "nonideal" and is related to the velocity where growth and stabilization of a vortex tangle takes place.

The critical velocity of the first type has theoretically been studied using classical theories, quantum mechanical theories and statistical mechanical theories. Many of the studies appeared before 1970. Therefore, chapter 8 of Keller (1969) is still useful as a reference. The general result from studies on grounds of the generation of vortex ring alike filaments is that the $v_c d$ product (where d is a characteristic length) is constant or changes slightly with d and is roughly in agreement with Feynman's proposal. The agreement with v_c in flow experiments is not so good. Maybe this is due to the existence of primordial vortex lines and in that case a nonideal critical velocity occurs.

The nonideal critical velocity could be determined with the Vinen model, where as a result $v_c d$ was found to be constant for a specified geometry. Due to the increase in calculating power of computers, nowadays the evolution of a vortex tangle can be simulated numerically. This work was pioneered by Schwarz (1968-1990). From dimensional analysis of the equation of motion for the vortices it follows that (Kuerten (1987b), Schwarz (1988)):

$$v_c d = \beta \,, \tag{5.39}$$

and $$\beta = \frac{\kappa}{4\pi} \ln\left[\frac{cR}{a_0}\right] \tag{5.40}$$

where c = constant of order unity
R = average local radius of curvature
a_0 = effective core radius.

In papers by Swanson (1985a,b) this scaling is discussed in more detail. Using their technique a better overall agreement of v_c with temperature was found (Tough (1982)).

A discussion of critical velocities in relation with phase slip experiments was held at the Nato Workshop on Excitations in 2D and 3D quantum liquids by Varoquaux (1990). In this paper different methods are used to account for observed critical velocities. It is evident that it is a difficult problem which seems hard to solve for complex geometries.

In general it follows from the theoretical studies that the $v_c d$ product is of importance. At present, however, no detailed theoretical account of the critical velocity, which is found in the flow experiments is known. Maybe future simulations of vortex tangles can explain the critical velocity in a real simulated setup.

5.6.2 THE EFFECT OF ^{3}He ON ^{4}He VORTICES.

As the origin of the creation of vortices in pure ^{4}He II is unclear it is even more difficult to speculate about the effect of ^{3}He on the formation of vortices. Ohmi (1969a) calculated the effect of ^{3}He impurities captured in the vortex core on the radius of the core from thermodynamics. He showed that the radius increases and can be relatively large ($\gg$10Å) for saturated mixtures. Ohmi (1969b) calculated that for small densities the binding energy of the ^{3}He particles to the vortex core is 3.5 K and the vortex radius increases with a factor 2.5 compared with that in pure ^{4}He. The tension of the vortex will decrease and the inertial mass will change. Rent (1969) also showed that the interaction of ^{3}He with a vortex is attractive leading to an increase of the vortex core radius. Using statistical mechanics and thermodynamics Senbetu (1978) found that the binding energy of the ^{3}He to the vortex core was 0.78 K. For a 1% solution the vortex core radius was estimated to be about 6.5 Å, in good agreement with the value found by Ohmi (1969a).

Experiments of Rayfield and Reif (1964) showed evidence that ^{3}He indeed condenses on the vortex core. Glaberson and Ostermeyer and Williams and Packard, see Glaberson (1986), revealed that small impurities of ^{3}He have a large effect on ion trapping on vortices and mobility of trapped ions. Concerning critical velocities Ostermeyer and Glaberson (1975) derived a criterion at which for axial flow along a helical deformed vortex the deformation grows or decays. They also showed that the axial critical velocity increases significantly when only 10 ppm ^{3}He was added to the pure ^{4}He. Williams (1974) used a 0.5% mixture showed that this led to a strong damping of the vortex motion. In this way he could make photographs of a vortex array.

Muirhead (1984) and Bowley (1984a) gave an explanation for the formation of vortices by ions. Muirhead (1985), Nancolas (1985) and Bowley (1984b) showed that if ^{3}He is bound to the ion, nucleation of vortices might take place at a lower velocity, but the effect is small (10 %). Varoquaux (1986) showed experimentally that 5% ^{3}He decreases the critical velocity by a factor 2 in comparison with pure ^{4}He.

The critical velocity for formation of vortices does not seem to be influenced very much by the presence of ^{3}He. This could mean that the stability of a vortex tangle is not greatly affected by the presence of ^{3}He.

5.6.3 RELATED WORK, IN MIXTURES.

In this section a short discussion is presented concerning related research in other laboratories on the hydrodynamics of mixtures of ^{3}He and ^{4}He II, in which evidence for superfluid turbulence is reported

At Leiden University Mudde and Van Beelen (1987, 1989, 1990) carried out counterflow experiments in ^{3}He-^{4}He II mixtures of molar concentrations up to 11.0% in a glass capillary with diameter $d=100\ \mu m$ in the 1.3 K-1.7 K temperature range. The ^{3}He component moves with the normal component of the ^{4}He. They determined the ^{4}He chemical potential differences from the measured temperature, pressure and concentration differences which were subsequently analyzed in terms of vortex line densities. The critical velocity was estimated. At a critical velocity ($v_n \simeq 3$ cm/s) mutual friction appeared. The values of v_cd scatter for the three ^{3}He concentrations used in their experiments and there was a temperature dependence observed. The value of v_cd at $T=1.3$ K approaches our results.

In Japan, measurements were carried out in which ^{4}He II is forced to flow through a capillary via a superleak (Satoh (1987)). For small superfluid velocities there was no normal fluid flow and no mutual friction. Above a first critical velocity mutual friction appeared and the normal component moved with the superfluid, but $v_n < v_s$. At still higher velocities v_n approaches v_s. The same experiments were carried out with a 6%

mixture (Okuyama (1988)). At about the same velocity as in pure ^{4}He the velocity of the ^{3}He became nonzero. Now the ^{3}He is dragged along with the normal ^{4}He component and a situation appeared with a vortex tangle in a mixture.

In France, experiments were carried out by Avenel (1985) and Varoquaux (1986) where discrete phase slip events were observed. In ^{4}He II they observed a critical velocity v_c where presumably the motion of the vortices was initiated at an orifice. They reported a temperature dependence of v_c. They also showed that minute traces of ^{3}He changed v_c. For a 5% mixture v_c decreased with about 40%. The ^{3}He atoms have a large influence on the nucleation of the vortices. The nucleation process of the vortices in the experiment of Avenel and Varoquaux was discussed in Schwarz (1987a), Brewer (1986) and Avenel (1986, 1987).

In New Mexico, Ecke (1987, 1989) Haucke (1983, 1987) and Maeno (1985) studied the convective behaviour of the mixture in a Rayleigh-Bénard cell between 0.70 K and 1.05 K and studied the different attractors of the system. In their 1987 article they discussed noisy states which are history dependent. From power spectra they suggest that superfluid turbulence occurs in the ^{4}He II and they showed that at about 0.13 cm/s a critical velocity occured.

These four different researches show that critical velocities are general phenomena in mixtures and give additional support for the analysis described in this thesis.

5.7 COMPARISON OF MUTUAL FRICTION IN PURE ^{4}He II WITH MUTUAL FRICTION IN MIXTURES.

5.7.1 PARAMETERS AND VORTEX LINE DENSITIES.

In section 5.3 vortex line densities were discussed. The results in circular tubes can be interpreted in terms of Vinen's model. Vortex line densities are dependent on the parameter B and the interpretation of figure 21 in terms of L is only possible if the parameters γ or δ are known. If we assume that the vortex-wall interaction in mixtures is the same as in pure ^{4}He II then we may assume that $\delta \simeq 1$. This means that from our measurements with circular tubes it follows that the parameter γ is on the order of 0.5 s/mm^2. In pure ^{4}He this parameter has a value between 0.5 and 3 s/mm^2 for circular and square channels.

The parameter B is not known for a ^{3}He-^{4}He II mixture. For ^{4}He II the value of B is about 1, (Barenghi (1983a)). If this value is assumed for our situation we get $\sqrt{L} = 50 - 200$ mm^{-1}, at velocities just above the critical value. These values are of the same order of magnitude as in pure ^{4}He II (Tough (1982)).

5.7.2 CIRCULAR FLOW CHANNELS.

For a complete discussion of the various phenomena mentioned in this section we refer to the review of Tough (1982) and the references therein. In ^{4}He II two turbulent flow states are distinguished: TI and TII. The transition from laminar flow to the TI state is characterized by a slow rising of the temperature difference above the laminar temperature difference. In general the first critical velocity (v_{c1}) is difficult to determine below 1.6 K. The temperature differences are very small. These two critical velocities were already observed by Brewer and Edwards (1956, 1961a,b, 1962) in the period 1956-1961. In more recent publications of the Ohio State group (Lorenson (1985), Martin (1983)) it is mentioned that a discontinuous transition occurs from the laminar state to the TI state.

At a velocity of about twice v_{c1} a transition occurs from TI to a TII state. At this transition the temperature increases rapidly with the velocity. The question whether v_{c2} is related with turbulence in the normal fluid component is left open by Tough (1982).

Above v_{c1} transient effects are observed and these were studied by different workers in the sixties and seventies Cambridge, Leiden and Moscow. In the eighties detailed studies were carried out by Slegtenhorst (1982) and Marees (1985, 1986) in Leiden. It was found that if the velocity was steadily increased it was possible to keep the flow state laminar for velocities larger than v_{c1}. A disturbance like a tap on the apparatus caused the turbulent state to set in. Hysteresis was observed as by decreasing the flow the turbulent state disappeared at $v \simeq v_{c1}$. The critical velocity may also be influenced by surface roughness. In metal tubes large transient effects, hysteresis and multiple flow states were observed, but in some experiments no effects of wall roughness on the flow properties were observed (Courts (1988), Hedge (1980)).

Comparing our results in mixtures with those of pure ^{4}He II we can remark that qualitatively we observed the same phenomena. In glass tubes we observed a more gradual transition perhaps indicating v_{c1}, followed by a steep transition resembling v_{c2}, see figure 19b,c. However, in general $2v_{c1} \neq v_{c2}$.

In the metal tubes the transition was sharp and discontinuous most of the time. Usually only one transition was observed. In a few measurements with metal tubes there was also a change in slope in the curves indicating a second transition. More evidence for the presence of a second critical velocity is presented in chapter 6. No hysteresis was observed. With increasing as well as decreasing flow the transition occured at the same velocity value. Perhaps the vibrations of the dilution refrigerator were too large. The value of the critical velocity we observed is a little lower than values of v_{c2} observed in ^{4}He II counterflow, see section 5.5.

It has to be noted that in our experiments many tubes are placed parallel. The studies carried out with pure ^{4}He II discussed above were carried out with one tube and so in that case the experimental conditions are more ideal. Another aspect which was already noted is the strong influence of the different velocity fields v_n and v_s on the mutual friction and on the critical velocity. This complicates the comparison. For further reading we refer for instance to Marees (1985-1987), Slegtenhorst (1977-1982) and Courts (1988, 1989).

5.7.3 ANNULAR FLOW CHANNELS.

Experiments with flow in slits date back to Kapitza's (1938) classical experiments in 1938. Many of the early experiments are described in Atkins (1959). At Ohio State University, Ladner (1978, 1979) and Henberger (1981, 1982) carried out experiments with glass rectangular slits with spacing 37 μm-101 μm. They observed only one turbulent flow state named TIII. In general the transition from laminar flow to TIII occurs gradually. Sometimes it occurs more discontinuous. Hysteresis can occur in the way as observed in the circular tubes. "A detailed high resolution study could be very illuminating", as Ladner (1979) remarks.

The critical velocity is determined by interpolation of the measured data to the laminar flow part. At 1.4 K values of v_{ns}, in slits with d between 37 μm and 101 μm, of 8 cm/s to 3 cm/s were found respectively. Yarmchuck and Glaberson (1978, 1979) used slits with a spacing d=0.5 mm in which also critical velocities were observed at values of about 1 cm/s. They also studied critical velocities in case the channel rotated leading to an increase of v_c and vortex depinning. They also studied the effects of surface roughness in relation with vortex depinning, see also Hedge (1980). In experiments carried out by Winkel (1954, 1955a,b), Hammel (1961), Craig (1965) and Keller (1960) short plan parallel and annular slits with spacing d in the order of microns were used. With heat flow and in gravitational experiments critical superfluid velocities v_{sc} in the order of 10 cm/s were found. It is of interest that the vortex line density coefficient γ obtained in the micrometer slits is the same as in case slits with a spacing of 100 microns are used.

The apparent transition we observe with mixtures is also gradual and the value of v_{ca} (Table 3) corresponds with those measured in ^{4}He II. No hysteresis was observed in our experiments. In section 5.5 it was argued that the observed critical velocity was only an apparent one and was determined by measuring accuracy. We do not know if this also holds for the phenomena in pure ^{4}He II. In pure ^{4}He II, Chase (1962, 1963) also carried out experiments with different geometries. Citing Chase: ".......W_c is determined mostly by the outer boundaries of the channel". If he inserted rods in a circular channel, realizing an annular spacing as in our experiments the critical velocity did not change much. So there is evidence from ^{4}He II experiments that in these annular channels it is the channel diameter D which determines the critical velocity. Presumably the proposal of Glaberson and Donnelly (1966) that the critical velocity is determined by the minimum inductive velocity which is determined by the largest vortex curvature fitting in the tube is correct.

It is possible that at the first critical velocity, vortex ring like structures can start to grow in a tube. These ideas were also discussed by Geurst (1979, 1990). At higher velocities perhaps at the second critical velocity, these vortex rings might get unstable and grow to a turbulent vortex tangle. However, the nucleation process is still unknown. There is experimental evidence that there are always remanent vortex lines in the fluid, see Vinen (1961b), Whitmore (1965-1968) and Awschalom (1984). Then it is the way in which they grow which determines the critical velocity.

More detailed measurements in pure ^{4}He II and in mixtures together with numerical simulations can resolve the discussion and lead to a better understanding of the critical velocity phenomenon.

5.8 CONCLUSION.

In metal circular capillaries the critical velocity appears as a rather abrupt change in the flow properties. In glass capillaries it is more gradual. There are indications that there is a first and a second critical velocity.

It is possible to interpret our measurements of circular flow tubes in terms of Vinen's model. If the parameter B is assumed to be equal to one, the vortex line density is roughly the same as in with pure ^{4}He II experiments. The values of the adjustable parameters of the model in the velocity region where the turbulence appears ($v \geq v_{c1}$)

are different from the values in the well developed turbulent regime ($v \gg v_{c1}$).

In annular flow channels the critical velocity lies below our detection limit. The adjustable parameters derived from the measured chemical potential differences are comparable with the well developed turbulence in circular tubes. The Vinen model can only explain this behaviour if it is assumed that the parameter δ is strongly dependent on the tube geometry. The turbulence in annular flow impedances strongly resembles that in the high mutual friction limit of circular capillaries. The Vinen parameters of both systems are the same.

The product of critical velocity and tube diameter has the same order of magnitude as in pure ^{4}He II. The $v_c d$ dependence rises with d perhaps following a log(d) dependence. Below 200 mK the critical velocity weakly depends on the temperature.

The flow of ^{3}He through a background of ^{4}He II in circular as well as in annular flow channels shows a remarkable resemblance with thermal counterflow in pure ^{4}He II.

CHAPTER 6

FLUCTUATION EXPERIMENTS

6.1 INTRODUCTION.

Fluctuations are related to many aspects of classical hydrodynamics. During the past 30 years it has become clear that in turbulent flows as for instance in pipe flow, fluctuations, intermittency and coherence phenomena play a role, see Hussain (1986), Cantwell (1981), Roshko (1976).

The transition from laminar to turbulent flow follows a characteristic route along various characteristic flow states. Typical examples of such routes are demonstrated by Taylor-Couette flow and by Rayleigh-Bénard convection (Swinney (1985)). Mostly the flow state develops from an orderly situation to a chaotic flow state (see for instance Bergé (1986), Tatsumi (1984) and Ottino (1990)).

In pipe flow of ordinary liquids turbulence develops locally in so called "puffs" ($2000 < Re_d < 2700$) and "slugs" ($2700 < Re_d < 4000$), (Wygnanski (1973,1974), Bandyopadhyay (1986)). This is sometimes called plug flow. If the velocity is measured locally an intermittent and strongly fluctuating signal is observed. These phenomena observed in normal fluids stimulated us to study the fluctuations which we observed around the critical velocity.

While we were investigating the flow characteristics of the flow impedances, as described in chapter 4, transient effects were observed when the flow rate was adjusted to a new value. There were two kinds of effects: relaxation of the measured quantities to a new equilibrium value and fluctuations in the pressure transducer signal. In the pressure signal it was observed that the relaxation was fast for velocities below the critical velocity and slow above the critical velocity. Furthermore, above the critical velocity the fluctuations in the pressure were small and increased passing the critical velocity. The characteristic time of the fluctuations was about one second. These transient effects were observed in experiments with flow impedances consisting of bundles of circular capillaries.

To obtain more information about the transient effects two preliminary experiments were carried out. The first was aimed at the changes in the relaxation processes as a function of the flow velocity. The time constant of the relaxation was studied. In the second experiment a study was made of the fluctuations by slowly changing the flow velocity and monitoring the pressure signal on an xt-recorder. These experiments are described in section 6.2. Stimulated by the results of these experiments the pressure fluctuations were studied in more detail using a Fast Fourier Transform (FFT) analysis. In these experiments we investigated in particular the dependence of the FFT-fluctuation spectra on the critical velocity. The steady state results of these experiments are presented in section 6.3 and the fluctuation spectra are discussed in section 6.4. Although interesting results were obtained concerning the first critical velocity, at present the physical meaning of the second critical velocity did not become quite clear. Section 6.5 discusses our results comparing them with related work in pure ^{4}He and concludes this chapter.

6.2 TRANSIENT EFFECTS.

6.2.1 TIME CONSTANTS OF THE DETECTORS.

Before an investigation is made of transient effects it is important to know the time constants of the various quantities and the detectors by which they are measured.

The time constants of all the detectors are small in comparison with the relaxation time of the quantities. The thermometer readings can be recorded with a time constant of about 0.5 s although, due to Kapitza resistance, the thermometer itself cannot respond faster than within (estimated) 10 seconds. The concentration capacitor and the pressure transducer can be measured with a time constant of 1 ms. The instrumental time constant of the pressure transducer is not known accurately, but it can follow fluctuations of at least 50 Hz. The flowmeter is a relatively slow instrument and has a time constant on the order of a minute.

The thermometers and the concentration capacitor are placed in two rather large volumes and the thermal time constant (this can be thought of as a RC-time) to detect changes, is on the order of a few minutes. Therefore these instruments are not suited to study fluctuations. In the steady flow experiments the thermometers, concentration capacitor and the flowmeter always showed a slow relaxation to a new equilibrium value. This was not the case with the pressure transducer. We observed, specially below the critical velocity, a fast response on the order of a few seconds to a new installed flow rate value. The pressure transducer is therefore the most suitable instrument to investigate fluctuations and relaxation phenomena.

6.2.2 THE RELAXATION PHENOMENON.

The experiment was carried out with the setup shown in figure 27a. The connection between the mixing chamber and the experimental space consisted of two flow channels in parallel. One was flow channel Z_D and the other was a single capillary with the same length and diameter as the capillaries contained in Z_D (see table 2). A vibrating wire viscometer (see chapter 7) was placed downstream of the tube system. A second vibrating wire was placed inside a tube of diameter 1 mm in series with the shunting capillary. The vibrating wire signal provides a measure of the temperature due to the temperature dependency of the viscosity of the fluid (chapter 7). These vibrating wires were installed for two reasons. The first was that from results of other experiments we knew that, if a detector (for instance a capacitor) is placed directly downstream of the flow impedance, a much faster response to flow changes is observed. If the response is fast enough this could provide an independent check of the relaxation by the pressure transducer. The second reason was that we hoped that fluctuations perhaps due to vortices could be observed in particular with the small vibrating wire.

In the experiment a constant voltage (V_0) is applied to the still heater with superposed on it a square wave with an amplitude about 2% of V_0 and a period of about 2000 s. This is long enough to complete the relaxation process.

Figure 27b is a recorder trace of the two vibrating-wire signals and the pressure transducer signal in the velocity region $v>v_c$. Also shown is the heater voltage. In the figure we observe a relatively fast response in about 1-2 minutes followed by a much slower relaxation of about 15 minutes. The latter is due to temperature relaxation of the mixing chamber caused by a temporary off balance of the dilution refrigerator, see figure 10.

Figure 27c shows measurements at $v \simeq v_c$, during one half period $v>v_c$ and in the other half $v<v_c$. Now the changes in the vibrating wire signals are small because the temperature changes are small, but the pressure transducer shows a clear response. The first change occurs in a short time. The second relaxation results again from the relaxation of T_m in a similar way as above v_c.

There is a distinct difference in the response above or below v_c. When v is increased from below v_c first a fast pressure drop is observed followed by a fast increase. If v is decreased from above v_c the decrease is monotonic. This behaviour is indicated in figure 27c with arrows. Evidence for this behaviour was also observed from the vibrating wire signals. In figure 27c it can be seen that also the magnitude of the fluctuations in the pressure changes around v_c. This feature is discussed in section 6.2.3.

In figure 27d an enlargement of the pressure transition for different flow velocities is presented. The detailed changes occurring in the relaxation can be observed and also the dependence on the velocity. At present the details of the transient effects are not well understood but we think that the superfluid turbulent state of the ^{4}He has a large effect on the observed time constant.

However, the time dependent phenomena we hoped to observe in the vibrating wire signal did not show up.

A relaxation time τ_r is defined as the time after which 50% of the total change of the various signals occurred. In figure 28 the results are shown. It is clear that at the critical velocity the relaxation time increases sharply and that the results of the three devices are in agreement with each other.

When the still heating power ($\dot{Q}_s$) is changed, a second-sound wave propagates from the still via the heat exchangers to the experimental space, (Kummer (1977)). At these low temperatures this is actually a counterflow wave in which the ^{3}He represents the normal fluid part. The wave will be overdamped by viscosity in the small capillaries (Murdock (1982)). Eventually the change in flow velocity will be communicated via the tube to the mixing chamber. The experiments show that at the critical velocity this transfer process changes. This must be due to the existence of the vortex tangle in the capillaries, which leads to an increase of the flow resistances. It resembles the increase of the time constant upon entering turbulent flow in thermal counterflow in pure ^{4}He II.

Fig.27a *Mixing chamber, including two vibrating wire viscometers and the pressure transducer.*
All measurements were carried out at an approximately constant mixing chamber temperature of 51 mK. The signals in figures b, c and d are shifted in the flow direction over a small distance due to recorder pen position.

27b *Relaxation experiment when $v>v_c$. Both viscometer signals (VWI and VWII) and the pressure transducer signal (C_p) are shown. The square wave of the still heater and T_e are also indicated.*

27c *Same as figure 27b, but now $v \simeq v_c$.*

27d *Enlargement of the transition above and below v_c.*

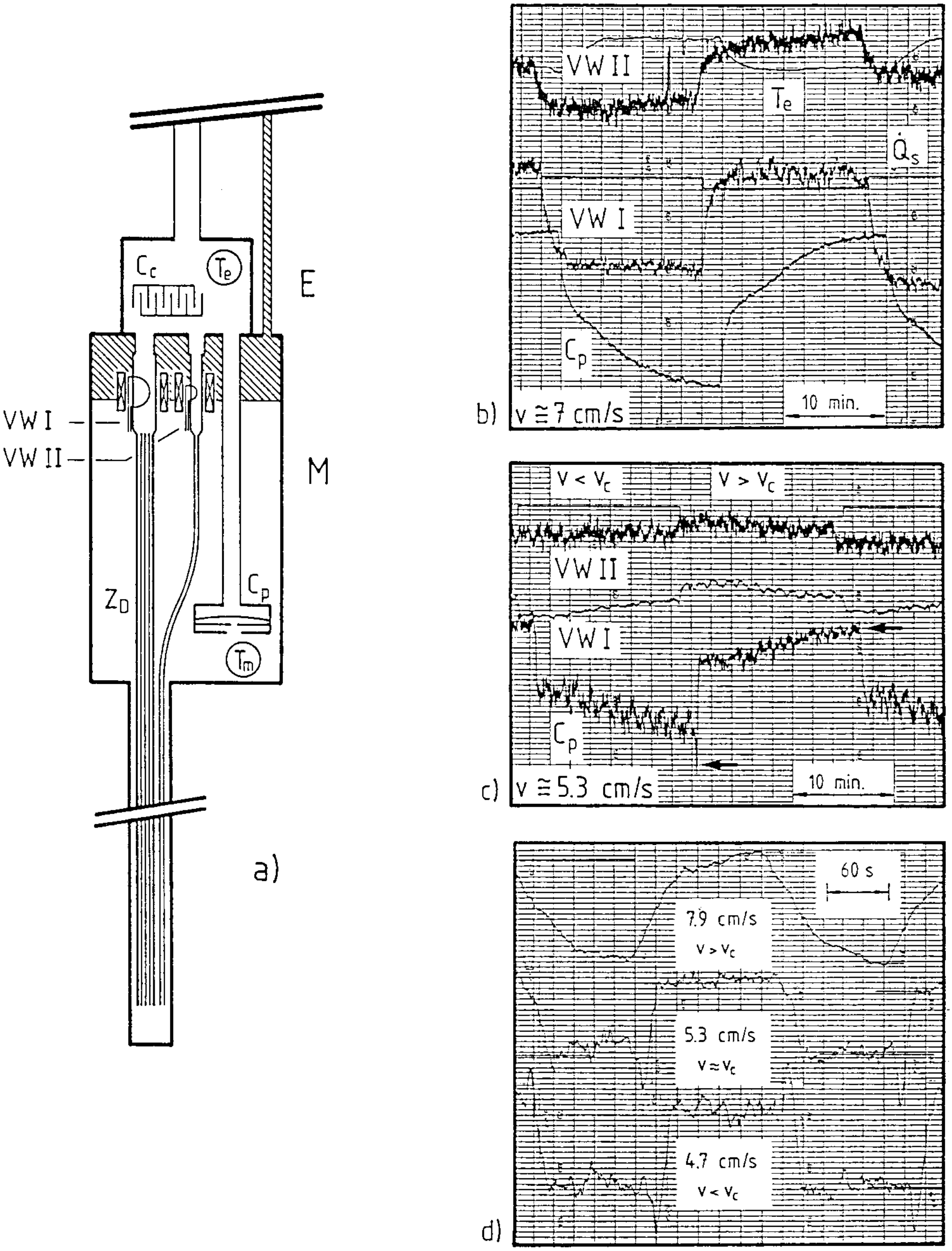
Cc
Te
E
VW I
VW II
M
ZD
Cp
Tm
a)
VW II
Te
Q̇s
VW I
Cp
b) v ≅ 7 cm/s
10 min.
v < vc
v > vc
VW II
VW I
Cp
c) v ≅ 5.3 cm/s
10 min.
60 s
7.9 cm/s
v > vc
5.3 cm/s
v ≈ vc
4.7 cm/s
v < vc
d)

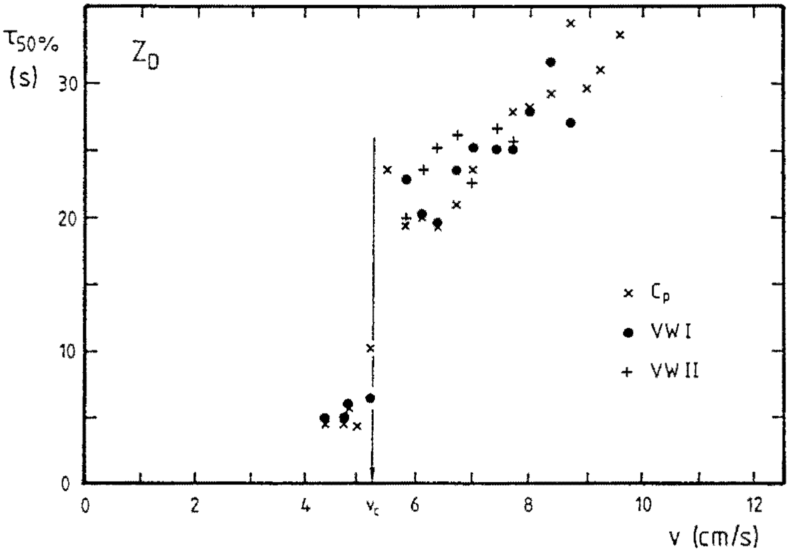

Fig.28 *The relaxation time τ_r as a function of the flow velocity. The abrupt change in τ_r corresponds with v_c.*

An experiment was carried out where the period of the square wave on the still heater was decreased. We observed that the highest frequency which can penetrate from the still to the mixing chamber is about 0.5 Hz at low flow rates below the critical velocity. The relaxation time constant is about four seconds for these velocities. The periodic perturbations of 0.5 Hz are in agreement with this relaxation time. At higher flow rates these 0.5 Hz oscillations cannot be observed anymore

The results of these experiments show that it would be interesting to carry out detailed measurements with second sound transducers normal to the flow direction to probe the turbulent state in our flow channels. Kuerten (1987b) proved that, by investigating the damping of second sound, critical velocities may be measured with this technique in ^{3}He-^{4}He II mixtures in wide tubes.

6.2.3 THE PRESSURE FLUCTUATIONS.

To investigate the dependence of the pressure fluctuations on velocity the pressure signal was recorded while the flow was increased slowly. The impedance Z_B was used to obtain the pressure-time recorder plot shown in figure 29.

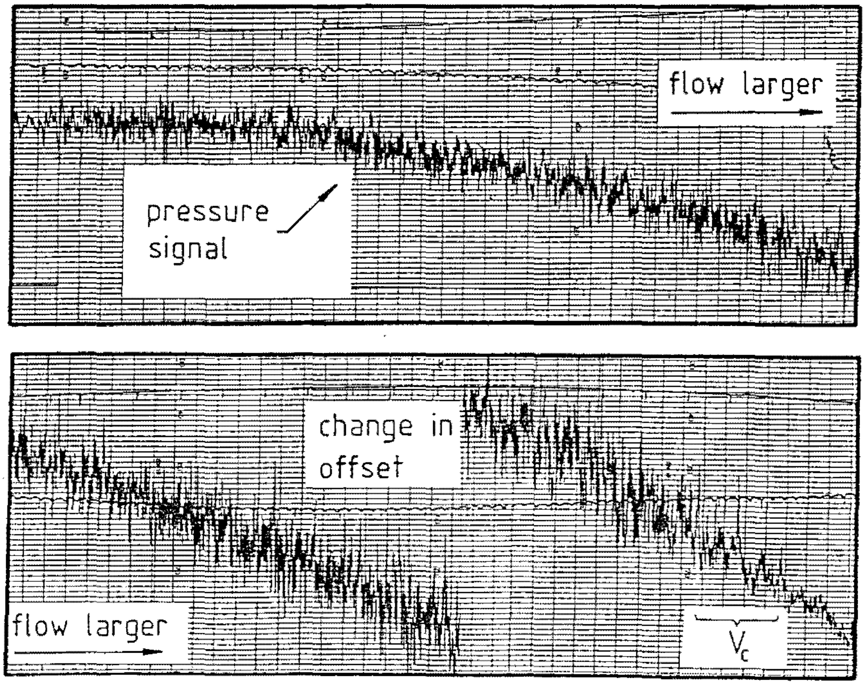

Fig.29 *Pressure signal as a function of time. Flow is steadily increased. The critical velocity is indicated. The velocity was increased from 2.6 cm/s to 7.2 cm/s in about 80 minutes, yielding a rate of increase of 0.06 cm/s per minute.*

At low velocities the fluctuations are small. They increase with flow velocity. Just below v_{c1} they are large and at v_{c1} their magnitude changes abruptly, becoming very small just above v_c. This effect was seen in many experiments with different flow impedances. The fluctuations must be related to the state of turbulence which is developing in the flow impedance. Whether this is due to the entrapment of quantized circulation as discussed in chapter 5 is not clear up to now.

6.2.4 THE FLUCTUATION SPECTRA.

The relaxation and fluctuation studies discussed in section 6.2.3 only give a qualitative picture of the phenomena. In order to obtain more quantitative information we determined the spectral behaviour of the fluctuations of the pressure signal of flow channels Z_K and Z_U. In the flow channel Z_K, which was coiled up with a diameter of curvature of 125 mm, the first and second critical velocity could be distinguished from the time averaged signal as well as in the fluctuation spectra. For the annular flow channel Z_U an apparent critical velocity could be discerned only in the time averaged measurement, whereas nothing special showed up in the fluctuations. However, from the amplitude of the spectra, obtained with different flow impedances, plotted as a function of the flow rate, a flow-dependent peak showed up which nearly coincides with the second critical velocity in Z_K. So one should be cautious about the interpretation of these peaks in terms of the critical velocity.

When a superleak was placed parallel to the flow impedance the fluctuation spectra did not show any feature at all. This provided evidence that the spectral techniques can indeed be used for the determination of the first and second critical velocity being it that the second critical velocity phenomenon will need more investigation to clear up its physical meaning.

6.3 THE STEADY STATE BEHAVIOUR.

The experimental setup is the one described by figure 7c, where flow channels can be installed outside of the mixing chamber. Two different experiments will be discussed. In one experiment only the flow channel was installed. In the other the channel was shunted by a superleak which consisted of a large diameter (12 mm) tube filled with densely packed jewelers rouge. The superfluid ^{4}He, dragged along with the ^{3}He through the flow channel when the critical ^{3}He flow rate is surpassed towards the experimental space E, now circulates back to the mixing chamber via the superleak. There is thus an internal circulation of ^{4}He between experimental space and mixing chamber, see figure 30. This flow situation resembles Staas' (1961) flow experiments in which the normal and superfluid component of the ^{4}He move together in the same direction with -apart from a small slip velocity- the same velocity. Further investigations to this type of flow were conducted by Van der Heijden (1972) - called NRS flow-, De Haas (1976) and Slegtenhorst (1979, 1981) among others. In the experiments in pure ^{4}He the chemical potential was observed to be zero. However, there still exists a vortex tangle, so L is nonzero. Van der Heijden (1974) suggests that the zero chemical-potential difference is fulfilled due to a superfluid friction F_s balancing the mutual friction F_{sn} and accounting for an extra momentum transfer to the walls.

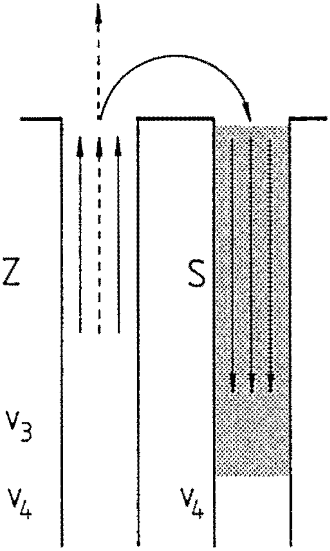

Fig.30 Schematical representation of the internal ^4He flow when a superleak is placed parallel. - - - ^3He flow, ——— ^4He flow.

In figure 31 temperature–, concentration–, pressure–, chemical potential differences and the T^2-x diagram measured with and without the superleak in parallel with this flow channel are presented. In figure 31 a–c it can be seen that for velocities below about 1.2 cm/s the results with and without the superleak both coincide with the mechanical vacuum model. At the critical velocity a nonzero chemical potential difference develops in the measurement without the superleak (figure 31d). If the velocity is increased further a kink occurs at about 2.3 cm/s. We already named the velocity at which this occurs the second critical velocity.

Figure 31 shows that in case the superleak is installed the ^{4}He chemical potential difference stays zero within experimental accuracy.

The pressure difference in case a superleak was mounted is larger than calculated with equation (2.16) over the whole measured velocity range. This can be caused by two effects or a combination of both. The first is due to the superfluid friction as mentioned by Van der Heijden (1974). However, for low velocities no such a difference should be observed. A second reason could be the curvature of the flow channel. The relevant dimensionless parameter which describes the state of the flow in a coiled tube is the Dean number De, which is defined as:

$$\mathrm{De} = \left[\frac{\mathrm{d}}{\mathrm{d_c}}\right]^{\frac{1}{2}}\left[\frac{\mathrm{d}v\rho_\mathrm{n}}{\eta}\right]. \tag{6.1}$$

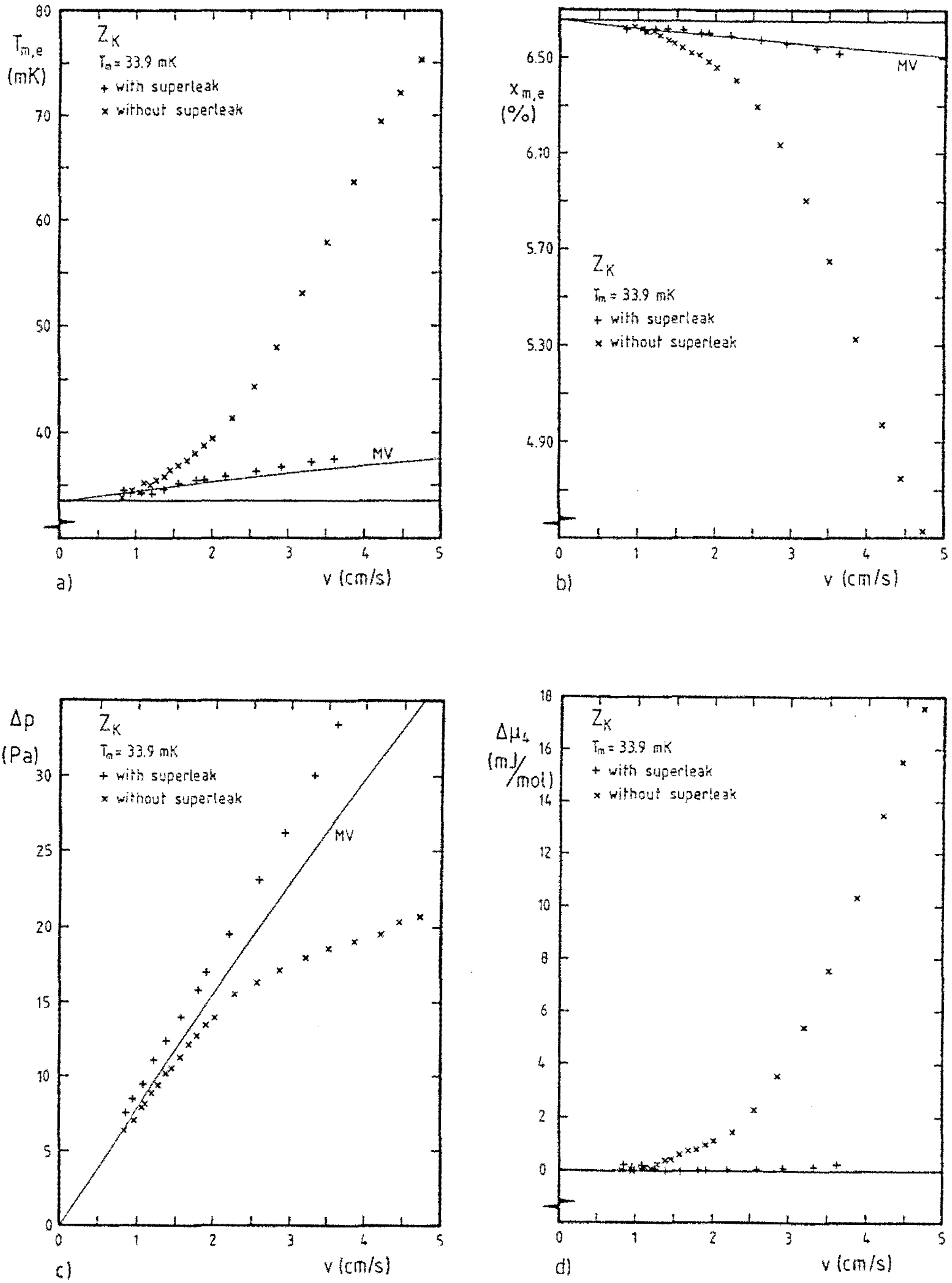
$T_{m,e}$ (mK)
80
70
60
50
40
Z_K
T_m = 33.9 mK
+ with superleak
× without superleak
MV
0 1 2 3 4 5
v (cm/s)
a)
$x_{m,e}$ (%)
6.50
6.10
5.70
5.30
4.90
Z_K
T_m = 33.9 mK
+ with superleak
× without superleak
MV
0 1 2 3 4 5
v (cm/s)
b)
Δp (Pa)
30
25
20
15
10
5
0
Z_K
T_m = 33.9 mK
+ with superleak
× without superleak
MV
0 1 2 3 4 5
v (cm/s)
c)
$\Delta\mu_4$ (mJ/mol)
18
16
14
12
10
8
6
4
2
0
Z_K
T_m = 33.9 mK
+ with superleak
× without superleak
0 1 2 3 4 5
v (cm/s)
d)

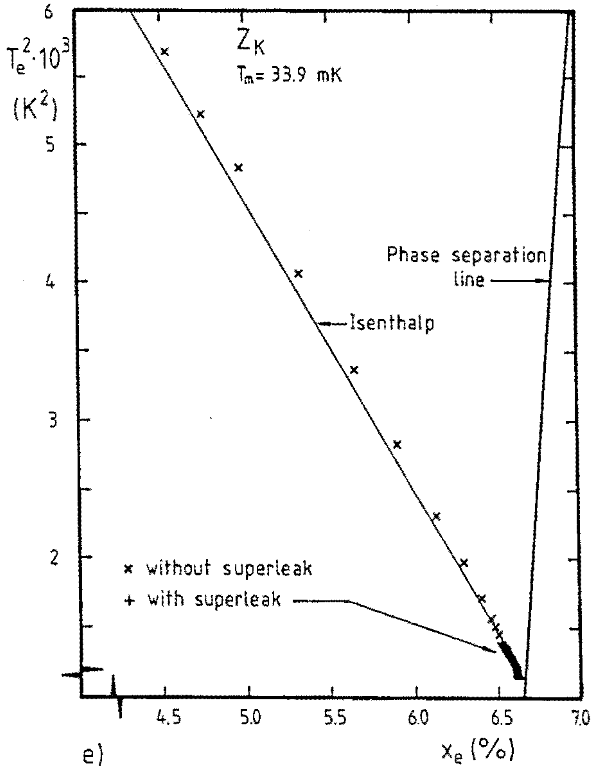

Fig.31 *The measurement with tube system* Z_K.
a) Temperature; b) concentration; c) pressure; d) chemical potential;
e) T^2*-x-diagram.*

The Dean number is equal to the ratio of the square root of the product of the inertial and centripetal forces to the viscous force. Due to the centrifugal forces a secondary flow may develop in the tube which mainly consists of two recirculating eddies along the tube axis. For Z_K, in the absence of a superleak, De≈10 at the highest flow rate. With the superleak parallel the ^{4}He moves with the ^{3}He and the total density ρ has to be used, instead of the normal component density ρ_n. In that case the Dean number can be as high as 150. This can lead to a deviation from the Poiseuille flow pattern, (Berger (1983)). As a result the pressure difference can increase by 50%. However, for the flow velocities below v_{c1} this argument does not hold as then De is too small to have influence and besides the substitution $\rho \rightarrow \rho_n$ does not hold. We think that the difference in pressure of both measurements is real, because the two measurements were carried out in two succeeding measuring runs, without dismounting the pressure transducer and only a difference in zero value of the capacitance of 0.5 % was observed between both measurements. On the basis of these results a definite conclusion cannot be drawn and the effect might be an interesting subject for future investigations.

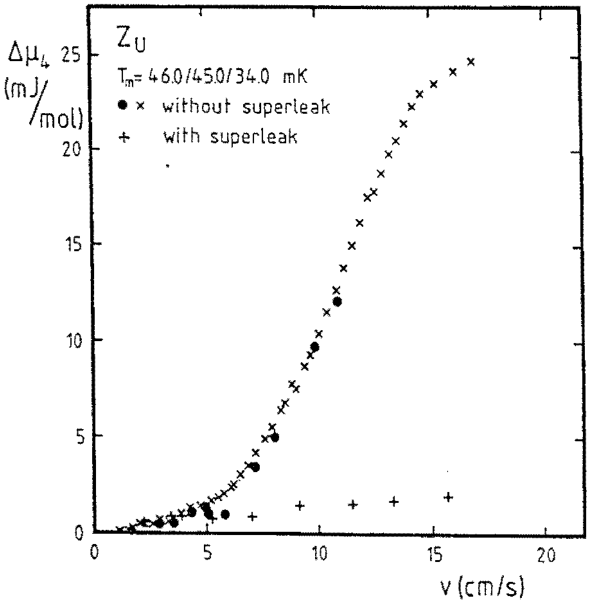

Fig.32 *Chemical potential difference for the flow channel Z_U.*

The measurements with flow channel Z_U were already presented in figures 13d–17d. Only $\Delta\mu_4$ is shown here (figure 32). In case no superleak is mounted this leads to the nonzero $\Delta\mu_4$ as usual. With a superleak $\Delta\mu_4$ is small but increases slightly with increasing velocity presumably due to a small but measurable chemical potential difference developing across the connecting tube. However, the overall behaviour with this flow channel is the same as in the case of Z_K.

6.4 THE FLUCTUATIONS.

6.4.1 FOURIER SPECTRA; INFLUENCE OF A SUPERLEAK.

The data acquisition and analysis system is schematically shown in figure 33. The capacitance of the pressure transducer is measured with the capacitance bridge in combination with a lock-in amplifier. The off-balance signal from the analogous output of the lock-in amplifier is fed to one of the ADC converters of a plotter (HP 7090A). The plotter communicates with a personal computer on IEEE basis.

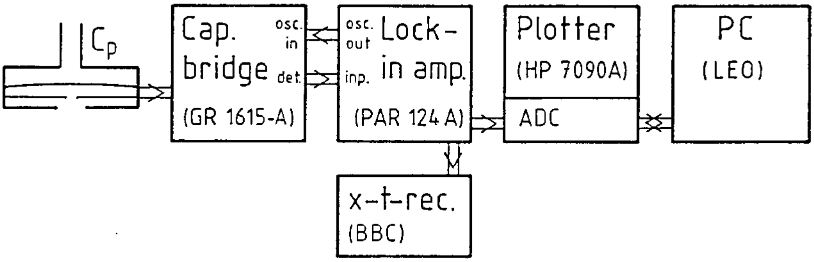

Fig.33 Experimental setup for the measurement and analysis of the pressure fluctuations.

Data are sampled with a sampling time between 3 ms and 100 ms. The Fast Fourier Transform method requires that the number of data points (n) is chosen in such a way that $n = 2^i$ where i is an integer, (Oran-Brigham (1988)). The maximum number of data points which can be handled is 4096 ($= 2^{12}$), which means that there is an upper limit to the frequency resolution in the FFT-spectra. The frequency lies in practice between 0.01 Hz and 150 Hz. Due to the finite sampling rate, frequencies above the Nyquist-frequency ($f_c = 1/2T$) can appear in the FFT spectrum at frequencies below f_c. This is called aliasing and can be prevented by removing these higher frequencies before analog-digital conversion takes place. It means that the time constant of the lock-in amplifier may not be less than the sampling time. If the time constant is taken equal to the sampling time the shape of the spectrum near the Nyquist frequency is modified, but this can be corrected for.

We have the impression that the interesting frequency range of the pressure fluctuations lies between 0.5 Hz and 5 Hz. Above 5 Hz no striking features appeared in the spectra.

We will discuss the experimental results with sampling time and time constant both 100 ms. In figure 34a-c results of the Fourier spectra are presented as obtained for flow channel Z_K without a superleak. Arbitrary units are used, which are the same in all diagrams in this section except figure 38. The results are smoothed by averaging every measurement with the two nearest neighbour points on both sides.

Figure 34a represents the FFT spectrum at a velocity of 0.58 cm/s, which is below the first critical velocity ($v_{c1} \simeq 1.2$ cm/s). There is no clear structure except for the irrelevant region at frequencies below 0.5 Hz.

The velocity of 1.06 cm/s (figure 34b) is about equal to v_{c1}. Some peaks are observed with a magnitude which is about 20-40 times higher than the amplitude of the spectrum of figure 34a. There are peaks at 0.8 Hz, 1.4 Hz and 3.4 Hz with a magnitude of 2, 4 and 2 respectively. The amplitude in the frequency range between the peaks is 7 to 8 times larger than the corresponding region of figure 34a.

In figure 34c the velocity is about equal to the second critical velocity v_{c2}. Clearly two peaks around 0.8 Hz and 1.75 Hz, with a magnitude of about 7 and 4 respectively, can be seen. The region of the spectrum between the peaks has an amplitude of a factor 10-20 times that of figure 34a.

In case a superleak is placed parallel to the flow channel the fourier spectrum changes. Figure 35 represents the situation with a velocity of 1.07 cm/s, which is the value of v_{c1} in the absence of a superleak. Due to an unstable flow during this measurement there is a large background at low frequencies. Apart from an interference at 3.85 Hz no further peaks can be distinguished. The same general behaviour occurred at all velocities which were studied. We can conclude that the phenomena as observed in the spectra clearly show the influence of the superfluid turbulence.

In figure 36 the amplitude of the spectrum at a fixed frequency is shown now as a function of the flow velocity for flow channel Z_K without the superleak in parallel. For a frequency of 0.85 Hz two strong peaks show up at two distinct velocities of about 1 cm/s and 2 cm/s. Similar behaviour is observed at other frequencies. The effect was also observed at different temperatures and in different flow systems and under different experimental conditions.

With a superleak in parallel there are no velocities at which peaks appear. The level of the FFT is on the order of 0.1-1.0, which is significantly lower than in figure 36 (not shown).

The spectra measured with the annular flow channel (Z_U) resemble those of the circular tubes. Again two peaks appeared in the spectra at about 0.9 Hz and 1.9 Hz without a superleak. These will not be discussed.

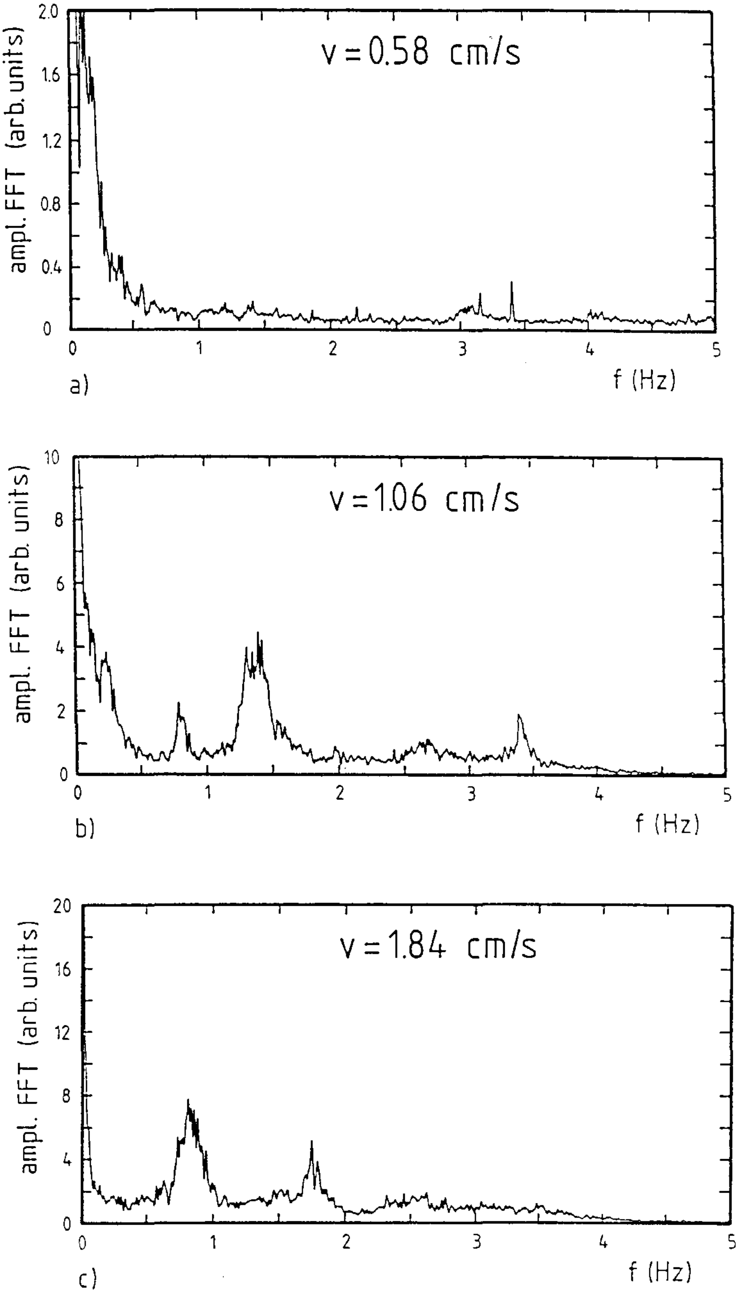

Fig.34 *FFT-spectra 0 Hz < f < 5 Hz of the pressure measurements for different flow velocities in flow channel* Z_K *without a superleak. a) v = 0.58 cm/s, b) v = 1.06 cm/s, c) v = 1.84 cm/s.*

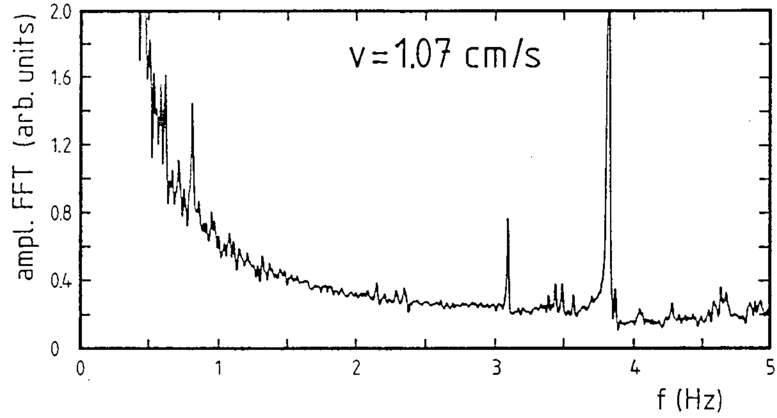

Fig.35 *FFT-spectrum 0 Hz<f<5 Hz of the pressure measurements for a flow velocity of 1.07 cm/s in flow channel Z_K in the presence of a superleak.*

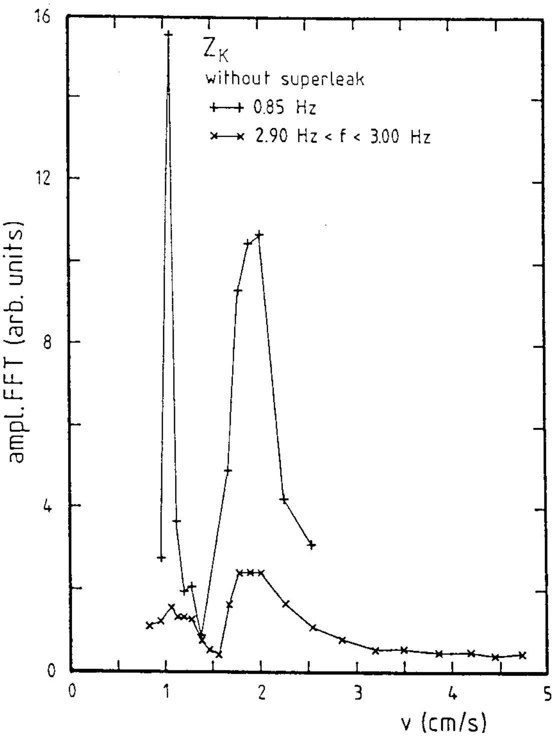

Fig.36 *Amplitude of the FFT spectrum at some frequencies as a function of the flow velocity without a superleak parallel.*

The velocity dependence of the amplitude of the spectrum at these frequencies is shown in figure 37. A peak occurs at about v=6 cm/s, but this does not coincide with the apparent critical velocity. The origin of the peak at 6 cm/s is not clear.

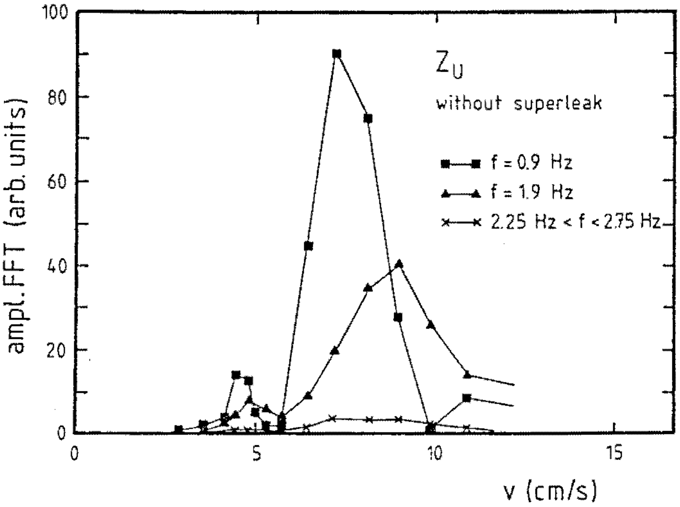

Fig.37 *Amplitude of the Fourier spectrum as a function of the flow velocity for some frequencies for flow impedance Z_U when the flow channel is not shunted by a superleak.*

When the superleak is placed in parallel, the amplitude of the Fourier signal is much smaller and no peaks occur and confirms the behaviour as was observed with Z_K.

The measurement with the annular tube was carried out with three different pressure transducers (see section 3.2.3) simultaneously mounted in the mixing chamber. All the transducers exhibit the same spectra with the same characteristic peaks at the same velocity. So the fluctuations do not depend on the type of pressure transducer.

Concerning the dependence of the amplitude of the spectra at fixed frequency on the flow channel we carried out measurements with flow channels Z_B, Z_Y, Z_M and Z_J. In figure 38 the FFT spectra are collected now plotted as a function of the molar flow rate for the frequency of 0.9 Hz. The original graphs are multiplied by a scaling factor in such a way that the magnitude of the peak around 0.5 mmol/s is the same for all flow impedances.

We observed at all frequencies a peak at ^{3}He circulation rates between 0.35 mmol/s and 0.8 mmol/s. The peak is absent when a superleak is present. Apparently, this peak is

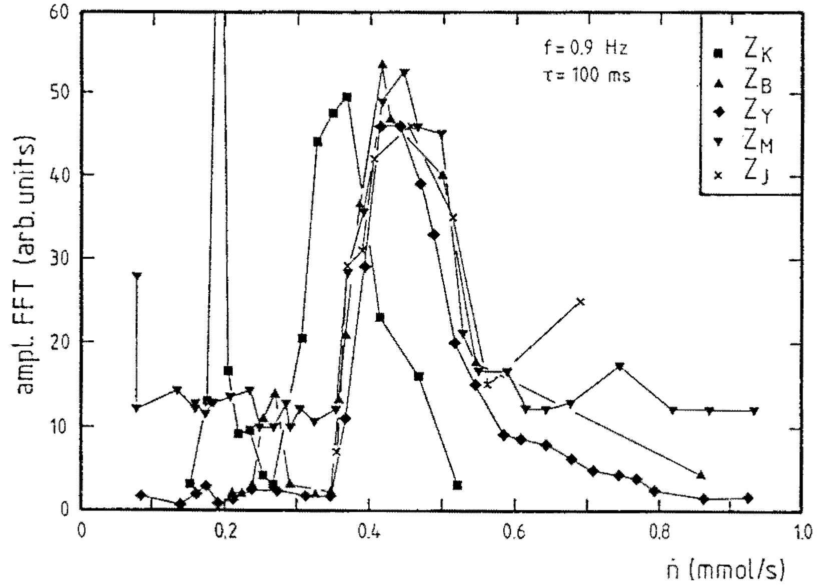

Fig.38 *The fluctuation amplitude for a frequency of 0.9 Hz as a function of the flow rate for different flow systems. The vertical scale of the different curves are multiplied by a scaling factor.*

not primarily a property of the flow channel but rather some resonance effect in the dilution refrigerator as a whole. This peak can mask a real critical velocity in our measurements or give an impression that there is a critical velocity. The origin of this resonance is unknown but must be related with the turbulence, as it disappears when a superleak is placed in parallel. The measurement with the circular tubes as discussed in section 6.3.3 is also plotted in figure 38 and does not coincide with the other curves.

One can speculate on the origin of the peak in the frequency spectrum. It is possible that in the critical velocity region vortices develop in the form of plugs, become unstable and decay again, leading to a periodic instability. This does not only remind one of the classic flow experiments of Reynolds (1883) at the end of the nineteenth century, but also on recent experiments by Griswold (1986, 1987a,b) where in pure ^{4}He, fluctuations due to vortex turbulence were observed. If vortex slippage has also influence then for the flow channels consisting of one single tube no fluctuations should occur at v_{c1}. This is in agreement with the observations with Z_M.

6.4.2 SOME ADDITIONAL EXPERIMENTS.

One may raise the question whether the FFT technique can be used to find the critical velocity in case the temperature jump at v_c is too small to be observed, e.g. because the flow channel has a low impedance. From the flow impedances Z_B and Z_K the first critical velocity could be resolved from the FFT spectra and although in the time averaged measurements the first critical velocity could be discerned also in Z_J and Z_M, the spectra did not give evidence for this. So, at present, unfortunately the FFT technique is not more sensitive to detect critical velocities. Temperature-, concentration- and pressure measurements in a stationary situation are still the best methods to reveal the critical velocity.

We also investigated whether it would be possible to measure fluctuations in the temperature. In the experiment carried out with the flow impedance Z_M a thermometer was placed inside the tube about 20 diameters (8 cm) from the end of the flow channel. This thermometer was a RuO_2 type resistor chip Bosch (1986). It was ground to a thickness of about 50 μm. An estimation of the Kapitza thermal boundary resistance (Lounasmaa (1974)) and the heat capacity (Love (1987)) yields a thermal time constant which is smaller than 100 ms at temperatures above 50 mK. Using a resistance bridge

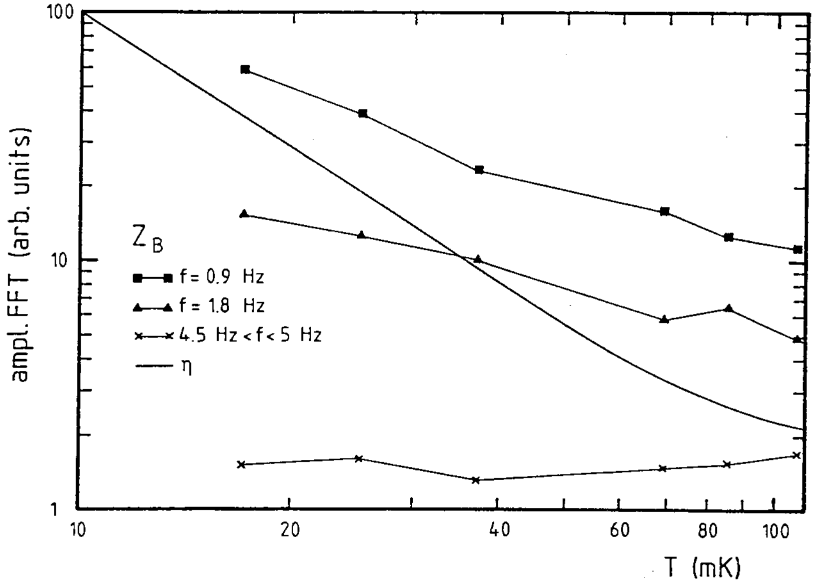

Fig.39 *Temperature dependence of the FFT spectra for three different frequencies, measured with flow channel Z_B. The temperature dependence of the viscosity is drawn multiplied by a scaling factor.*

we took spectra of the resistance fluctuations. The spectrum turned out to be flat irrespective of the flow rate. The reason why no significant temperature fluctuations were observed may be due to a rather low sensitivity which was 0.1 mK in our case. So we cannot draw a definitive conclusion.

In order to study the dependence of the fluctuations on the viscosity the FFT spectrum was measured at constant flow rate as a function of the temperature. Results are shown for three different frequencies in figure 39.

For increasing temperature the amplitude of the fluctuations decreases. The viscosity (see chapter 7), however, decreases more than the fluctuation amplitude. So the viscosity (η) is not the only parameter which determines the fluctuations. This is not surprising as we know that the fluctuations are strongly nonlinear on the flow velocity. In this context a suggested dependence of the fluctuations on a Reynolds number will not be correct.

6.5 DISCUSSION AND CONCLUSION.

In pure ^{4}He II fluctuations and oscillations in several quantities have been observed. In particular in the studies carried out at Leiden by Marees and Slegtenhorst (1977-1987) temperature fluctuations were observed in metal and glass capillaries which were caused by plugs of turbulence moving up and downstream. Fluctuations have also been studied by means of other techniques, see for instance Griswold (1986, 1987a,b) and related work. Griswold also analyzed the signal of a pressure transducer by means of spectral methods. He observed that, in the transition region TI→TII, the amplitude of the fluctuations is large and outside this region it is small. The characteristic frequencies were found to lie in between 0.1 Hz and 5 Hz. So Griswold's work is qualitatively in agreement with our results in mixtures as we observe large fluctuation amplitudes at v_{c1} and at the possible v_{c2} and outside this region the amplitude is small. The characteristic frequencies we observe lie in between 0.5 Hz and 5 Hz.

Concluding we can remark that for the first time fluctuation spectra of the pressure difference across a flow channel have been measured in a dilution refrigerator. The pressure transducer is an instrument capable of measuring frequencies at least up to 50 Hz and is therefore fast in comparison with thermometry at low temperatures. At the first critical velocity the fluctuation amplitude of the pressure is strongly velocity dependent. Furthermore it is shown that these fluctuations are related with the development of superfluid turbulence as, in the case that a superleak is mounted parallel to the flow channel, the fluctuations practically disappear. Indications of a second critical velocity were found. The results should be analyzed carefully as measurements with different flow impedances show that at some specific ^{3}He flow rate a maximum occurs for all impedances. The behaviour observed in the pressure difference, when a superleak is mounted in parallel, shows that there is an analogy of our experiments with pure ^{4}He experiments, where the normal and superfluid component move together with the same velocity in one direction.

The spectral technique is possibly a powerful expedient to detect v_{c1} and v_{c2} and might be used to analyze the vortex dynamics in the flow of mixtures. Temperature and concentration fluctuations have not been seen up to now and are a challenge for the future.

CHAPTER 7

VISCOSITY MEASUREMENTS

7.1 INTRODUCTION.

In chapter 4 it was shown that in the mechanical vacuum approximation our measured pressure differences did not agree with pressure differences based on equation (2.16). Therefore it was decided to measure the shear viscosity of the mixture along the phase separation line as a function of the temperature by an independent method. A list of experimental data of the viscosity of ^{4}He, ^{3}He and mixtures is given in appendix A.

Measurements along the phase separation line have been carried out by Black (1971) and Kuenhold (1972, 1973a,b), and for temperatures below 10 mK by Guénault (1982, 1983) and Bradley (1982a). No detailed values of the viscosity between 10 and 200 mK were available at the time this work was started. However, recently during the finishing stages of this thesis, the work of Bradley (1990) appeared and at the 19th International Conference on Low Temperature Physics measurements on the viscosity of mixtures along the phase separation line were presented by König (1990). We will come back to these measurements in section 7.5.

We decided to use the vibrating wire viscometer because it is a relatively small instrument, it is simple to construct and it measures the viscosity locally and fast. To develop it as a reliable viscometer a device was built in which different wires could be tested and a variable magnetic field could be applied. The reliability of the measuring technique could be verified by comparing our results with the known viscosity in pure ^{4}He.

In section 7.2 the theory of the vibrating wire viscometer will be summarized. In section 7.3 the results of the experiments in pure ^{4}He are summarized. Section 7.4 deals with the setup and technique used for the determination of the viscosity of mixtures. Section 7.5 deals with the results of the measurements of the viscosity of ^{3}He-^{4}He II mixtures along the phase separation line between 7 mK and 200 mK. Section 7.6 concludes this chapter.

7.2 THEORY OF THE VIBRATING WIRE VISCOMETER.

The basis for the measurement of the viscosity using a vibrating wire is the damping of an oscillating circular cylinder in a liquid due to viscosity. Stokes (1851) derived the equations for the force acting on a circular cylinder vibrating in a liquid from the Navier Stokes equation. Tough (1963-1965) introduced the application of a vibrating wire for the measurement of the viscosity of liquid helium. Since then the vibrating wire has been used at many laboratories to measure the viscosity of quantum fluids. A detailed presentation of the theory can be found in Retsina (1986, 1987). In the treatment below only the main results will be described.

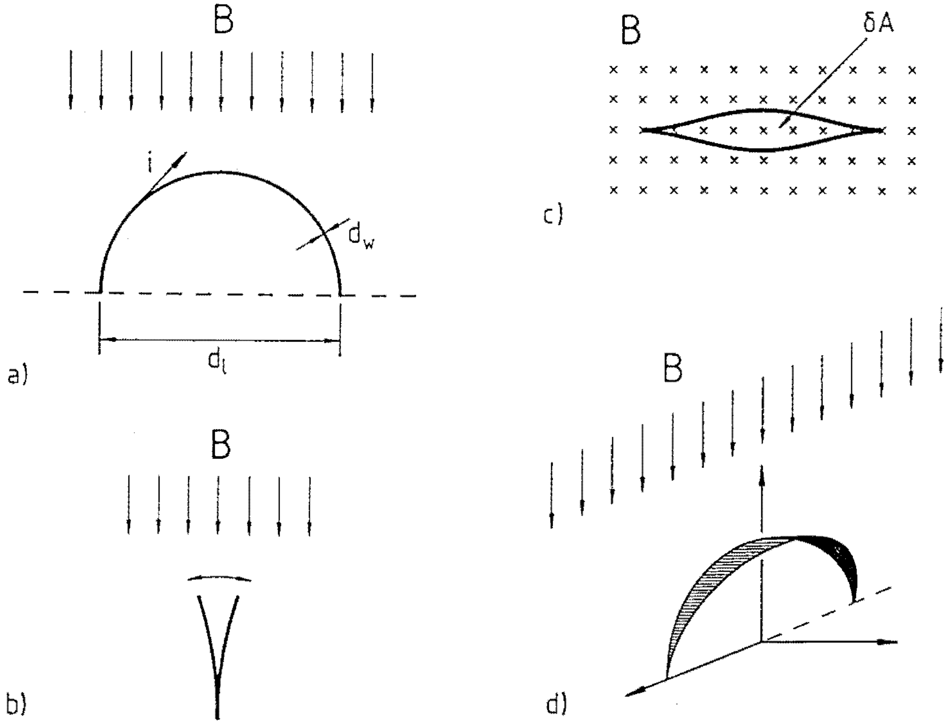

Fig.40a–d Vibrating wire viscometer in different projections.

We used a vibrating wire viscometer consisting of a half circular loop with loop diameter d_l and wire diameter d_w placed in a magnetic field B (figure 40). If an a.c. current:

$$i = i_0 e^{j\omega t} \tag{7.1}$$

is passed through the wire then, due to the Lorentz force, the wire oscillates with an angular frequency (ω). The elastic spring force tends to drive the wire back to its equilibrium position. In a liquid, there is also a force on the wire due to the liquid. Due to the motion of the wire the magnetic flux in the voltage loop changes (figure 40d). The induced voltage is measured.

In Retsina (1986) the equation of motion is derived. We will only treat the main results. The force by the liquid on the wire plays an important role and will be discussed in somewhat more detail.

For a circular cylinder oscillating with a displacement:

$$u = u_0 e^{j\omega t}\ , \tag{7.2}$$

the force on the wire due to the liquid per unit of length is given by:

$$F_d = -\omega^2 M' u_0 e^{j\omega t}(-k + jk') \tag{7.3}$$

where M' $= \frac{1}{4}\rho\pi d_w{}^2$, which is the mass of the displaced fluid
ρ = density of the fluid
k,k' = Stokes functions, these will be discussed below.

The force F_d is the force as derived by Stokes in the linear regime. The reduced amplitude of displacement (u_0/d_w) of the wire is small.

The Stokes functions are functions of the parameter m, which is defined as:

$$m = \frac{d_w}{4\delta_v} \tag{7.4}$$

where δ_v is the viscous penetration depth, defined as:

$$\delta_v = \sqrt{\eta/\rho\omega}\ . \tag{7.5}$$

This penetration depth is the characteristic length over which vorticity diffusion takes place. These functions are tabulated in Stokes' paper. They can also be calculated using the analytic form of the functions. We used the equation of Goodwin (1968) with an accuracy of 1% for m>0.1 as defined:

$$m = m_0 - 0.02383 \exp(-0.3602 m_0) \tag{7.6}$$

$$m_0 = \sqrt{2}\,\frac{1+\sqrt{1+k'}}{2k'} \,. \tag{7.7}$$

The functions k' and k are shown in figure 41.†

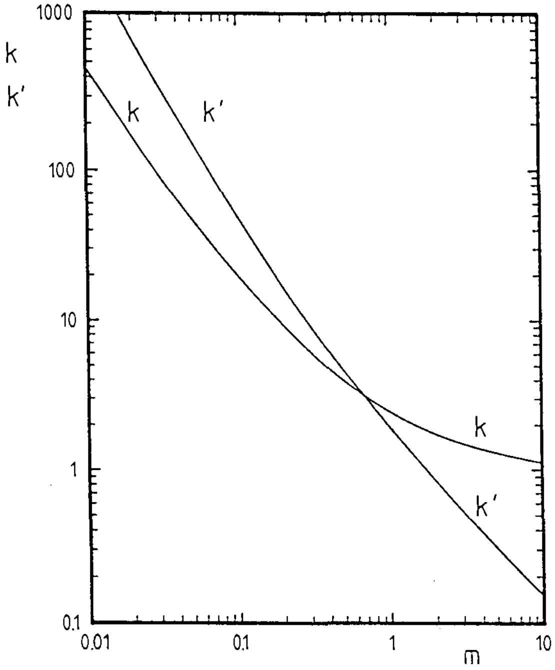

Fig.41 The functions k and k'.

Equation (7.3) contains a term $-k\omega^2 M' u_0 e^{j\omega t} = kM'\ddot{u}$, where $\ddot{u} = d^2u/dt^2$, in which kM' represents the effective accelerated liquid mass. The second term in equation (7.3) given by $k'M'\omega\dot{u}$ causes the damping of the motion of the cylinder.

If in Retsina's treatment damping in the wire is neglected the equation of motion is obtained as:

$$(M+kM')\ddot{u} + \omega k' M' \dot{u} + M\omega_0^2 u = F_L \,. \tag{7.8}$$

In this equation F_L is the Lorentz force and M ($=\frac{1}{4}\pi\rho_w d_w^2$) is the mass of the wire per unit of length. The term $M\omega_0^2 u$, in which ω_0 is the resonance frequency in vacuum, results from linearization of the elastic forces. The amplitude u is in principle a function of the coordinate along the radius of the wire and the most detailed mathematical derivation is given in Retsina's work. For harmonic motion the induced voltage is given by:

---

† In Goodwin's thesis a misprint occurs: he quotes the value 0.2383 instead of the correct value 0.02383.

$$V_i = V_0(V_1 + jV_2) \tag{7.9}$$

where:

$$V_1 = \frac{\rho k' \omega^3}{\left[\rho_w \omega_0^2 - (\rho_w + \rho k)\omega^2\right]^2 + \rho^2 k'^2 \omega^4} \tag{7.10}$$

$$V_2 = \frac{\omega(\rho_w \omega_0^2 - (\rho_w + \rho k)\omega^2)}{\left[\rho_w \omega_0^2 - (\rho_w + \rho k)\omega^2\right]^2 + \rho^2 k'^2 \omega^4} \,. \tag{7.11}$$

V_0 is a parameter which depends on magnetic field, driving current, wire diameter and a constant geometry factor. The function V_1 is proportional to the voltage in phase with the current and is called the 0° signal. It has a maximum if:

$$\omega^2 = \frac{\omega_0^2}{1 + k\rho/\rho_w} \equiv \omega_r^2 \tag{7.12}$$

with ω_r the angular resonance frequency in the liquid. Equation (7.12) is correct provided that:

$$\rho(k + k')/\rho_w \ll 1 \,, \tag{7.13}$$

which is always satisfied in the experiments. The function V_2 is proportional to the 90° signal. Its magnitude is zero for $\omega = \omega_r$. It has a maximum for:

$$\omega^2 = \frac{\omega_0^2}{1 + (k + k')\rho/\rho_w} \equiv \omega_-^2 \tag{7.14}$$

and a minimum for:

$$\omega^2 = \frac{\omega_0^2}{1 + (k - k')\rho/\rho_w} \equiv \omega_+^2 \,. \tag{7.15}$$

In figure 42 the two signals are given as functions of ω. The width $\omega_+ - \omega_-$ of the resonance curve is related to the damping of the wire in the liquid. On the condition (7.13) it can be derived for a quantum liquid that:

$$\omega_+ - \omega_- = \Delta\omega_\eta = \omega_0 \frac{\rho_n k'}{\rho_d} \,. \tag{7.16}$$

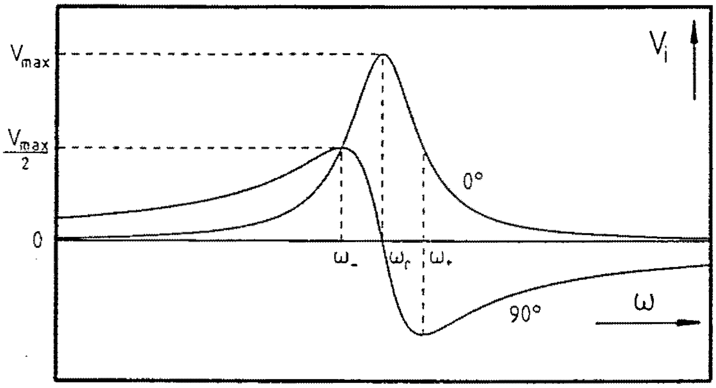

Fig.42 The 0° and 90° induced signal (equations (7.10) and (7.11)) as a function of the angular frequency.

In reality there is always a small non-zero internal damping which contributes to the measured peakwidth. Therefore the peakwidth in vacuum $\Delta\omega_0$ has to be measured and this value has to be subtracted from the measured peak width in the liquid to obtain the correct peakwidth due to viscous damping only. In general $\Delta\omega_0$ cannot always be determined accurately and to obtain reliable viscosity results it is important that the vacuum damping is as small as possible so that an error in $\Delta\omega_0$ hardly contributes to the viscosity.

From the measured peakwidth in the liquid and the resonance frequency in vacuum k′ can be calculated, provided that ρ_n and ρ_w are known. Using (7.6) and (7.7), m can be calculated. Finally η can be calculated using (7.3) and (7.4) by:

$$\eta = \frac{d_w^2 \rho_n \omega_r}{16 m^2} . \tag{7.17}$$

The frequencies occurring in the measurements are on the order of a kHz, whereas the peakwidth is in general on the order of 1 Hz and so is much smaller.

7.3 A SUMMARY OF THE RESULTS OBTAINED IN PURE ^{4}He.

The theory as presented in section 7.2 is only correct if a number of criteria are satisfied. In summary:

a) The liquid is assumed incompressible.
b) The non-linear terms in the Navier-Stokes equation are negligible.
c) The vibrating wire can be approximated as an infinitely long straight cylinder.
d) There is no influence of the non-zero mean free path.
e) Outer boundaries are sufficiently far removed from the wire.
f) Viscous heating and sound radiation effects are small.
g) In the case of mixtures there are no slip effects at the wire surface due to a thin pure ^{4}He boundary layer.

Most of these conditions (a,e,f,g) are in general satisfied.

Before we started the investigation to the viscosity of mixtures a number of different vibrating wires were studied in a separate setup. The specifications of the wires are shown in appendix B and are indicated with W_A-W_S. A detailed description of the setup, measuring technique and the experiments will be published elsewhere. From this investigation the following results were obtained (in summary).

The reduced amplitude (u_0/d_w) must be smaller than 0.1 for measurements in ^{4}He I and smaller than 0.03 in ^{4}He II. The Reynolds number, based on the diameter of the wire, has no influence on the measured viscosity for these small relative amplitudes up to at least Re = 100. This observation is in agreement with the literature, see for instance Stuart (1963), Riley (1966), Sarpkaya (1986), Bearman (1985) and Mostert (1989).

For NbTi multifilamentary wire a strong magnetic-field dependent peak width appears. This wire (W_G) is unsuitable for viscosity measurements.

The internal damping has to be determined at a gas pressure below 0.5 torr. It is recommended to carry out measurements at a constant induced voltage. The accurate determination of the vacuum peakwidth is important in the temperature range where the viscous damping is small. In mixtures below 80 mK and in ^{4}He II an incorrect vacuum peak may lead to sizable errors in the viscosity.

Stainless steel has a large internal damping, besides, the resistive heating is large and this material is not recommended for application as a viscometer.

The ratio d_l/d_w must not be smaller than 40.

The best choice for the wire materials are like Ta, Nb or Ir, in combination with a magnetic field below the critical field.

To check the accuracy and reliability of our techniques the measured viscosity of ^{4}He II at s.v.p. is presented here as a function of the temperature (figure 43).

In appendix A a collection of data is presented. Guided by this diagram and the

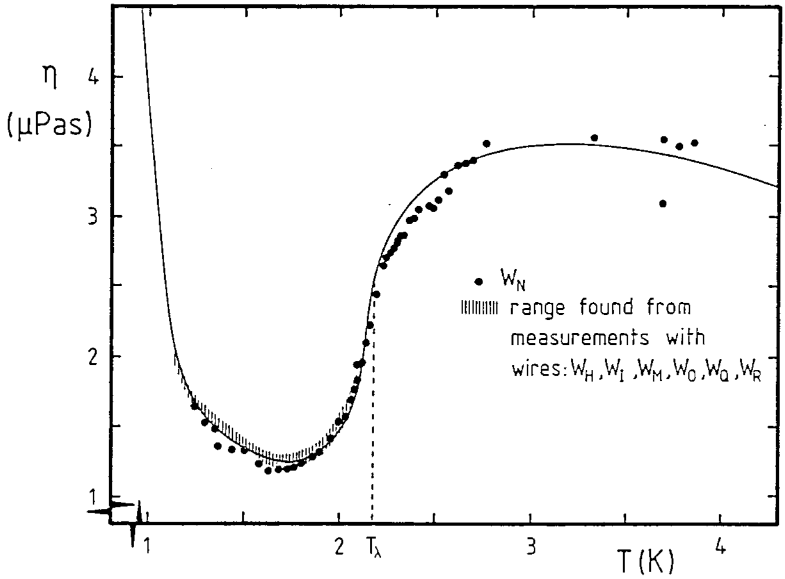

Fig.43 Viscosity results compared with literature values (full curve).

reviews of Barenghi (1981, 1983a) the full curve was drawn. Most of our measurements are situated in the shaded area. In the measurement using W_N a careful calibration of the thermometer was carried out and the viscosity was measured as accurate as possible. The agreement with the full curve is good.‡

Stimulated by this result we measured the viscosity of liquid ^{3}He-^{4}He mixtures of the dilute phase below 200 mK. This will be described in the next sections.

---

‡ Our measurements were carried out at a number of wire frequencies between 400 Hz and 2200 Hz. A similar experiment was also carried out by Nadirashvili (1978, 1979) using a stretched string as a vibrating wire. In contrast with Nadirashvili's results we did not observe any dependence of the viscosity on the frequency.

7.4 MEASUREMENTS IN THE DILUTION REFRIGERATOR.

7.4.1 EXPERIMENTAL SETUP.

The experiments were carried out with one or more viscometers placed in the saturated dilute phase in the mixing chamber. A viscometer holder was made of Araldite (figure 44).

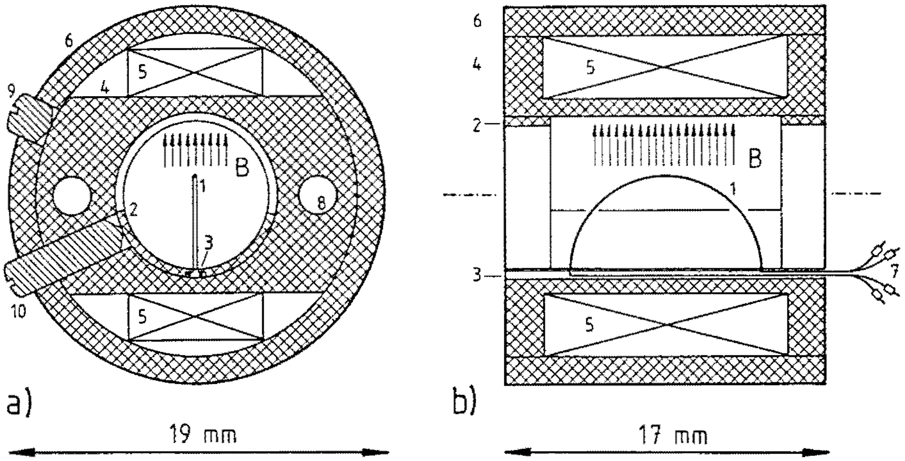

Fig.44 *Two cross sections of the vibrating wire viscometer holder, $B = 80\ mT$.*
a) Perpendicular to the loop. b) Parallel to the loop.
1) vibrating wire; 2) cylindrical wire holder; 3) slit for guiding wire connector; 4) magnets holder; 5) magnets; 6) bounding cylinder; 7) connectors; 8) M2 holes; 9)10) setscrews. The arrows give the direction of the magnetic field.

The support frame of the vibrating wire viscometer is formed by two cylinders between which two permanent magnets are clamped. The wire is supported by a thin walled (0.5 mm) cylinder which fits in the magnet holder. In the bottom of the wire holder a slit is made (0.5 mm × 0.3 mm) over the whole length. The vibrating wire is glued in two holes. The holes end in the slit which guides the leads to the current and voltage terminals. The threaded holes are used for mounting the assembly in the mixing chamber. The setscrews fix the components.

The magnets of this holder are made of neodymium and generate a field at the wire position of 80 mT. The maximum d_l which could be used without interference with the walls was about 6 mm.

Two more viscometer holders of a similar design were built with different magnetic fields. We will identify the viscometers by their magnetic fields as the 80 mT, 30 mT, 17 mT viscometer respectively.

These viscometers have a typical size of 2 cm. In fact they can even be made smaller, fitting in a cubic centimeter. A second advantage of this construction is that the vibrating wire can be replaced easily.

7.4.2 MEASUREMENT OF THE VISCOSITY.

The viscosity can be determined using the analysis of section 7.2. For the calculation of η, the normal fluid density (ρ_n) has to be determined for a mixture. To this end the concentration (x) is calculated from T according to equation (4.9). From the concentration the density ρ_3 of the ^{3}He in the mixture can be determined using an expression of Kuerten (1985) which holds for $x \geq 0.066$:

$$\rho_3 = 0.1437+104.5x. \tag{7.18}$$

In mixtures the density ρ_n has to be calculated using the effective mass $m^* = 2.46\ m_3$, (Kuerten (1985)):

$$\rho_n = \frac{m^*}{m_3}\rho_3 = 2.46\ \rho_3. \tag{7.19}$$

The determination of the temperature, was discussed in section 3.2.1. For T<20 mK we used CMN thermometry and for T>20 mK calibrated Speer resistors were used.

In the second table in appendix B the parameters of the wires which were used in the mixing chamber are shown. One viscometer was placed in the mixing chamber most of the time. In one occasion three viscometers, W_V, W_W and W_Y, were placed simultaneously in the mixing chamber. Viscometer W_U proved to be unreliable during a number of measurements and all the results were rejected.

Measurements of the peakwidth were carried out as a function of the temperature in a situation when the temperature was constant. Care was taken that the conditions under which the measurements were performed satisfied the criteria listed in section 7.3.

Apart from the measurements with the vibrating wire viscometers we also performed a viscosity measurement using the pressure transducer in combination with flow channel Z_Z. The slit width of this flow channel was machined very carefully with an accuracy of 1 μm. Furthermore, it was designed in such a way that even at mixing chamber temperatures of about 7 mK viscous heating could be neglected. Then it follows from (2.12):

$$\Delta p = -\eta \dot{n}_3 V_3 \zeta \ell \tag{7.20}$$

and η can be calculated directly from the pressure difference (Δp). Due to the low impedance ($\zeta\ell$) of the flow channel the contribution due to the connections, which amounted about 6%, had to be taken into account. The pressure differences were on the order of 0.02-0.5 Pa. We estimate the error of this technique about 2%.

7.5 THE VISCOSITY OF THE ^{3}He-^{4}He MIXTURE ALONG THE PHASE SEPARATION LINE.

7.5.1 THE RESULTS.

The results of our viscosity measurements with the viscometers and with the pressure difference method are presented in figure 45. The two methods yielded consistent results.

The viscosity was measured from about 7 mK to 400 mK. Above 200 mK, however, the results are unreliable because the temperature T_i becomes so large that presumably vapour bubbles are created in the ^{3}He flowing towards the mixing chamber. This leads to instabilities in density and temperature.

One of the drawn lines in figure 45 represents equation (2.13). A fit can be made to the data between 7 mK and 60 mK, leading to:

$$\eta = (7.6\pm1.6)\cdot10^{-8}/T^{1.80\pm0.08} \tag{7.21}$$

where η is expressed in Pas and T in K.

In figure 46 the product ηT^2 is plotted as a function of T. The difference with equation (2.13) is apparent. A linear fit was made to the ηT^2 data below 80 mK leading to:

$$\eta = \frac{(2.7\pm0.2)\cdot10^{-8}}{T^2} + \frac{(34\pm3)\cdot10^{-8}}{T} \tag{7.22}$$

where η is expressed in Pas and T in K.

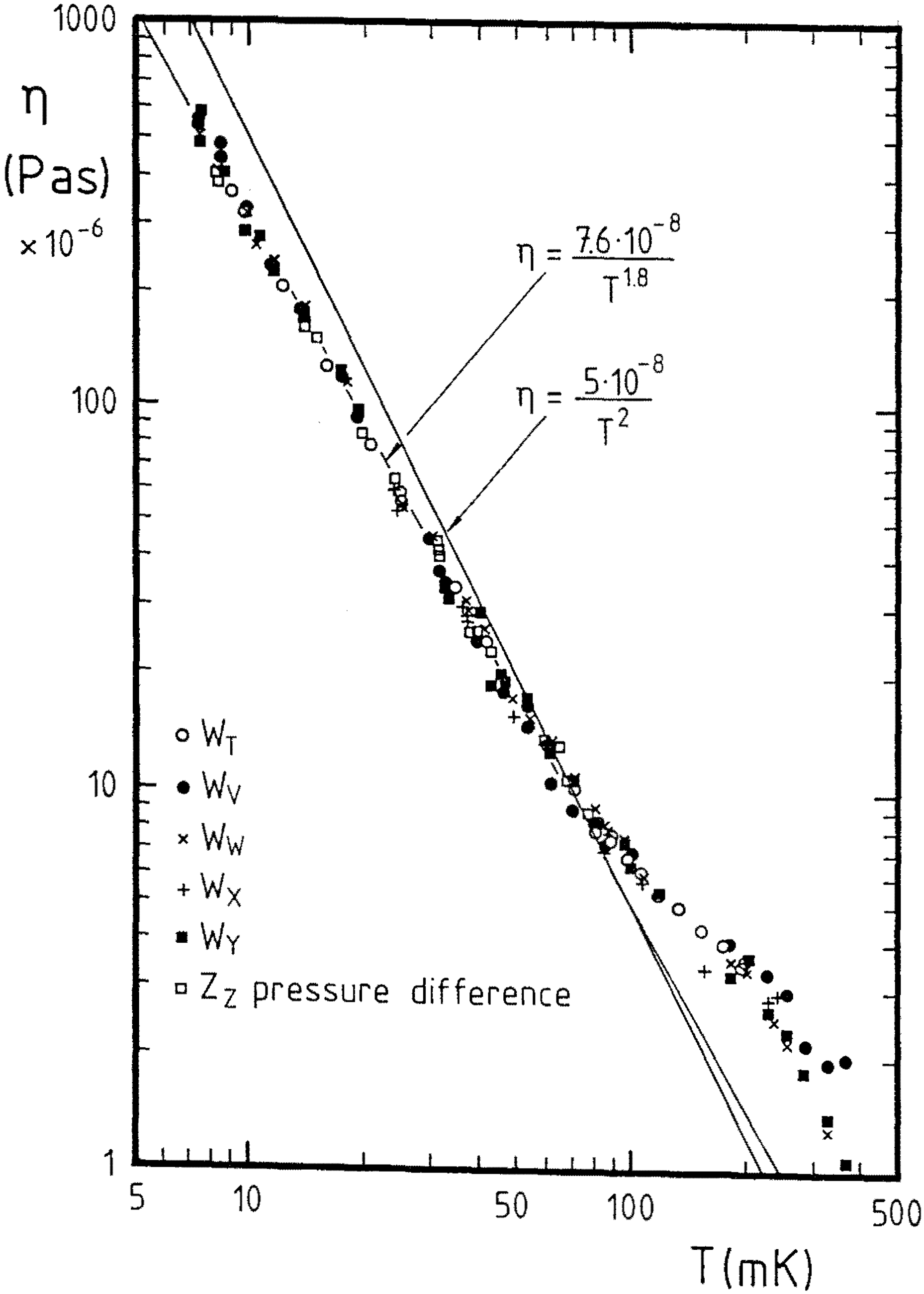

Fig.45 *The measured viscosity of the ^{3}He-^{4}He mixture along the phase separation line. The drawn lines represent equations (2.13) and (7.21).*

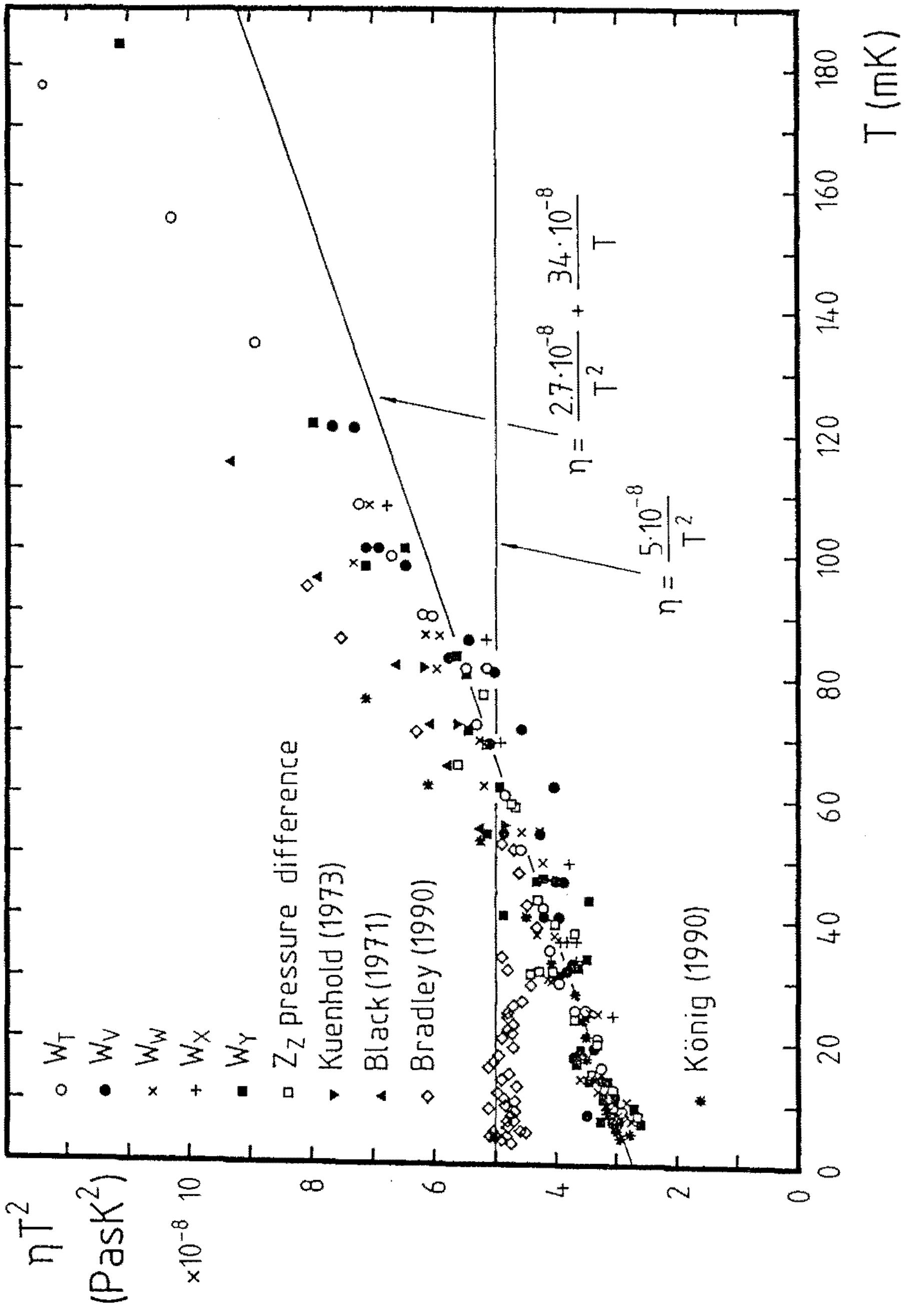

Fig.46 The product ηT^2 as a function of T.

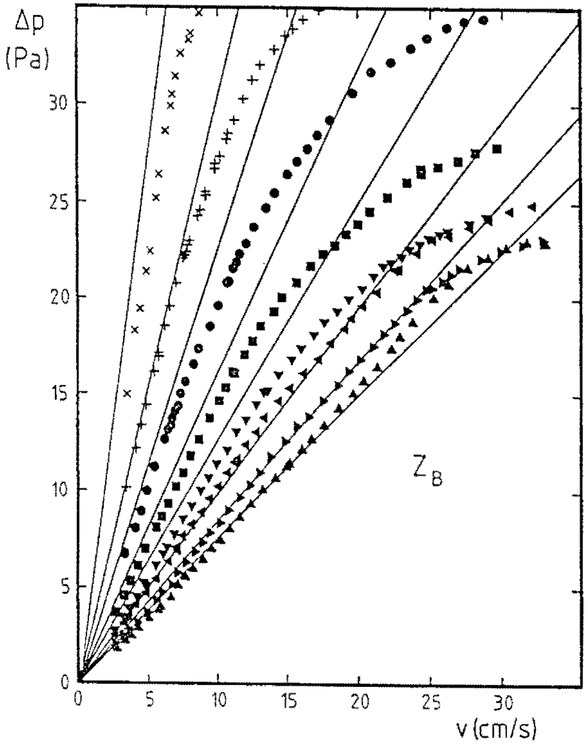

Fig.47 Pressure differences using Z_B. The drawn lines are calculated using the measured viscosity. For the meaning of the symbols compare figure 15e.

An interesting aspect of the measured η value is the improved agreement with the measured pressure differences. To show this the lower part of figure 15e is reproduced in figure 47 and the pressure differences are calculated using the measured viscosity data. (drawn lines). The agreement is much better now although not yet perfect. The small ℓ/d ratio, incorrect zero point estimation, and changes of the pressure cell calibration may lead to these errors.

7.5.2 COMPARISON WITH RELATED WORK.

Finally we compare our results with other work, see figure 46. In appendix A the viscosity measurements at higher temperatures and of pure ^{3}He are presented.

Measurements of the viscosity of ^{3}He-^{4}He mixtures were published by Kuenhold

(1972, 1973a,b) from the pressure difference across a capillary and by Fisk (1972, 1973) using a vibrating wire viscometer. Their values were in agreement with each other. Only a few data points were obtained by Kuenhold at the phase separation line indicated as triangles in figure 46 and are in reasonable agreement with our results.

The values of Black (1971) along the phase separation line down to 115 mK are also plotted in figure 46. They are systematically larger than our values. The deviation becomes larger at increasing temperature.

Guénault (1982, 1983) and Bradley (1982a) measured the viscosity below 10 mK. In their articles no viscosity values were given but we calculated η using their measured peak widths. The values are shown in the appendix figure A3. Their values are in agreement with ours. Below about 6 mK, effects of mean free path may no longer be neglected.

During the writing of this thesis the results of Bradley (1990a) were published. The viscosity was measured in the mixing chamber of a dilution refrigerator, in the same way as we did, from 3.7 mK up to about 100 mK. They used the phase separation line data of Kuerten (1985) and also used equation (7.19). Above 70 mK their values are somewhat larger than our values (figure 46). In the range 40 mK-70 mK they agree within error. Below about 40 mK their values follow a relation $\eta = 4.8 \cdot 10^{-8}/T^2$. Below 40 mK the difference between the measurements is substantial. However, via private communication (Pickett (1990)) we were informed that there may be a calibration problem of their thermometer at lowest temperature.

At the 19th International Conference on Low Temperature Physics the results of the Bayreuth group were presented (König (1990)). These results are also drawn in figure 46. Their values agree below about 40 mK with our data, so we tend to believe that our data are correct in this temperature range. In addition our measurements with vibrating wires and the pressure cell are consistent.

At temperatures above 60 mK our ηT^2 values are systematically about 10^{-8} PasK^2 lower than the measurements obtained at other laboratories. In this temperature range the accurate determination of the vacuum peakwidth is important.

7.6 CONCLUSION.

The vibrating wire is a small and efficient instrument to measure the viscosity. However, several constraints have to be satisfied. Especially the reduced amplitude should be smaller than 0.1 in normal liquids and smaller than 0.03 in quantum liquids.

An increase in magnetic field leads to an increase in peak width. This effect is very large for multifilamentary NbTi wire, which we advise not to use for viscosity measurements.

An accurate measurement of the viscosity in liquids with small η can only be carried out if the peak width in vacuum is known as a function of the reduced amplitude. Experiments have to be carried out using the same amplitude of the peak voltage.

A vibrating wire using permanent magnets can be made very small and is suited for the measurements of η of ^{3}He-^{4}He mixtures at low temperatures.

The viscosities measured in this work with many different viscometers in pure ^{4}He II and in mixtures are consistent. The values of the viscosity of ^{4}He II found in this work are in agreement with the literature.

Our measurements of the viscosity of a dilute mixture of ^{3}He-^{4}He along the phase separation line below 60 mK are in agreement with other workers. The difference at higher temperatures of about 10^{-8} PasK^2 in ηT^2 remains to be settled in the future and might be due to an incorrect determination of the vacuum peak. Using our measured viscosity better agreement is obtained with the pressure measurements as determined in the flow experiments described in chapter 4.

APPENDIX A

A SUMMARY OF VISCOSITY MEASUREMENTS IN THE HELIUM LIQUIDS

This appendix contains a survey of the data of the viscosity of pure ^{4}He (figure A1 and A2) and of pure ^{3}He and of ^{3}He-^{4}He mixtures (figure A3).

The measurements of the ^{4}He viscosity are presented in two groups, one in which oscillating disks, spheres and cylinders were used and the second group which includes all the other methods. In the oscillating systems the product $\rho_n\eta$ is measured so ρ_n must be known accurately. This implies that the temperature must be measured very carefully. But also the hydrodynamic constraints are important. For the rotating cylinder viscometers a discussion of these aspects was given by Donnelly (1987, 1988) and Barenghi (1988). We chose the preferred viscosity guided by Barenghi's paper (1981, 1983a).

The viscosity of mixtures down to very low temperatures was measured by Kuenhold (1972, 1973a,b), Fisk (1972, 1973), Ritchie (1987) Owers-Bradley (1989), Bradley (1990) and König (1990). In figure A3 a review diagram is given of the viscosity of pure ^{3}He and of ^{3}He-^{4}He mixtures as a function of temperature. Not shown in the diagram are: Berthold (1976), Betts (1963, 1965), Biskeborn (1975), Eisenstein (1980), Owers-Bradley (1989), Guénault (1990). We did not consider superfluid or polarized ^{3}He.

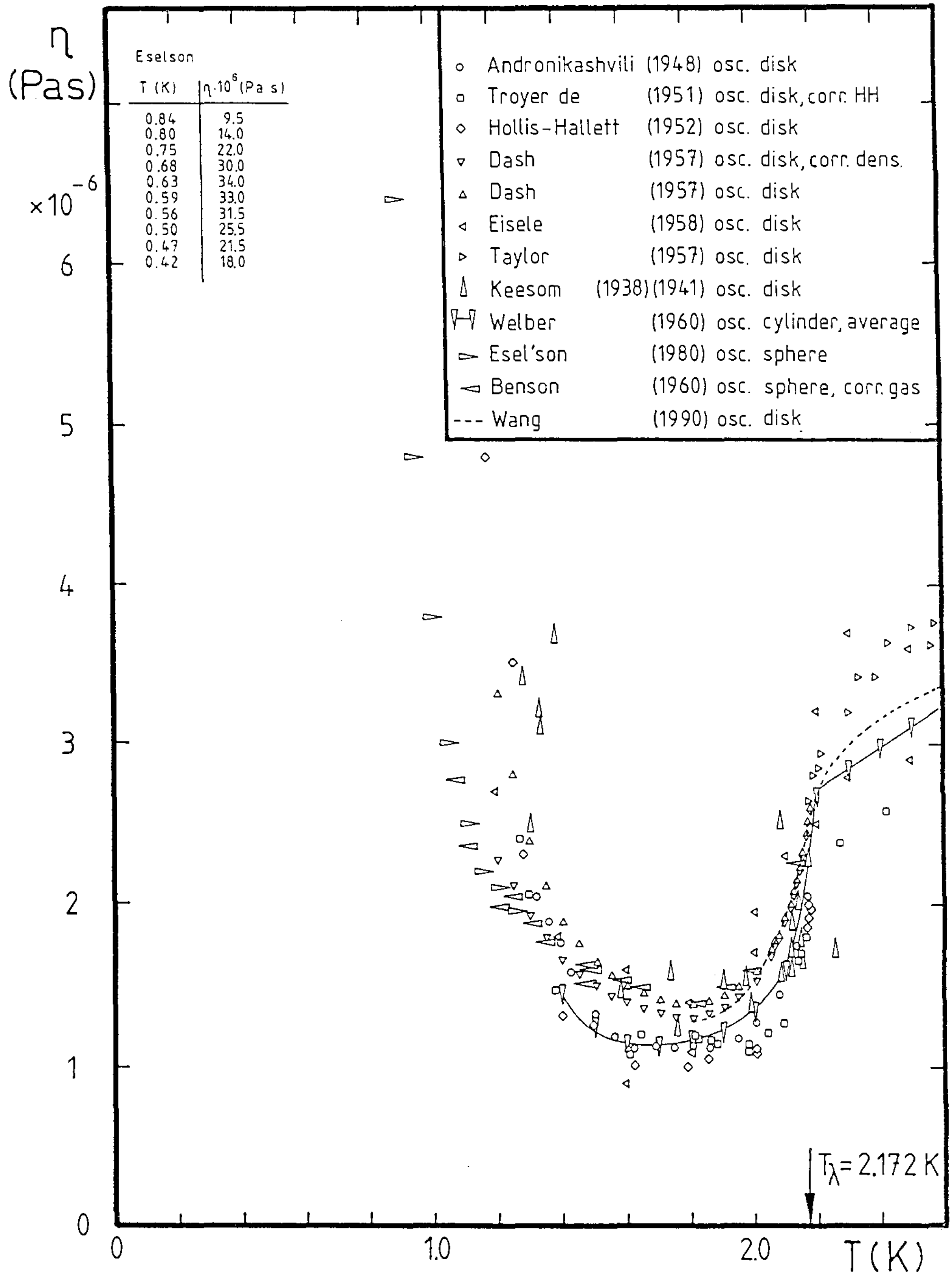

Fig. A1 *The viscosity of pure ^{4}He measured with oscillating systems.*

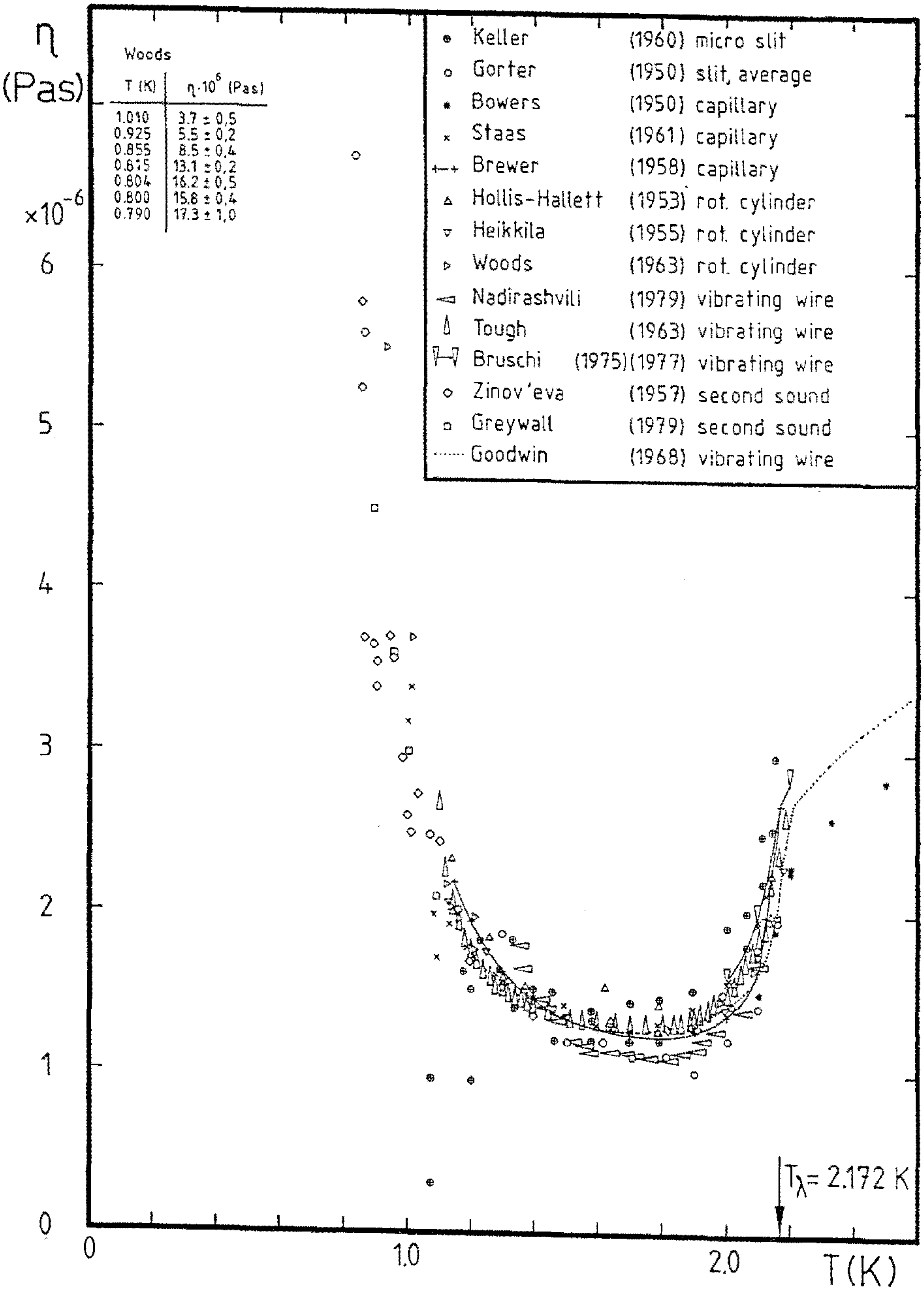

Woods

T (K)	$\eta \cdot 10^6$ (Pas)
1.010	3.7 ± 0,5
0.925	5.5 ± 0,2
0.855	8.5 ± 0,4
0.815	13.1 ± 0,2
0.804	16.2 ± 0,5
0.800	15.8 ± 0,4
0.790	17.3 ± 1,0

Fig.A2 *The viscosity of pure ^{4}He measured with other measuring techniques.*

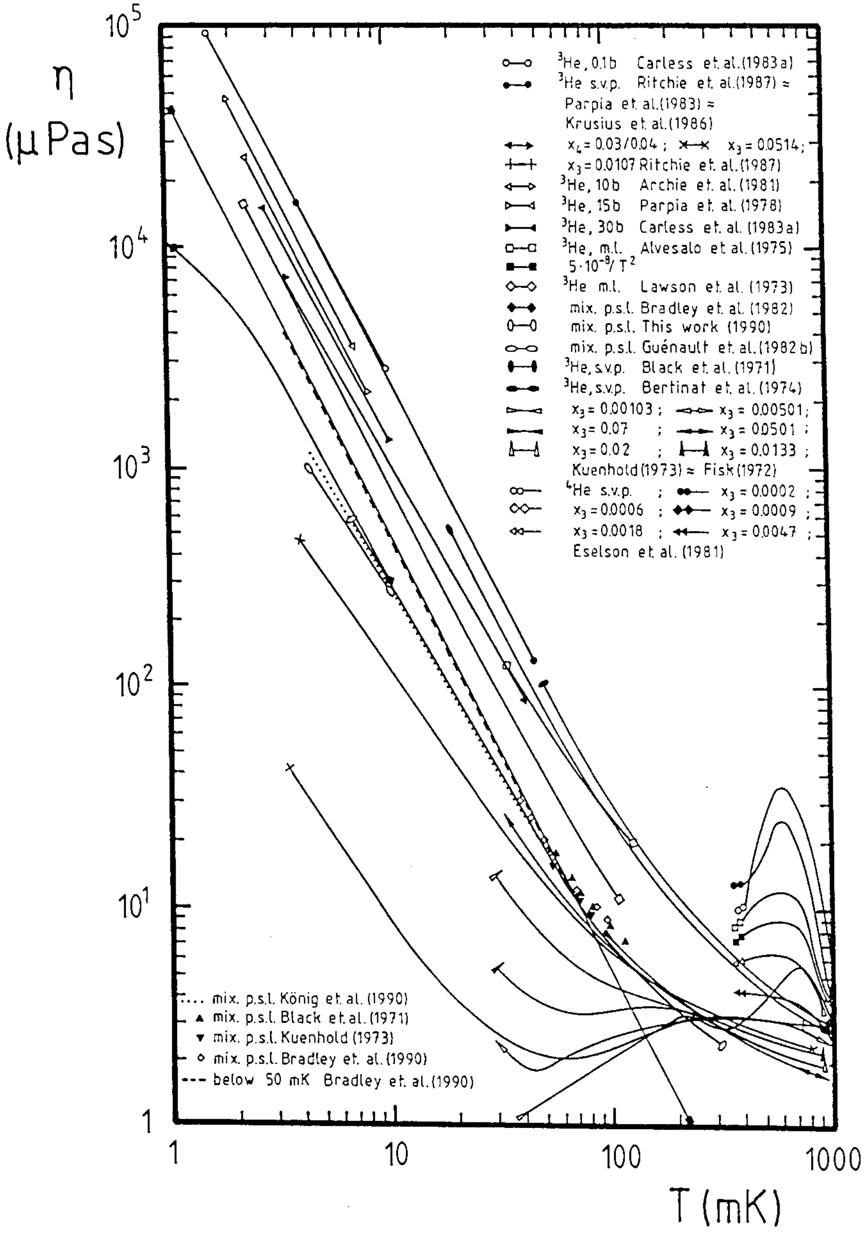

Fig. A3 *Survey graph of the measured viscosity of mixtures at temperatures below 1 K. The different curves can be distinguished by the end points corresponding with the explanation in the inset. s.v.p. means saturated vapour pressure, 10b, etc. means the pressure in bars, p.s.l. means phase separation line, m.l. means melting line.*

APPENDIX B

VIBRATING WIRE SPECIFICATIONS

This appendix contains two tables summarizing the parameters of the vibrating wire viscometers. Table B1 contains the data of the wires used in pure ^{4}He, table B2 those used for determining the viscosity of the mixtures.

The first column of table B1 indicates the index of the wire. The second column describes the material. NbTi means that one filament of a NbTi multifilamentary wire was used (IMI*), Nfil means the entire multifilamentary wire, W, Ir, St, Nb, Ta, mean tungsten, iridium, stainless steel, niobium and, tantalum respectively. In the third column the wire density is given. The density W_A-W_F is an estimation, the density of W_G and W_Q was measured. For the other materials we used the values tabulated in Reed (1983). The fourth and fifth column give the wire diameter and the loop diameter respectively. We measured d_w with an accuracy of 1μm and d_l was determined with an accuracy of 0.2 mm. The sixth column gives the ratio d_l/d_w. Column 7 and 8 give the resonance frequency (f_0) and the resonance width (Δf_0) both in vacuum respectively. Column 9 gives the Q_0 factor, which is the ratio between f_0 and Δf_0. In the 10th column the range of viscous penetration depth (δ_v) is indicated and column 11 presents the m value. The two values in column 10 and 11 are calculated at 1.1 K (left) and T_λ (right) assuming that $\eta(1.1\ \mathrm{K}) \simeq \eta(T_\lambda) \simeq 2.4\ \mu$Pas (Barenghi (1981, 1983a)). Liquid variables as ρ and ρ_n were obtained from Brooks and Donnelly (1977), and Maynard (1976). The last column indicates ψ which is defined as the ratio of measured to the estimated resonance frequency.

To estimate f_0 we assumed the very simplifying model that the wire is a clamped circular cylinder with diameter d_w and length $\frac{1}{2}d_l$. The formula calculated in Morse (1968) for the fundamental resonance (f_{0c}) was used:

$$f_{0c} = 0.56\,\frac{d_w}{{d_l}^2}\sqrt{E/\rho_w} \tag{B1}$$

where E = the Youngs modulus, which is tabulated in Reed (1983). From table B1 it can be seen that the measured frequency is about half the estimated value.

Table B2 Summary of the basic data of the vibrating wire viscometers used in the experiments in pure ^{4}He.

No	Mat	ρ_w	d_w	d_l	$\frac{d_l}{d_w}$	f_0	Δf_0	Q_0	δ_v	m	ψ
		(kg/m^3)	(μm)	(mm)		(Hz)	(Hz)		(μm)		
W_A	NbTi	6550	4	3.0	750	–	–	–	–	–	–
W_B	NbTi	6550	4	1.4	350	2998	34	88	7.8–0.9	0.1–1.0	0.64
W_C	NbTi	6550	4	1.0	250	5879	56	105	5.6–0.7	0.2–1.5	0.64
W_D	NbTi	6550	9	3.0	330	1091	9	121	13–1.6	0.2–1.4	0.47
W_E	NbTi	6550	9	1.4	160	5350	8	669	5.8–0.7	0.4–3.2	0.51
W_F	NbTi	6550	9	1.0	110	7340	70	105	5.0–0.6	0.4–3.8	0.35
W_G	Nfil	6580	113	8.0	70	1880	0.30	6270	9.9–1.2	2.8–24	0.46
W_H	W	19313	101	8.0	80	1885	0.20	9425	9.9–1.2	2.6–21	0.46
W_I	W	19313	19	8.0	420	420	0.09	4700	21–2.5	0.2–1.9	0.54
W_J	W	19313	101	6.0	60	3460	0.22	16000	7.3–0.9	3.4–29	0.47
W_K	W	19313	101	4.0	40	7638	3.4	2250	4.9–0.6	5.1–43	0.46
W_L	W	19313	101	2.0	20	32462	55	590	2.4–0.3	11–87	0.49
W_M	Ir	22659	49	8.0	160	1150	0.05	23000	13–1.5	1.0–8.2	0.54
W_N	Ir	22659	79	8.0	101	1770	0.066	27000	10–1.2	1.9–16	0.52
W_O	Ir	22659	101	8.0	80	2255	0.13	17300	9.0–1.1	2.8–23	0.52
W_P	Ir	22659	212	8.0	40	4535	1.5	3020	6.3–0.8	8.4–70	0.49
W_Q	St	8443	103	8.0	80	2220	0.34	6500	9.1–1.1	2.8–23	0.48
W_R	Nb	8616	133	8.0	60	2024	0.07	29000	9.5–1.1	3.5–30	0.49
W_S	Ta	16754	101	8.0	80	1452	0.04	36000	11–1.3	2.3–19	0.49

The setup of table B2 is the same as that of table B1 except column 2, which gives the B field of the viscometer. For the determination of the parameters δ_v and m (column 11 and 12) the viscosity assumed in equation (2.13) was used. The first value in these two columns corresponds with a temperature of 5 mK and the second value with 200 mK. The table starts at W_T in continuation of table B1.

Table B2 Summary of the basic data of the vibrating wire viscometers used for the measurements of the viscosity of mixtures.

No	B (mT)	mat	ρ_w (kg/m^3)	d_w (μm)	d_l (mm)	$\frac{d_l}{d_w}$	f_0 (Hz)	Δf_0 (mHz)	Q_0	δ_v (μm)	m	ψ
W_T	17	Ta	16754	101	20	200	233	5	47000	280-6	0.1-11	0.49
W_U	17	Ta	16754	249	20	80	585	35	16700	177-4	0.3-16	0.50
W_V	17	Ta	16754	249	24	96	410	17	23000	211-5	0.3-14	0.50
W_W	30	Ta	16754	101	10	99	960	25	38400	138-3	0.2-8	0.50
W_X	17	Ir	22659	101	12	119	1014	45	22500	135-3	0.2-9	0.52
W_Y	80	Ir	22659	101	10	99	1356	41	33070	116-2	0.2-10	0.48

CHAPTER 8

GENERAL CONCLUSIONS AND SUGGESTIONS FOR FURTHER STUDIES

8.1 GENERAL CONCLUSIONS.

This thesis treats the hydrodynamic properties of the flow of ^{3}He through ^{4}He at temperatures below 200 mK, where at a fixed entrance temperature the change of temperature, concentration and pressure across a flow impedance is determined experimentally as a function of the flow rate. This technique revealed many interesting flow phenomena. The experimental setup was highly reliable.

Basically two types of flow impedances were investigated: circular and annular tubes.

With circular tubes it was observed that for low velocities (below the first critical velocity) temperature, concentration and pressure difference along the flow channel are in agreement with the mechanical-vacuum model. The small differences between the model and the measurements are mainly due to the incorrect value of the viscosity as assumed in the model. The calculated ^{4}He chemical-potential difference across the flow channel is zero for these velocities.

In metal tubes, at the first critical velocity, the three measured quantities change discontinuously. At this velocity the ^{4}He chemical potential difference becomes nonzero. This is due to mutual friction between the flowing ^{3}He and the ^{4}He (which is macroscopically at rest) and is attributed to quantum vortices in the flow impedance. At intermediate flow rates the measurements do not follow the high-flow rate limiting value of the mutual-friction model. In glass tubes the transition is more gradual.

At very high velocities the flow state is dominated by mutual friction. In this highly turbulent flow state there is agreement with the mutual-friction model as formulated by Castelijns.

The product of the first critical velocity and channel diameter increases with the channel diameter and the values are comparable with pure ^{4}He counterflow data. The vortex line density which can be calculated (apart from a constant factor) is of the same order of magnitude as the values obtained in pure ^{4}He. If the measurements with circular tubes are interpreted in terms of the Vinen model of generation and decay of vortex lines, a consistent picture shows up. For the different tubes the fitting parameter is equal in the velocity range just above the first critical velocity. In the highly turbulent velocity range the parameter has a different value.

From pressure fluctuation studies it was observed that, at the first critical velocity the amplitude of the fluctuations of a time scale of one second is large. The amplitude of the Fourier spectrum for a fixed frequency as a function of the flow velocity shows a peak at the first and second critical velocity. In the case that a superleak is placed parallel the peaks are not observed and the amplitude of the fluctuations is very small. However, if for some impedances the amplitude at a fixed frequency is plotted as a function of the flow then a peak occurs at a certain flow rate region.

There are several indications for the existence of a second critical velocity. First of all the flow dependence of the quantities measured downstream of the flow channel show a kink at a velocity about twice the first critical velocity. Furthermore, from the analysis in terms of the Vinen theory it appeared that there are two regions of turbulence with different parameters. From the fluctuation studies it appeared that the amplitude of the spectra, plotted as a function of the flow rate, shows two peaks. One occurring at the first and the other at a second critical velocity. However, if for different flow impedances the amplitude of the spectra is plotted as a function of the flow rate a peak occurs for all flow impedances at the same flow rate, which nearly coincides with the second critical velocity.

In annular flow channels, for small velocities, the measurements agree with the mechanical-vacuum model. For these velocities the contribution of mutual friction to the ^{4}He chemical-potential gradient based on the third power law ($\chi \ell j^3$) is unmeasurably small. If the velocity is increased the measured quantities slowly deviate from the mechanical-vacuum model and the calculated chemical potential slowly starts to deviate from zero. The chemical-potential difference is in agreement with the highly turbulent flow state in circular flow channels. The critical velocity at which the ^{4}He chemical potential becomes nonzero is only an apparent one and depends on the tube length. The product of this critical velocity and the slit spacing disagrees strongly with the values found in circular flow channels. We think that the "real" critical velocity is much smaller than could be measured in our experiments. The Vinen model provides no adequate description for this observation. The pressure fluctuations do not show an abrupt change in amplitude at the apparent critical velocity. This conclusion is not entirely unambiguous as a flow rate dependent peak of the fluctuation amplitude interferes with the measurements. If the tube is shunted by a superleak the fluctuations decrease strongly. So presumably the quantum turbulence plays an important role in the appearance of the fluctuations.

In the vibrating wire viscometer the ratio between the vibrating wire amplitude and the wire diameter (reduced amplitude) is an important parameter. It should be smaller than 0.1 for normal fluids; for quantum fluids it should be smaller than 0.03. In multifilamentary NbTi the shift and width of the resonance peak are strongly magnetic field dependent. This material is unsuitable for the measurement of the viscosity. Normal metals, although suffering from a small B^2 dependency on peak width and shift, can be used. Superconducting metals are to be preferred in case $B < B_c$, yielding small vacuum-peak widths.

The measured viscosity of ^{4}He is in good agreement with literature so that application of the vibrating-wire technique to the measurement of the viscosity of mixtures is justified. The viscosity of the saturated dilute ^{3}He-^{4}He mixture below 60 mK is in agreement with results from different researchers. Using the measured viscosity data leads to a much better agreement of the measured pressure differences with the calculated values.

8.2 SUGGESTIONS FOR FUTURE RESEARCH.

It was suggested that the critical velocity in annular flow channels lies much lower than was reached in our experiments. It is of interest to measure the "real" critical velocity in an annular flow channel. Technically this will be difficult as very long tube lengths will be necessary. Another method to carry out this experiment is to use thermometers which can measure with an accuracy of microkelvins, for instance superconducting thermometric fixed point devices. The result of such an experiment could resolve an interesting aspect of the critical velocity, which would also be of importance for experiments carried out with pure ^{4}He II.

The fluctuation experiments were carried out with relatively short tubes most of the time. It is of interest to study the critical velocity using Fourier spectral techniques with flow channels with a large length where large fluctuations can be observed and then successively deviding the number of capillaries by two to study the higher velocity region. Using the same diameter but changing the number of tubes may also resolve the question of the existence of the second critical velocity. More research into the effects of inlet conditions and wall material would also be of interest.

The pressure transducer averages the pressure fluctuations over the whole flow channel. It is of interest to carry out local temperature measurements using very small thin film resistors or using a superconducting material (Ir) in its transition region as a very accurate thermometer to resolve at least 1 μK fluctuations. If fluctuations in temperature can be observed than it becomes possible to check whether turbulent plugs are formed in the flow channel indeed. It will be possible to carry out correlation studies using two or more sensors. In such a case the coherence of the flow may be probed.

More knowledge of the vibrating wire viscometer is of interest. Very pure superconductors can be tested achieving low vacuum peakwidths. Influence of external vibrations on the resonance properties should be studied to achieve more precise viscosity measurements. Also of interest is to investigate the peakwidth as a function of the ratio of the vibration amplitude and the wire diameter in liquid ^{4}He I and ^{4}He II. In general the technique to determine the viscosity of the mixture should be improved. The accurate determination of the viscosity of ^{3}He-^{4}He mixtures is important. It should be measured along the phase separation line and perhaps measurements up to higher temperatures are of interest. But also measurements at constant concentration are important. Of particular interest are measurements of pure ^{3}He with small additions of ^{4}He, which can give insight into the influence of the ^{4}He film on the viscometer.

The study of the critical velocity may be of importance for the design of dilution refrigerators. Especially for machines using high circulation rates (1 mmol/s) it is of importance that tubes at the dilute side are wide enough so that mutual friction has only a small effect.

The damping constants of second sound due to ^{4}He vortices, which are known for ^{4}He II, are not known for dilute mixtures at low temperature. It is very important that these parameters are studied by e.g. second sound, which can lead to a much better comparison of the pure ^{4}He and mixture vortex line distributions. That such a study is possible was put forward by Kuerten (1987b). For very large diameter tubes (> 5 mm) this technique can resolve critical velocities, which is impossible with the methods used in this work. Pre-eminently of use are the second sound transducers as used in the research group of R.J. Donnelly in Oregon. Such transducers may also be used to probe vortex-line density fluctuations in the mixture, this eventually in combination with temperature or pressure fluctuations.

The validity of the Vinen approach should be reconsidered. Numerical simulation of the evolution of a vortex tangle might explain the difference of the critical velocity between annular and circular flow channels.

Now that the viscosity of the mixture is determined it is perhaps possible to determine the excess pressure which might show up if superfluid turbulence occurs in flow channels. Furthermore, the determination of the temperature dependency of the viscosity supplies new data with respect to the transport properties of mixtures at low temperatures. This can be of influence with respect to the superfluid transition temperature of mixtures, which is of interest at present.

REFERENCES

Abraham B.M., Brandt O.G., Eckstein G., Manarin J. Relative molar volume and limiting solubility of ^{3}He in superfluid ^{4}He. Phys. Rev. 188(1969)309.
Agosta C.C., Wang S., Cohen L.H., Meyer H. Transport properties of helium near the liquid-vapor critical point. IV The shear viscosity of ^{3}He and ^{4}He. J. of Low Temp. Phys. 67(1987)237.
Ahlers G. On the viscosity of ^{4}He near the superfluid transition. Phys. Lett. 37A(1971)151.
Air Capacitors. Alfred Tronser GmbH., Postbox 63, D7543 Engelsbrand, W-Germany.
Allen J.F., Reekie J. Momentum transfer and heat flow in helium II. Proc. of the Cambr. Phil. Soc. 35(1939)114.
Alphen W.M. van, Haasteren G.J. van, Bruyn-Ouboter R. de, Taconis K.W. The dependence of the critical velocity of the superfluid on channel diameter and film thickness. Phys. Lett. 20(1966)474.
Alphen W.M. van. Flow phenomena in superfluid helium. Ph.D. Thesis, Leiden University, Leiden, The Netherlands(1969),.
Alvesalo T.A., Collan H.K., Loponen M.T., Lounasmaa O.V., Veuro M.C. The viscosity and some related properties of liquid ^{3}He at the melting curve between 1 and 100 mK. J. of Low Temp. Phys. 19(1975)1.
Anderson A.C. Carbon resistance thermometry. Temperature, its measurement and control in science and industry. Vol.4, Part 2, ed. by H.H. Plumb, Pittsburgh, Instrument Society of America, Pennsylvania (1972)p.773.
Anderson P.W. Considerations of the flow of superfluid helium. Rev. of Mod. Phys. 38(1966)298.
Andronikashvili E.L. The temperature dependence of the normal density of helium II. Zh. Eksper. i Teor. Fiz. 18(1948a)424.
Andronikashvili E.L. Investigation of the viscosity of the normal component of helium II. Zh. Eksper. i Teor. Fiz. 18(1948b)429.
Araldite. Ciba-Geigy, VIBA N.V., Postbox 29801, The Hague, Netherlands.
Asyst. Asyst Software Technologies Inc. 100 Corporate Woods, Rochester, N.Y. 14623, U.S.A.
Atkins K.R. Liquid helium, Cambridge Univ. Press, Cambridge (1959).
Avenel O., Varoquaux E. Observation of singly quantized dissipation events obeying the Josephson frequency relation in the critical flow of superfluid ^{4}He through an aperture. Phys. Rev. Lett. 55(1985)2704.
Avenel O., Varoquaux E. Reply to D.F. Brewer. Phys. Rev. Lett. 57(1986)921.
Avenel O., Varoquaux E. Reply to K.W. Schwarz. Phys. Rev. Lett. 59(1987)1168.
Awschalom D.D., Milliken F.P., Schwarz K.W. Properties of superfluid turbulence in a large channel. Phys. Rev. Lett. 53(1984a)1372.
Awschalom D.D., Schwarz K.W. Observation of a remanent vortex line density in superfluid helium. Phys. Rev. Lett. 52(1984b)49.

Bandyopadhyay P.R. Aspects of equilibrium puff in transitional pipe flow. J. of Fluid Mech. 163(1986)439.

Barenghi C.F., Lucas P.G.J., Donnelly R.J. Cubic spline fits to thermodynamic and transport parameters of liquid ^{4}He above the λ transition. J. of Low Temp. Phys. 44(1981)491.

Barenghi C.F., Swanson C.E., Donnelly R.J. Induced vorticity fluctuations in turbulent counterflow of superfluid helium. Phys. Rev. Lett. 48(1982a)1187.

Barenghi C.F. Experiments on quantum turbulence. Ph.D. Thesis, Oregon University, Eugene, Oregon, U.S.A. (1982b).

Barenghi C.F., Donnelly R.J., Vinen W.F. Friction on quantized vortices in helium II. A review. J. of Low Temp. Phys. 52(1983a)189.

Barenghi C.F., Swanson C.E., Donnelly R.J. Axial homogeneity, anisotropy and drift of a tangle of quantum vortices in He II. 75 th Jubilee Conference on helium-4, St. Andrews Scotland, 1-5 Aug. 1983, ed. by J.G.M. Armitage., World Scientific, Singapore (1983b).

Barenghi C.F., Jones C.A. The stability of the Couette flow of helium II. J. of Fluid Mech. 197(1988)551.

Bearman P.W., Dawnie M.J., Graham J.M.R., Obasaju E.D. Forces on cylinders in viscous oscillatory flow at low Keulegan-Carpenter numbers. J. of Fluid. Mech. 154(1985)337.

Beelen H. van, Joolingen W. van, Yamada K. On a balance equation for superfluid vorticity in capillary flow of helium II. Physica B153(1988)248.

Benson C.B., Hollis-Hallett A.C. The oscillating sphere at large amplitudes in liquid helium. Can. J. of Phys. 34(1956)668.

Benson C.B., Hollis-Hallett A.C. Viscosity measurements in liquid helium II. Can. J. of Phys. 38(1960)1376.

Bergé P., Pomeau Y., Vidal C. Order within chaos, John Wiley & Sons, New York (1986).

Berger S.A., Talbot L. Flow in curved pipes. Ann. Rev. of Fluid. Mech. 15(1983)461.

Berthold J.E., Giannetta R.W., Smith E.N., Reppy J.D. Determination of the ^{3}He superfluid density tensor for the A and B phases. Phys. Rev. Lett. 37(1976)1138.

Bertinat M.P., Betts D.S., Brewer D.F., Butterworth G.J. Effective viscosity of dilute solutions of liquid ^{3}He in ^{4}He between 20 mK and 1K. Phys. Rev. Lett. 28(1972)472.

Bertinat M.P., Betts D.S., Brewer D.F., Butterworth G.J. Damping of torsional oscillations of a quartz crystal cylinder in liquid helium at low temperatures. Viscosity of pure ^{3}He. J. of Low Temp. Phys. 16(1974)479.

Betts D.S., Osborne D.W., Welber B., Wilks J. The viscosity of liquid helium-3. Phil. Mag. (ser.8)8(1963)977.

Betts D.S., Keen B.E., Wilks J. The viscosity and acoustic impedance of liquid helium-3. Proc. of the Roy, Soc. of London A289(1965)34.

Betts D.S., Brewer D.F., Lucking R. Effective viscosity of liquid helium isotope mixtures. Proc. of the 13 th Conf. on Low Temp. Phys. ed. by K.D. Timmerhaus, W.J. O'Sullivan and E.F. Hammel, Vol.1, p.559, Plenum Press, New York (1973).

Betts D.S. Refrigeration and thermometry below one Kelvin, chapter 3. Sussex University Press, London (1976).

Betts D.S. An introduction to millikelvin technology. Cambridge University Press, Cambridge (1989).

Biskeborn R., Guernsey R.W. Critical exponents for the shear viscosity of ^{4}He at $T_\lambda{}^*$. Phys. Rev. Lett. 34(1975)455.

Black M.A., Hall H.E., Thompson K. The viscosity of liquid helium-3. J. of Phys. C, Solid State Phys. 4(1971)123.

Bosch W.A., Mathu F., Meyer H.C., Willekers R.W. Behaviour of thick film resistors (Philips type RC-01) as low temperature thermometers in magnetic fields up to 5T. Cryogenics 26(1986)3.

Bowers R., Mendelssohn K. Viscosity and superfluidity in liquid helium. Proc. of the Phys. Soc. 62(1949)394.

Bowers R., Mendelssohn K. The viscosity of liquid helium between 2 and 5 K. Proc. of the. Roy. Soc. of London A204(1950)366.

Bowley R.M. Nucleation of vortex rings by negative ions in liquid helium at low temperatures. J. of Phys. C, Solid St. Phys. 17(1984a)595.

Bowley R.M., Nancolas G.G., McClintock P.V.E. Vortex nucleation in ultradilute superfluid ^{3}He/^{4}He solutions. Phys. Rev. Lett. 52(1984b)659.

Bradley D.I., Guénault A.M., Keith V., Pickett G.R., Pratt W.P. The effect of mean free path and boundary limitations on the behaviour of a vibrating wire in a saturated ^{3}He-^{4}He solution at 0.5 bar down to 0.9 mK. J. of Phys. C, Solid St. Phys. 30(1982a)L501.

Bradley D.I., Oswald R. Viscosity of the ^{3}He-^{4}He dilute phase in the mixing chamber of a dilution refrigerator. J. of Low Temp. Phys. 80(1990)89.

Bradley D.I., Pickett G.R. Private Communication (1990).

Brewer D.F., Edwards D.O., Mendelssohn K. The onset of friction in helium II. Phil. Mag. (ser.8)1(1956)1130.

Brewer D.F., Edwards D.O. The heat conductivity and viscosity of liquid helium II. Proc. of the Roy. Soc. of London A251(1959)247.

Brewer D.F., Edwards D.O. Heat conduction by liquid helium II in capillary tubes. I Transition to supercritical condition. Phil. Mag. (ser.8)6(1961a)775.

Brewer D.F., Edwards D.O. Heat conduction by liquid helium II in capillary tubes. II Measurements of the pressure gradient. Phil. Mag. (ser.8)6(1961b)1173.

Brewer D.F., Edwards D.O. Heat conduction by liquid helium II in capillary tubes. III Mutual friction. Phil. Mag. (ser8)7(1962)721.

Brewer D.F., Edwards D.O. The effect of pressure on the normal component viscosity and critical velocities of liquid helium II. Proc. of the 8 th Int. Conf. on Low Temp. Phys. London 16-22 Sept. 1962, ed. by R.O. Davies, Butterworths, London (1963)p.96.

Brewer D.F. Phase coherence and quantized circulation transitions in superfluid helium. Phys. Rev. Lett. 57(1986)920.

Broese van Groenou A., Poll J.D., Delsing A.M.G., Gorter C.J. The viscosity of the normal part of liquid helium II from heat conduction experiments. Physica 22(1956)905.

Brooks J.S., Donnelly R.J. The calculated thermodynamic properties of superfluid helium-4. J. of Phys. Chem. Ref. Data 6(1977)51.

Bruschi L., Santini M. Vibrating wire viscometer. Rev. Sci. Instr. 46(1975a)1560.

Bruschi L., Mazzi G., Santini M., Torzo G. Measurements of ^{4}He viscosity near the superfluid transition. J. of Low Temp. Phys. 18(1975b)487.

Bruschi L., Mazzi G., Santini M., Torzo G. The behaviour of the ^{4}He viscosity near the superfluid transition. J. of Low Temp. Phys. 29(1977)63.

Bruschi L., Santini M. The ^{4}He viscosity near the superfluid transition under pressure. J. of Low Temp. Phys. 33(1978)357.

Cantwell B.J. Organized motion in turbulent flow. Ann. Rev. of Fluid Mech. 13(1981)457.

Carless D.C., Hall H.E., Hook J.R. Vibrating wire measurements in liquid ^{3}He. I The normal state. J. of Low Temp. Phys. 50(1983a)583.

Carless D.C., Hall H.E., Hook J.R. Vibrating wire measurements in liquid ^{3}He. II The superfluid B phase. J. of Low Temp. Phys. 50(1983b)605.

Castelijns C.A.M., Kuerten J.G.M., Waele A.T.A.M. de, Gijsman H.M. ^{3}He flow in dilute ^{3}He-^{4}He mixtures at temperatures between 10 and 150 mK. Phys. Rev. B32(1985)2870.

Castelijns C.A.M. Flow properties of ^{3}He in dilute ^{3}He-^{4}He mixtures at temperatures between 10 and 150 mK. Ph.D. Thesis, Eindhoven University of Technology, Eindhoven, The Netherlands (1986).

Celoron, Celoron is a product name and is a cotton based phenolic resin. Merrem and la Porte, Postbox 50, 5300 AB Zaltbommel, The Netherlands.

Chase C.E. Thermal conduction in liquid helium II. I Temperature dependence. Phys. Rev. 127(1962)361.

Chase C.E. Thermal conduction in liquid helium II. II Effects of channel geometry. Phys. Rev. 131(1963)1898.

Childers R.K., Tough J.T. Critical velocities as a test of the Vinen theory. Phys. Rev. Lett. 31(1973)911.

Childers R.K., Tough J.T. Observation of multiple Vinen states in He II counterflow. J. of Low Temp. Phys. 15(1974a)53.

Childers R.K., Tough J.T. Observation of a new flow state in He II counterflow. J. of Low Temp. Phys. 15(1974b)63.

Childers R.K., Tough J.T. He II counterflow: Temperature and pressure difference data and analysis in terms of the Vinen theory. Phys. Rev. B13(1976)1040.

Collaudin B. Stabilisation d'hydrogene atomique polarise en champ magnétique intense (B $\leq$ 14 T). Ph.D. Thesis, Grenoble University, Grenoble, France (1986).

Coops G.M., Waele A.T.A.M. de, Gijsman H.M. The multiple mixing chamber. Cryogenics 19(1979)659.

Coops G.M. Dilution refrigerator with multiple mixing chambers. Ph.D. Thesis, Eindhoven University of Technology, Eindhoven, The Netherlands (1981).

Coops G.M., Waele A.T.A.M. de, Gijsman H.M. Experimental evidence for mutual friction between ^{3}He and superfluid ^{4}He. Phys. Rev. B25(1982)4879.

Courts S.S., Tough J.T. The transition to superfluid turbulence in two fluid flow of HeII. Phys. Rev. B38(1988)74.

Courts S.S., Tough J.T. Dissipation in two fluid flow in He II. Phys. Rev. B39(1989)3924.

Craig P.P., Keller W.E., Hammel E.F. Flow of liquid helium II under large temperature and pressure gradients. Ann. of Phys. 21(1965)72.

Dash J.G., Taylor R.D. Hydrodynamics of oscillating disks in viscous fluids: density and viscosity of normal fluid in pure ^{4}He from 1.2 K to the lambda point. Phys. Rev. 105(1957a)7.

Dash J.G., Taylor R.D. Density and viscosity of normal fluid in dilute solutions of ^{3}He in ^{4}He. Phys. Rev.107(1957b)1228.

Donnelly R.J., Swanson C.E. Quantum turbulence. J. of Fluid Mech. 173(1986)387.

Donnelly R.J., La Mar M.M. Absolute measurement of the viscosity of classical and quantum fluids by rotating cylinder viscometers. Phys. Rev. A36(1987)4507.

Donnelly R.J., La Mar M.M. Flow and stability of helium II between concentric cylinders. J. of Fluid Mech. 186(1988)163.

Ebner C., Edwards D.O. The low temperature thermodynamic properties of superfluid solutions of ^{3}He in ^{4}He. Phys. Repts. 2(1971)77.

Ecke R., Haucke H., Wheatley J.C. Superfluid turbulence in convecting dilute solutions of ^{3}He in superfluid ^{4}He. Phys. Rev. Lett. 58(1987)499.

Ecke R., Haucke H. Noise induced intermittency in the quasiperiodic regime of Rayleigh-Bénard convection. J. of Stat. Phys. 54(1989)1153.

Eisele K.M., Hollis-Hallett A.C. The viscosity of liquid helium at frequencies of 11.8 and 35.5 kc/sec. Can. J. of Phys. 36(1958)25.

Eisenstein J.P., Swift G.W., Packard R.E. Effect of the quasiparticle mean free path on Poiseuille flow in normal liquid ^{3}He. Phys. Rev. Lett. 45(1980)1199.

Esel'son B.N., Nosovitskaya O.S., Pogorelov L.A., Sobolev V.I. Characteristics of the viscosity of liquid helium below 1 K. J.E.T.P. Lett. 31(1980)31.

Esel'son B.N., Nosovitskaya O.S., Pogorelov L.A., Sobolev V.I. Shear viscosity and parameters of kinetic processes in superfluid helium. Physica 107B(1981)41.

Fetter A.L. Vortices and ions in helium. Chapter 3 of: The physics of liquid and solid helium. ed. by K.H. Benneman and J.B. Ketterson, John Wiley & Sons, New York (1976).
Feynman R.P. Application of quantum mechanics to liquid helium. Prog. in Low Temp. Phys. 1(1955)17, ed. by C.J. Gorter.
Fisk D.J. The viscosity of dilute solutions of helium-3 in liquid helium-4 below 0.1 K. Ph.D. Thesis, Manchester University, Manchester (1972).
Fisk D.J., Hall H.E. The viscosity of ^{3}He-^{4}He solutions. Proc. of the 13 th Int.Conf. on Low Temp. Phys, University of Colorado, Boulder, Colorado, Aug. 21-25, 1972, ed. by K.D. Timmerhaus, W.J. O'Sullivan, E.F. Hammel, Vol.1 p.568, Plenum Press, New York (1973).
Frossati G., Godfrin H., Hébral B., Schumacher G., Thoulouze D. Conventional cycle dilution refrigerator down to 2.0 mK. Physics at Ultralow Temperatures. Proc. of the Int. Symp. at Hakoné, Japan, Sept. 5-9 (1977), ed. by T. Sugawara, S. Nakajima, T. Ohtsuka, T. Usui.

Geurst J.A. Mutual friction in the laminar flow of superfluid helium II through capillary tubes. Phys. Lett. 71A(1979)78.
Geurst J.A. Hydrodynamics of quantum turbulence in He II: Vinen's equation derived from energy and impulse of the vortex tangle. Physica B154(1989)321.
Geurst J.A. Private Communication (Feb.1990).
Glaberson W.I., Donnelly R.J. Growth of pinned vortex lines in helium II. Phys. Rev. 141(1966)208.
Glaberson W.I., Donnelly R.J. Structure, distribution and dynamics of vortices in helium II. Prog. in Low Temp. Phys. 9(1986)1, ed. by D.F. Brewer.
Goeje M.P. de. On second and fourth sound in helium II and their application as acoustical probes of superfluid turbulence. Ph.D. Thesis, Leiden University, Leiden, The Netherlands(1986).
Goeje M.P. de, Beelen H. van. Turbulent counterflow of helium II investigated with a sixfold helmholtz resonator for second sound. Physica 133B(1985)109.
Goodwin J.M. The pressure dependence of viscosity in liquid helium. Ph.D. Thesis, Washington University, Washington, U.S.A. (1968).
Goodwin J.M. A vibrating wire viscometer for measurements at elevated pressures. J. of Phys. E, Scient. Instr. 6(1973)452.
Goodwin J.M. The viscosity of pressurized ^{4}He above T_λ. Physica 76(1974)177.
Gorter C.J., Mellink J.H. On the irreversible processes in liquid helium II. Physica 15(1949)285.
Gorter C.J., Kasteleyn P.W., Mellink J.H. Discussion of the properties of helium II on the basis of the two fluid model. Physica 16(1950)113.
Greywall D.S. Measurements of the second sound damping in dilute ^{3}He-^{4}He solutions. Phys. Rev. Lett. 42(1979)1758.
Greywall D.S., Busch P.A. High precision ^{3}He-vapor pressure gauge for use to 0.3 K. Rev. of Sci Instr. 51(1980)509.
Griffioen W., Frossati G. Small sensitive pressure transducer for use at low temperatures. Rev. of Sci. Instr. 56(1985)1236.
Griswold D. Dynamics of the vortex line density in superfluid turbulence. Ph.D. Thesis, Ohio State University, Columbus, U.S.A. (1986).
Griswold D., Lorenson C.P., Tough J.T. Intrinsic fluctuations of the vortex-line density in superfluid turbulence. Phys. Rev. B35(1987a)3149.
Griswold D., Tough J.T. Noise induced bistability at the TI/TII transition in superfluid ^{4}He II. Phys. Rev. A36(1987)1360.
Guénault A.M., Keith V., Kennedy C.J., Pickett G.R. Mean free path effects and a search for superfluidity in ^{3}He-^{4}He solutions near the solubility maximum from 0.4 to 4 mK. Phys. Lett. 90A(1982)432.

Guénault A.M., Keith V., Kennedy C.J., Pickett G.R. Transition from hydrodynamic to ballistic quasiparticle behaviour in a Fermi gas: The response of a vibrating-wire resonator in a ^{3}He-^{4}He solution from 0.3 to 10 mK. Phys. Rev. Lett. 50(1983)522.

Guénault A.M., Nichols T.R., Pickett G.R. The damping of a vibrating wire resonator in 0.003% and 0.1% ^{3}He-^{4}He solutions below 120 mK. The effective viscosity of a 0.1% solution. J. of Low Temp. Phys. 81(1990)179.

Haas W. de. A synthesis of flow phenomena in He II. Ph.D. Thesis, Leiden University, Leiden, The Netherlands (1975). Physica 75(1974)311.

Haas W. de, Beelen H. van. A synthesis of flow phenomena in helium II. Physica 83B(1976)129.

Haeringen W. van, Staas F.A., Geurst J.A. On ^{3}He-^{4}He dilution refrigerators, part I. Philips J. of Res. 34(1979a)107.

Haeringen W. van, Staas F.A., Geurst J.A. On ^{3}He-^{4}He dilution refrigerators, part II. Philips J. of Res. 34(1979b)127.

Haeringen W. van. On the choice of tube lengths and diameters in a ^{3}He-^{4}He dilution refrigerator system. Cryogenics 20(1980)153.

Hall H.E., Vinen W.F. The rotation of liquid helium II. I Experiments on the propagation of second sound in uniformly rotating helium II. Proc. of the Roy. Soc. of London A238(1957a)204.

Hall H.E., Vinen W.F. The rotation of liquid helium II. II The theory of mutual friction in uniformly rotating He II. Proc. of the Roy. Soc. of London A238(1957b)215.

Hall H.E. The viscosity of ^{3}He-^{4}He solutions. Liquid and solid helium, Proc. of the Europ. Phys. Soc. Top. Conf., Haifa, 1-4 July 1974, ed. by C.G. Kuper, S.G. Lipson, M. Revzen. John Wiley & Sons, New York (1975)p.375.

Hammel E.F., Keller W.E. Fountain pressure measurements in liquid helium II. Phys. Rev. 124(1961)1641.

Hansen A., Nelkin M. Absence of small scale structure in homogeneous superfluid turbulence. Phys. Rev. B34(1986)4894.

Haucke H., Maeno Y. Phase space analysis of convection in a ^{3}He-superfluid ^{4}He solution. Physica 7D(1983)69.

Haucke H., Ecke R. Mode locking and chaos in Rayleigh-Bénard convection. Physica 25D(1987)307.

Hedge S.G., Glaberson W.I. Pinning of superfluid vortices to surfaces. Phys. Rev. Lett. 45(1980)190.

Heikkila W.J., Hollis-Hallett A.C. The viscosity of liquid helium II. Can. J. of Phys. 33(1955)420.

Henberger J.D.,Tough J.T. Geometric effects on superfluid turbulence, rectangular, square and circular tubes compared. Phys. Rev. B23(1981)413.

Henberger J.D., Tough J.T. Uniformity of the temperature gradient in the turbulent counterflow of He II. Phys. Rev. B25(1982)3123.

Heijden G. van der. Forces in the flow of liquid helium II. Ph.D. Thesis, Leiden University, Leiden, (1972a).

Heijden G. van der, Voogt W.J.P. de, Kramers H.C. Forces in the flow of liquid helium II. I Flow with small superfluid velocity. Physica 59(1972b)473.

Heijden G. van der, Boog A.G.M. van der, Kramers H.C. Forces in the flow of liquid helium II. 3 Flow with v_n and v_s unequal zero. Physica 77(1977)487.

Hollis-Hallett A.C. Oscillating disk experiments in liquid helium II. Proc. of the Phys. Soc. A63(1950)1367.

Hollis-Hallett A.C. Experiments with oscillating disk systems in liquid helium II. Proc. of the Roy. Soc. of London A210(1952)404.

Hollis-Hallett A.C. Experiments with a rotating cylinder viscometer in liquid helium II. Proc. of the Cambr. Phil. Soc. 49(1953)717.

Hollis-Hallett A.C. Oscillating disks and rotating cylinders in liquid helium II. Prog. in Low Temp. Phys. 1(1955)64. ed. by C.J. Gorter.

Højgaard Jensen H., Smith H., Wölfle P., Nagai K. Boundary effects in fluid flow. Application to quantum fluids. J. of Low Temp. Phys. 41(1980)473.

Hudson R.P., Marshak H., Soulen R.J., Utton D.B. Review paper: recent advances in thermometry below 300 mK. J. of Low Temp. Phys. 20(1975)1, especially chapter 8.

Hussain A.K.M.F. Coherent structures and turbulence. J. of Fluid Mech. 173(1986)303.

Kapitza P. Viscosity of liquid helium below the λ-point. Nature 141(1938)74.

Kapton Foil. DuPont de Nemours Int. SA, Polymer Products Department Films Div., 50-52 Route des Acasias CH-1211, Geneva 24, Switzerland. Kindly supplied to us by P. Wassenaar, M. Seher & Co., Kompasstraat 3, 2901 AM Capelle aan de IJssel.

Keesom W.H., MacWood G.E. The viscosity of liquid helium. Physica 5(1938)737.

Keesom W.H., Keesom P.H. On the viscosity of liquid helium in the neighbourhood of the lambda point. Physica 8(1941)65.

Keller W.E., Hammel E.F. Heat conduction and fountain pressure in liquid He II. Ann. of Phys. 10(1960)202.

Keller W.E. Helium-3 and helium-4. Plenum Press, New York (1969).

Khalatnikov I.M. An introduction to the theory of superfluidity. W.A. Benjamin (1965), New York. Reissued Addison Wesley Publ. Co. Inc., New York (1989).

Kierstead H.A. Dielectric constant, molar volume and phase diagram of saturated liquid ^{3}He-^{4}He mixtures. J. of Low Temp. Phys. 24(1976)497.

König R., P. Smeibidl and F. Pobell. Private Communication at 19 th Int. Conf. on Low Temp. Phys. at Brighton: Refrigeration and viscosity of liquid ^{3}He and of liquid ^{3}He-^{4}He mixtures.

Krusius M., Nenonen S., Salmelin R., Haavasoja T., Tsakadze Dzh.S., Nadirashvili Z.Sh. Viscosity of normal liquid helium-3 near Tc. Sov. J. of Low Temp. Phys. 12(1986)191.

Kuenhold K.A., Crum D.B., Sarwinski R.E. The viscosity of dilute solutions of ^{3}He in ^{4}He at low temperatures. Phys. Lett. 41A(1972)13.

Kuenhold K.A. The viscosity of dilute solutions of helium-3 in liquid helium-4 below 0.1 K. Ph.D. Thesis, Ohio State University, Columbus, U.S.A., (1973a).

Kuenhold K.A., Crum D.B., Sarwinsky R.E. The viscosity of dilute solutions of ^{3}He in ^{4}He at low temperatures. Proc. of the 13 th Int. Conf. on Low Temp. Phys., University of Colorado, Boulder, Colorado, Aug. 21-25, 1972. ed.by K.D. Timmerhaus, W.J. O'Sullivan, E.F. Hammel, Vol.1, p.559. Plenum Press, New York (1973b).

Kuerten J.G.M., Castelijns C.A.M., Waele A.T.A.M. de, Gijsman H.M. Thermodynamic properties of liquid ^{3}He-^{4}He mixtures at zero pressure for temperatures below 250 mK and ^{3}He concentrations below 8 %. Cryogenics 25(1985a)419.

Kuerten J.G.M. Private communication (1985b).

Kuerten J.G.M., Castelijns C.A.M., Waele A.T.A.M. de, Gijsman H.M. Flow of ^{3}He in superfluid ^{4}He. Phys. Scripta T13(1986a)109.

Kuerten J.G.M., Castelijns C.A.M., Waele A.T.A.M. de, Gijsman H.M. Comprehensive theory of flow properties of ^{3}He moving through superfluid ^{4}He. Phys. Rev. Lett. 56(1986b)2288.

Kuerten J.G.M. ^{3}He-^{4}He II mixtures: Thermodynamic and hydrodynamic properties. Ph.D. Thesis, Eindhoven University of Technology, Eindhoven, The Netherlands (1987a).

Kuerten J.G.M., Zeegers J., Waele A.T.A.M. de, Gijsman H.M. Dissipative effects in dilution refrigerators. Proc. of the 18 th Int. Conf. on Low Temp. Phys., Kyoto (1987). Jap. J. of Appl. Phys. 26(1987b)29.

Kuerten J.G.M. Private communication (1987c).
Kummer R.B., Narayanamurti V., Dynes R.C. Ballistic phonons and the transition to second sound in dilute mixtures of ^{3}He in liquid ^{4}He. Phys. Rev. B16(1977)1046.

Ladner D.R., Tough J.T. Helium II counterflow at large heat currents: Profound effects of geometry. Phys. Rev. B17(1978)1455.
Ladner D.R., Tough J.T. Temperature and velocity dependence of superfluid turbulence. Phys. Rev. B20(1979)2690.
Landau L.D. The theory of superfluidity of helium II. J. of Phys. U.S.S.R. 5(1941)71, Collected Papers, ed. by D. ter Haar, Pergamon Press, Oxford, (1965)p.301.
Landau L.D., Lifshitz E.M. Fluid Mechanics, 2nd ed., Pergamon Press, Oxford (1959).
Landau J., Tough J.T., Brubaker N.R., Edwards D.O. A sensitive nonmagnetic pressure transducer for use at very low temperatures. Rev. Sci. Instr. 41(1970)444.
Lawson D.T., Gully W.J., Goldstein S., Reppy J.D., Lee D.M. Richardson R.C. The low temperature viscosity of normal liquid ^{3}He. J. of Low Temp. Phys. 13(1973)503.
London H. Proc. of the Int. Conf. on Low Temp. Phys., Oxford (1951)p.157, ed. by R. Bowers.
London H., Clarke G.R., Mendoza E. Osmotic pressure of ^{3}He in liquid ^{4}He, with proposals for a refrigerator to work below 1 K. Phys. Rev. 128(1962)1992.
Lorenson C.P, Griswold D., Nayak V.U., Tough J.T. Dynamic features of superfluid turbulence near the second critical heat current. Phys Rev. Lett. 55(1985)1494.
Lounasmaa O.V. Experimental principles and methods below 1 K. Academic Press, London (1974).
Love M.S., Anderson A.C. Heat capacity of thick film resistance thermometers below 1 K. Rev. of Sci. Instr. 58(1987)1113.

Maeno Y., Haucke H., Ecke R.E., Wheatley J.C. Oscillatory convection in a dilute ^{3}He superfluid ^{4}He solution. J. of Low Temp. Phys. 59(1985)305.
Marees G., Beelen H. van. On the disappearance of the flow impedance of helium II when mass and entropy flow in opposite directions. Physica 133B(1985)21.
Marees G. Transient phenomena and nonuniform superfluid turbulence in the flow of helium II. Ph.D. Thesis, Leiden University, Leiden, The Netherlands (1986).
Marees G., Mudde R.F., Beelen H. van. On the motion of plugs of turbulence in the flow of helium II. Physica 144B(1987a)292.
Marees G., Slot P.J.M. van der, Beelen H. van. Subcritical and supercritical non-turbulent flow of mass and entropy in superfluid ^{4}He. Physica 144B(1987b)209.
Marees G., Beelen H. van. On various processes of redistribution of superfluid turbulence in capillary flow of helium II. Physica 145B(1987)21.
Martin K.P., Tough J.T. Evolution of superfluid turbulence in thermal counterflow. Phys. Rev. B27(1983)2788.
Maynard J. Determination of the thermodynamics of He II from sound velocity data. Phys. Rev. B14(1976)3868.
Mostert R., Gulik P.S. van der, Berg H.R. van der. The working equations of a vibrating wire viscometer. Physica A156(1989)909.
Mudde R.F., Beelen H. van. Capillary flow of superfluid ^{3}He-^{4}He mixtures. Proc. of the 18 th Int. Conf. on Low Temp. Phys., Kyoto (1987). Jap. J. of Appl. Phys. 26(1987)103. ed. by Y. Nagaoka.
Mudde R.F. Thermal counterflow in ^{3}He-^{4}He mixtures, Ph.D. Thesis, Leiden University, Leiden, The Netherlands, (1989).
Mudde R.F., Beelen H. van. Counterflow in superfluid ^{3}He-^{4}He mixtures. I The laminar case. Physica B162(1990)197.

Muirhead C.M., Vinen W.F., Donnelly R.J. The nucleation of vorticity by ions in superfluid ^{4}He. I Basic theory. Phil. Trans. of the Roy. Soc. of London A311(1984)433.

Muirhead C.M., Vinen W.F., Donnelly R.J. The nucleation of vorticity by ions in superfluid ^{4}He. II Theory of the effect of dissilved ^{3}He. Proc. of the Roy. Soc. of London A402(1985)225.

Murdock E.S., Corruccinni L.R. The attenuation of second sound in dilute ^{3}He-^{4}He solutions below 1 K. J. of Low Temp. Phys. 46(1982)219.

Mylar sheet, aluminized. Superinsulation NRC-2, 7 μm thick. Oxford Instruments Lim., Eynsham, Oxford OX8 1TL, England. Also delivered by Goodfellow, Cambridge Science Park, Cambridge CB4 4DJ, England. A 2 μm thickness sample was kindly supplied to us by S. van der Werf, K.V.I., Groningen.

Nadirashvili Z.Sh., Tsakadze D.S. Measurements of the normal component viscosity in liquid helium II at various frequencies. Sov. J. of Low Temp. Phys. 4(1978)711.

Nadirashvili Z.Sh., Tsakadze J.S. Dependence of helium II viscosity properties on oscillation frequency. J. of Low Temp. Phys. 37(1979)169.

Nakamura M., Fujii Y., Shigi T., Nagao K. Solubility of ^{4}He in liquid ^{3}He at very low temperatures. J. of the Phys. Soc. of Jap. 57(1988)1676.

Nancolas G.G., Bowley R.M., McClintock P.V.E. The breakdown of superfluidity in liquid ^{4}He. IV Influence of ^{3}He isotopic impurities on the nucleation of quantized vortex rings. Phil. Trans. of the Roy Soc. of London A313(1985)537.

Niinikoski T.O. A horizontal dilution refrigerator with very high cooling power. Nucl. Instr. and Meth. 97(1971)95.

Ohmi T., Tsuneto T., Usui T. Phase separation in rotating helium. Prog. in Theor. Phys. 41(1969a)1395.

Ohmi T., Usui T. Superfluid vortex, trapping neutral impurities. Prog. in Theor. Phys. 41(1969b)1401.

Okuyama M., Satoh T., Satoh T. Adiabatic flow of helium II. II Motion of normal fluid component and vortices. Physica 154B(1988)116.

Onsager L. Statistical hydrodynamics. Nuovo Cim.(Ser.9)6(1949)249 & 279.

Oran-Brigham E. The fast fourier transform and its applications. Prentice Hall International, London (1988).

Ostermeier R.M., Glaberson W.I. Instability of vortex lines in the presence of axial normal fluid flow. J. of Low Temp. Phys. 32(1975)191.

Ottino J.M. Mixing, chaotic advection and turbulence. Ann. Rev. of Fluid Mech. 22(1990)207.

Owers-Bradley J.R., Main P.C., Church R.J., Hampson T.M.M., McHale G., Bowley R.M. Measurements of the viscosity of a spin polarized ^{3}He-^{4}He solution. Proc. of the Conf. on Spin Polarized Quantum Systems, ed. by S. Stringari, World Scientific, Singapore (1989)p.169. To be published in J. of Low. Temp. Phys. 77.

Parpia J.M., Sandiford D.J., Berthold J.E., Reppy J.D. Viscosity of liquid ^{3}He-B near the superfluid transition. Phys. Rev. Lett. 40(1978)565.

Parpia J.M., Rhodes T.L. First observation of Knudsen minimum in normal liquid ^{3}He. Phys. Rev. Lett. 51(1983)805.

Pickett G.R. Private communication (1990).

Putterman S.J. Superfluid hydrodynamics. North Holland Publ. Co., Amsterdam (1974).

Radebaugh R. Thermodynamic properties of ^{3}He-^{4}He solutions with applications to the ^{3}He-^{4}He dilution refrigerator. Nat. Bur. Stand., NBS Tech. Note 362(1967).

Rayfield G.W., Reif F. Quantized vortex rings in superfluid helium. Phys. Rev. 136 (1964)A1194.

Reed R.P., Clark A.F. Materials at low temperatures. American Society for Metals, Metals Park, Ohio (1983).

Rent L.S., Fisher I.Z. Adsorption of atomic impurities on quantized vortices in liquid helium II. Sov. Phys. J.E.T.P. 28(1969)375.

Retsina T., Richardson S.M., Wakeham W.A. The theory of a vibrating rod densimeter. Appl. Sci. Res. 43(1986)127.

Retsina T., Richardson S.M., Wakeham W.A. The theory of a vibrating rod viscometer. Appl. Sci. Res. 43(1987)325.

Reynolds O. An experimental investigation of the circumstances which determine whether the motion of water shall be direct or sinuous, and of the law of resistance in parallel channels. Phil. Trans. of the Roy. Soc. of London A174(1883)935.

Richardson R.C., Smith E.N. Experimental techniques in condensed matter physics at low temperatures. Addison-Wesley, New York (1988).

Riley N. On a sphere oscillating in a viscous fluid. Quart. J. of Mech. and Appl. Math. 19(1966)461.

Ritchie D.A., Saunders J., Brewer D.F. Momentum transfer between ^{3}He quasiparticles and surfaces: The effective viscosity of dilute solutions of ^{3}He in ^{4}He. Phys. Rev. Lett. 59(1987)465.

Roshko A. Structure of turbulent shear flows: A new look. A.I.A.A. J. 14(1976)1349.

Sarpkaya T. Force on a circular cylinder in viscous oscillatory flow at low Keulegan-Carpenter numbers. J. of Fluid Mech. 165(1986)61.

Satoh T., Satoh T., Ohtsuka T., Okuyama M. Adiabatic flow of superfluid helium II. I Thermohydrodynamic description with a new type of mutual friction force. Physica 146B(1987)379.

Schooley J.F., Soulen R.J., Evans G.A. Preparation and use of superconductive fixed point devices, SRM 767. Nat. Bur. of Stand. Special Publication 260-44, U.S. Dept. of Commerce, Nat. Bur. Stand. (1972).

Schwarz K.W. Interaction of quantized vortex rings with quantized vortex lines in rotating He II. Phys. Rev. 165(1968)323.

Schwarz K.W., Jang P.J. Creation of quantized vortex rings by charge carriers in superfluid helium. Phys. Rev. A8(1973)3199.

Schwarz K.W. Spherical probes and quantized vortices: hydrodynamic formalism and simple approximations. Phys. Rev. A10(1974)2306.

Schwarz K.W. Onset of phase slip in superflow through channels. Phys. Rev. B12(1975)3658.

Schwarz K.W. Theory of turbulence in superfluid ^{4}He. Phys. Rev. Lett. 38(1977)551.

Schwarz K.W. Turbulence in superfluid helium: Steady homogeneous counterflow. Phys. Rev. B18(1978)245.

Schwarz K.W. Vortex pinning in superfluid helium. Phys. Rev. Lett. 47(1981a)251.

Schwarz K.W., Smith C.W. Pulsed ion study of ultrasonically generated turbulence in superfluid ^{4}He. Phys. Lett 82A(1981b)251.

Schwarz K.W. Generation of superfluid turbulence deduced from simple dynamical rules. Phys. Rev. Lett. 49(1982)283.

Schwarz K.W. Critical velocity for a self sustaining vortex tangle in superfluid helium. Phys. Rev. Lett. 50(1983)364.

Schwarz K.W. Three dimensional vortex dynamics in superfluid ^{4}He. I Line-line and line-boundary interactions. Phys. Rev. B31(1985)5782.

Schwarz K.W. Dissipative flow of liquid ^{4}He in the limit of absolute zero. Phys. Rev. Lett. 57(1986)1448.

Schwarz K.W. Temperature dependence of discrete dissipative events in superfluid ^{4}He. Phys. Rev. Lett. 59(1987a)1167.

Schwarz K.W. Reply on comment T.F. Buttke. Phys. Rev. Lett. 59(1987b)2118.

Schwarz K.W. Three dimensional vortex dynamics in superfluid ^{4}He. II Homogeneous superfluid turbulence. Phys. Rev. B38(1988)2398.

Schwarz K.W. Phase slip and turbulence in superfluid ^{4}He: A vortex mill that works. Phys. Rev. Lett. 64(1990a)1130.

Schwarz K.W. Note on the validity of vortex tangle simulations of homogeneous superfluid turbulence. J. of Comp. Phys. 87(1990b)237.

Senbetu L. Effect of ^{3}He impurities on the structure of quantized vortex lines and the lifetime of negative ions trapped on vortices. J. of Low Temp. Phys. 32(1978)571.

Slegtenhorst R.P., Beelen H. van. Discrete flow states in capillary flow of He II. Physica 90B(1977)245.

Slegtenhorst R.P., Beelen H. van. Analysis of an experiment on thermally driven flow of helium II in two coupled capillaries. Physica 97B(1979)25.

Slegtenhorst R.P. On the flow of helium II under the influence of a heat current. Ph.D. Thesis, Leiden University, Leiden, The Netherlands (1981a).

Slegtenhorst R.P., Beelen H. van. A survey of experimental data on capillary flow of helium II in the temperature range between 1 K and 2 K. Physica 106B(1981b)200.

Slegtenhorst R.P., Marees G., Beelen H. van. Observation of steady inhomogeneous flow states in capillary flow of helium II. Physica 108B(1982c)367.

Slegtenhorst R.P., Marees G., Beelen H. van. Steady flow of helium II in the presence of a heat current. Physica 113B(1982a)341.

Slegtenhorst R.P., Marees G., Beelen H. van. Transient effects in superfluid turbulence. Physica 113B(1982b)367.

Soulen R.J., Dove R.B. SRM 768: Temperature reference standard for use below 0.5 K. Nat. Bur. of Stand. Special Publication 260-62. U.S. Dept. of Commerce, Nat. Bur. of Stand. (1979).

Staas F.A., Taconis K.W., Fokkens K. Viscosity of liquid ^{3}He-^{4}He mixtures in the helium II region above 1 K. Physica 26(1960)669.

Staas F.A., Taconis K.W., Alphen W.M. van. Experiments on laminar and turbulent flow of He II in wide capillaries. Physica 27(1961)893.

Stokes G.G. On the effect of the internal friction of fluids on the motion of pendulums. Proc. of the Cambr. Phil. Soc. 9(1851)8.

Stuart J.T. Unsteady boundary layers. Chapter 7 of Laminar Boundary Layers. ed. by L. Rosenhead, Oxford at the Clarendon Press, Oxford (1963).

Stycast 1266/2850GT. Emerson & Cuming, W.R. Grace & Co., Nijverheidsstraat 7, 2431 Westerlo, Belgium.

Swanson C.E. A study of vortex dynamics in counterflowing He II. Ph.D. Thesis, Oregon University, Eugene, Oregon U.S.A. (1985a).

Swanson C.E., Donnelly R.J. Vortex dynamics and scaling in turbulent counterflowing helium II. J. of Low Temp. Phys. 61(1985b)363.

Swinney H.L., Gollub J.P. Hydrodynamic instabilities and the transition to turbulence. Topics in Appl. Phys. 45, second ed., Springer Verlag, Berlin, (1985).

Tatsumi T. Turbulence and chaotic phenomena in fluids. Proc. of the Int. Symp. on Turbulence and Chaotic Phenomena in Fluids, Kyoto, Japan 5-10 Sept. 1983. North Holland, Amsterdam (1984).

Taylor R.D., Dash J.G. Hydrodynamics of oscillating disks in viscous fluids: Viscosities of liquid ^{3}He and ^{4}He. Phys. Rev. 106(1957)398.

Tilley D.R., Tilley J. Superfluidity and superconductivity, second ed. Adam Hilger Ltd., Bristol (1986).

Tjerkstra H.H. The influence of pressure on the viscosity of liquid helium I. Physica 18(1952)853.

Tough J.T., McCormick W.D., Dash J.G. Viscosity of liquid helium II. Phys. Rev. 132(1963)2373.

Tough J.T., McCormick W.D., Dash J.G. Vibrating wire viscometer. Rev. of Sci. Instr. 35(1964)1345.

Tough J.T., McCormick W.D., Dash J.G. Effects of turbulence in He II counterflow. Phys. Rev. 140(1965)A1524.

Tough J.T. Superfluid turbulence. Prog. in Low Temp. Phys. 8(1982)135, ed. by D.F. Brewer.

Tritton D.J. Physical fluid dynamics, second ed. Clarendon Press, Oxford (1988).

Troyer A. de, Itterbeek A. van, Berg G.J. van den. Measurements on the viscosity of liquid helium by means of the oscillating disk method. Physica 17(1951)50.

Varoquaux E., Meisel M.W., Avenel O. Onset of the critical velocity regime in superfluid ^{4}He at low temperature. Phys. Rev. Lett. 57(1986)2291.

Varoquaux E., Zimmerman W. Jr., Avenel O. Phase slippage studies of the critical velocity in Helium-4. Nato Workshop on Excitations in 2D and 3D Quantum Liquids, Exeter Ag. 10-15 (1990)

Vinen W.F. Mutual friction in a heat current in liquid helium II. I Experiments on steady heat currents. Proc. of the Roy. Soc. of London A240(1957a)114.

Vinen W.F. Mutual friction in a heat current in liquid helium II. II Experiments on transient effects. Proc. of the Roy. Soc. of London A240(1957b)128.

Vinen W.F. Mutual friction in a heat current in liquid helium II. III Theory of the mutual friction. Proc. of the Roy. Soc. of London A242(1957c)493.

Vinen W.F. Mutual friction in a heat current in liquid helium II. IV Critical heat currents in wide channels. Proc. of the Roy. Soc. of London A243(1957d)400.

Vinen W.F. The detection of single quanta of circulation in liquid helium II. Proc. of the Roy. Soc. of London A260(1961b)218.

Vinen W.F. Critical velocities in liquid helium II. Proc. of the Int School of Phys. "Enrico Fermi", course 21, Varenna, July 3-15, 1961. Liquid helium, Academic Press, New York (1963)p.336.

Waele A.T.A.M. de, Kuerten J.G.M. Thermodynamics and hydrodynamics of ^{3}He-^{4}He mixtures. Prog. in Low Temp. Phys. to appear (1990). ed. by D.F. Brewer.

Wang S., Howald C., Meyer H. Shear viscosity of liquid ^{4}He and ^{3}He-^{4}He mixtures especially near the superfluid transition. J. of Low Temp. Phys. 79(1990)151.

Welber B., Quimby S.L. Measurement of the product of viscosity and density of liquid helium with a torsional crystal. Phys. Rev. 107(1957)645.

Welber B. Damping of a torsionally oscillating cylinder in liquid helium at various temperatures and densities. Phys. Rev. 119(1960)1816.

Wheatley J.C. Dilute solutions of ^{3}He in ^{4}He at low temperatures. Am. J. of Phys. 36(1968a)181.

Wheatley J.C., Vilches O.E., Abel W.R. Principles and methods of dilution refrigeration . Physics 4(1968b)1.

Wheatley J.C., Rapp R.E., Johnson R.T. Principles and methods of dilution refrigeration II. J. of Low Temp. Phys. 4(1971)1.

Whitmore S.C., Zimmerman W. Observation of stable superfluid circulation in liquid helium II. Phys. Rev. Lett. 15(1965)389.

Whitmore S.C. Observation of quantized circulation in superfluid helium. Ph.D. Thesis, Minnesota University, Minneapolis, U.S.A. (1966).

Whitmore S.C., Zimmerman W. Observation of quantized circulation in superfluid helium. Phys. Rev. 166(1968)181.

Williams G.A., Packard R.E. Photographs of quantized vortex lines in rotating liquid He II. Phys. Rev. Lett. 33(1974)280.

Winkel P. Wrijvingsverschijnselen in vloeibaar helium II. (Friction phenomena in liquid helium II (in Dutch)). Ph.D. Thesis, Leiden University, Leiden, The Netherlands (1954).

Winkel P., Delsing A.M.G., Poll J.D. On the existence of critical velocities in liquid helium II. Physica 21(1955a)331.

Winkel P., Broese van Groenou A., Gorter C.J. On the heat conduction in liquid helium II. Physica 21(1955b)345.

Woods A.D.B., Hollis-Hallett A.C. The viscosity of liquid helium between 1.1 K and 0.79 K. Physica 24(1958a)S140.

Woods A.D.B., Hollis-Hallett A.C. The viscosity of liquid helium between 0.78 K and 1.1 K. Can. J. of Phys. 36(1958b)253.

Woods A.D.B., Hollis-Hallett A.C. The kinematic viscosity of liquid helium II. Can. J. of Phys. 36(1958)1125.

Woods A.D.B., Hollis-Hallett A.C. The viscosity of liquid helium II between 0.79 K and the lambda point. Can. J. of Phys. 41(1963)596.

Wygnanski I.J., Champagne F.H. On transition in a pipe. Part 1. The origin of puffs and slugs and the flow in a turbulent slug. J. of Fluid Mech. 59(1973)281.

Wygnanski I.J., Friedman D., Sokolov M. On transition in a pipe. Part 2. The equilibrium puff. J. of Fluid. Mech. 69(1974)283.

Yamauchi J., Yamada K. Effects of boundary-vortex force in capillary flow of superfluid helium. Physica 128B(1985)45.

Yarmchuck E.J., Glaberson W.I. Thermorotation effects in superfluid helium. Phys. Rev. Lett. 41(1978)564.

Yarmchuck E.J., Glaberson W.I. Counterflow in rotating superfluid helium. J. of Low Temp. Phys. 36(1979)381.

Zeegers J., Kuerten J.G.M., Waele A.T.A.M. de, Gijsman H.M. Critical velocities in ^{3}He-^{4}He mixtures. Proc. of the 18 th Int. Conf. on Low Temp. Phys., Kyoto, Aug 20-26, 1987, ed. by Y. Nagaoka. Jap. J. of Appl. Phys. 26(1987)63.

Zeegers J., Aarts R.G.K.M., Waele A.T.A.M. de, Verbruggen M.H.W., Gijsman H.M. Fluctuation phenomena in ^{3}He-^{4}He hydrodynamics. Proc. of the Int. Conf. on Macroscopic Quantum Phenomena 18-22 Sept., 1989, p.228, Smolenice, Chechoslovakia. ed. by M. Kolac.

Zinov'eva K.N. Absorption of second sound in He II. Zh. Eksp. i Teor. Fiz. 25(1953)235.

Zinov'eva K.N. The coefficient of volume absorption of second sound and the viscosity of the normal component of helium II down to 0.83 K. Sov. Phys. J.E.T.P. 4(1957)36.

Zinov'eva K.N. Viscosity of liquid ^{3}He in the range 0.35-3.2 K and ^{4}He above the lambda point. Sov. Phys. J.E.T.P. 34(1958)421.

Zinov'eva K.N., Dubrovin A.V. Dissipation coefficients in helium II. Sov. J. of Low Temp. Phys. 9(1983)232.

LIST OF SYMBOLS

LATIN SYMBOLS

A	Gorter-Mellink constant	$\mathrm{mskg^{-1}}$
A	area of cross section of a tube	$\mathrm{m^{-2}}$
a	experimentally determined parameter (0.2 K^2)	K^2
a_0	vortex core radius	m
B	Hall Vinen parameter	-
b	coefficient in enthalpy conservation equation (0.2K^2)	K^2
C	capacity	F
C_0	^{3}He entropy coefficient (104.3 $\mathrm{Jmol^{-1}K^{-2}}$)	$\mathrm{Jmol^{-1}K^{-2}}$
D	annular diameter	m
d	tube diameter	m
d	slit spacing	m
d_c	diameter of the spiral	m
d_l	diameter of the wire loop	m
E	Young's modulus	Pa
F_d	viscous force per unit of wire length	$\mathrm{Nm^{-1}}$
F_l	Lorentz force per unit of wire length	$\mathrm{Nm^{-1}}$
F	mutual friction force density	$\mathrm{Nm^{-3}}$
f	frequency of oscillation	$\mathrm{s^{-1}}$
H_3^{os}	osmotic enthalpy per mole ^{3}He	$\mathrm{Jmol^{-1}}$
h	Planck's constant ($6.6\cdot10^{-34}$ Js)	Js
$\hbar$	Planck's constant devided by 2π ($1.05\cdot10^{-34}$ Js)	Js
i	current	A
j_3	^{3}He flow rate density	$\mathrm{mols^{-1}m^{-2}}$
k	parameter	$\mathrm{(molskg^{-1}m^{-2})^{\frac{1}{2}}}$
k, k'	Stokes functions	-
L	vortex line density	$\mathrm{m^{-2}}$
L_3	latent heat of ^{3}He	$\mathrm{Jmol^{-1}}$
ℓ	length of tube	m
M	wire mass per unit of wire length	$\mathrm{kgm^{-1}}$
M'	displaced fluid mass per unit of wire length	$\mathrm{kgm^{-1}}$
m	Womersley parameter	-
m_0	constant	-
m^*	effective mass (2.46 m_3)	kg
N	number of flow channels	-
$\dot{n}$	flow rate	$\mathrm{mols^{-1}}$
p	pressure	Pa
Q	heating power	W
r	radius	m
S	entropy per mol	$\mathrm{Jmol^{-1}K^{-1}}$
T	temperature	K
T_λ	lambda temperature (2.172 K)	K
t	time	s

u	displacement	m
V	molar volume	m^3mol^{-1}
v	velocity	ms^{-1}
W_c	critical velocity × diameter	m^2s^{-1}
w	dimensionless velocity	-
x	^{3}He concentration	-
x	dimensionless line length	-
z	length along the tube	m

GREEK SYMBOLS

α	constant	$(molm^2kg^{-1}s^{-1})^{\frac{1}{2}}$
β	constant	$(kgm^2mol^{-1}s^{-1})^{\frac{1}{2}}$
β	scaling parameter	m^2s^{-1}
γ	χ_1'/χ_2	$m^{-2}s$
γ''	mutual friction coefficient ($14\cdot10^{-9}$ $s^3m^5mol^{-3}$)	$s^3m^5mol^{-3}$
δ	constant of order unity	-
δ_v	viscous penetration depth	m
ϵ_r	relative dielectric constant	-
ζ	impedance factor	m^{-4}
η	dynamic viscosity	Pas
η_d	viscosity coefficient ($5\cdot10^{-8}$ $PasK^2$)	$PasK^2$
κ	thermal conductivity	$Wm^{-1}K^{-1}$
κ	quantum of circulation ($1.0\cdot10^{-7}$ m^2s^{-1})	m^2s^{-1}
λ	dimensionless length	-
μ	chemical potential	$Jmol^{-1}$
ν	crossing rate of vortex lines	s^{-1}
ξ	dimensionless parameter	-
Π	osmotic pressure	Pa
ρ	density	kgm^{-3}
σ	flow rate coefficient	-
τ	time	s
υ	coefficient relating T_e with T_h	-
χ	mutual friction coefficient ($11\cdot10^{-9}$ $kgsm^7mol^{-4}$)	$kgsm^7mol^{-4}$
χ	constants related with Vinen's model	- or m^2s^{-1}
ψ	ratio of measured to estimated resonance frequency	-
ω	angular frequency	$rads^{-1}$

FREQUENTLY USED INDEXES

d	referring to downstream of impedance
e	referring to experimental space
i	referring to inlet of mixing chamber
m	referring to mixing chamber or quantity per mole or mixture
n	referring to normal fluid component
s	referring to superfluid component or to the still
w	referring to the wire
η	referring to the viscosity
3	referring to ^{3}He
4	referring to ^{4}He

SAMENVATTING

Gedurende het promotieonderzoek zijn de stromingseigenschappen bestudeerd van vloeibare ^{3}He-^{4}He II mengsels bij temperaturen tussen 10 mK en 200 mK nabij de mengkamer van een mengkoelmachine. Er is in het bijzonder onderzocht wat de temperatuurstijging is als ^{3}He onder adiabatische condities door superfluïde ^{4}He stroomt in capillairen met diameter $50\ \mu m < d < 5$ mm. Dit is gedaan bij een constante ingangstemperatuur als functie van de stroomsnelheid. Behalve de temperatuurtoename zijn ook concentratieafname en drukverschil gemeten en daaruit is onder andere de chemische potentiaal van het ^{4}He berekend. De meetresultaten zijn vergeleken met een tweetal in het verleden opgestelde modellen, waarbij in het ene model de viscositeit in rekening wordt gebracht bij lage stroomsnelheden en in het andere model de bijdrage van de wederkerige wrijving wordt meegenomen bij relatief hoge stroomsnelheden. De wederkerige wrijving wordt toegeschreven aan de aanwezigheid van gequantiseerde wervels in het ^{4}He.

In de snelheidsgebieden waar de modellen toepasbaar zijn is er overeenstemming met de meetresultaten. Het is daarbij gebleken dat er, pas boven een zekere kritische snelheid v_c, dissipatie optreedt tengevolge van wederkerige wrijving tussen het ^{3}He en het ^{4}He II naast de altijd aanwezige viskeuze dissipatie. Ook de invloed van het wandmateriaal en de diameter van de capillairen op de kritische snelheid is onderzocht. Behalve aan ronde capillairen zijn er metingen uitgevoerd aan kanalen waarbij de doorsnede bestond uit een annulaire spleet. In deze annulaire impedanties treedt in tegenstelling tot de ronde capillairen een geleidelijke overgang op naar wederkerige wrijving. Er is een duidelijke invloed van de geometrie op de kritische snelheid. Er zijn voorts gegevens verkregen over de wervellijndichtheid boven de kritische snelheid en deze is in overeenstemming met data uit de literatuur.

Het optreden van kritische snelheden en de daarmee gepaard gaande wervellijndichtheid wordt beschreven met het Vinen model. Met dit model kunnen de metingen in ronde capillairen goed beschreven worden. Echter, het is niet consistent toepasbaar op metingen met annulaire stromingsimpedanties indien dezelfde modelparameters gehanteerd worden. Dit belangrijke resultaat vraagt om een nieuwe beschrijving van het optreden van kritische snelheden.

Behalve het stationaire stromingsgedrag zijn ook de fluctuaties in het drukverschil over de stromingskanalen onderzocht omdat deze in de omgeving van de kritische snelheid sterk bleken te variëren. Een eerste resultaat laat zien dat het fourier spectrum in de omgeving van de kritische snelheid pieken vertoont. Ook zijn er aanwijzingen voor een tweede kritische snelheid. Definitieve conclusies hierover zijn echter op dit moment nog niet te trekken. Dit onderwerp vormt een mogelijkheid voor verder onderzoek.

Uit het totaalbeeld van al het onderzoek is het duidelijk dat de stroming van ^{3}He door een achtergrond van superfluide ^{4}He en de daarbij optredende verschijnselen grote overeenkomst vertoont met het zogenaamde "counterflow" experiment in zuiver ^{4}He.

Gedurende het onderzoek is ook een viscositeitsmeter ontwikkeld die werkt op basis van de demping van een trillende draad in de vloeistof. Daarmee is de viscositeit van het ^{3}He-^{4}He mengsel gemeten. Deze is in overeenstemming met resultaten van de drukmeting uit het stromingsonderzoek. Het lijkt erop dat de gebruikelijke uitdrukking voor de viscositeit niet in overeenstemming is met de gemeten waarden. Dit heeft gevolgen voor de berekening van de drukgradiënt in de stromingsimpedanties. De nieuwe waarde van de viscositeit kan eveneens gevolgen hebben voor de grootte van de parameters in de microscopische beschrijving van ^{3}He-^{4}He mengsels.

SUMMARY.

In this work the flow properties of liquid ^{3}He-^{4}HeII mixtures were studied at temperatures between 10 mK and 200 mK near the mixing chamber of a dilution refrigerator. In particular, the temperature rise was investigated if ^{3}He flows through superfluid ^{4}He II in capillaries with a diameter between 50 μm and 5 mm under adiabatic conditions. Apart from the temperature increase, the concentration decrease and pressure difference were measured at a constant inlet temperature as functions of the flow velocity. From these quantities the chemical potential of ^{4}He was calculated. The results are compared with two models formulated in the past. In one model the viscosity is taken into account at low flow velocities while in the other model the contribution of mutual friction is taken into account at relatively high velocities. The mutual friction is attributed to the presence of quantized vortices in the ^{4}He. In the velocity ranges where the models are applicable there is agreement with the measurements.

From the experiments it has become evident that above a critical velocity v_c, dissipation appears because of a mutual friction between the ^{3}He and ^{4}He together with the viscous dissipation which is always present. The influence of wall material and the diameter of the capillaries on the critical velocity has also been studied. Apart from circular capillaries measurements were carried out with flow impedances where the cross section consisted of an annular slit. In these annular flow impedances a gradual transition to mutual friction occurs, contrary to the circular capillaries. So there is a distinct influence of the geometry on the critical velocity. Furthermore, data were obtained about the vortex line density for velocities above the critical velocity, which is in agreement with data from literature.

The occurrence of critical velocities and associated vortex line density is described in the literature with the Vinen model. With this model the measurements in circular capillaries can be interpreted. However, the model cannot be applied consistently to the measurements with annular flow impedances when the same model parameters are used.

Apart from the stationary flow behaviour, fluctuations in the pressure over the flow channels were studied because these were observed to vary strongly at the critical

velocity. The fourier spectrum of these fluctuations shows a peak in the critical velocity region. There are also indications in the spectrum of a second critical velocity. At present a final conclusion cannot be drawn and this subject might be a suggestion for future studies.

The overall picture of this research is that the flow phenomena of ^{3}He through a background of superfluid ^{4}He resemble those in pure ^{4}He counterflow.

A viscosity meter was developed which is based on the damping of a vibrating wire in the liquid. The design criteria and the dependence of magnetic field were studied. This viscometer was tested in pure ^{4}He between 1.1 K and 4.2 K in a separate setup. With these results the viscosity of the ^{3}He-^{4}He mixture was measured between 7 mK and 200 mK. A detailed comparison is made with the literature. The simple expression used for the viscosity of mixtures at low temperatures is not in agreement with the measurements. The new value of the viscosity influences the calculated pressure difference. Furthermore it can have influence on the magnitude of the parameters in the microscopic description of ^{3}He-^{4}He mixtures.

NAWOORD

Het in dit proefschrift beschreven onderzoek is uitgevoerd in de groep Lage Temperaturen, onder leiding van Prof. dr. H.M. Gijsman, van de faculteit Technische Natuurkunde van de Technische Universiteit Eindhoven. Aan het tot stand komen van dit proefschrift is een bijdrage geleverd door vele personen, van wie ik er op deze plaats graag enkele met name wil noemen, zonder hiermee volledigheid te betrachten.

Fons de Waele stond mij als directe begeleider altijd met raad en daad bij. Mede dankzij zijn stimulans en grote inzicht in de natuurkunde is dit onderzoek zo succesvol verlopen. Ik ben hem erkentelijk voor de vrijheid waarmee ik dit onderzoek heb kunnen uitvoeren.

Hans Kuerten leverde via zijn goede inzicht in de theoretische natuurkunde een grote bijdrage met veel suggesties t.a.v. het uitvoeren van diverse metingen.

Ronald Aarts heeft door zijn grote kennis van meetsystemen en computer-automatisering alsmede zijn inzet in begeleiding van afstudeerders het mogelijk gemaakt dat drukfluctuaties onderzocht konden worden.

Leo van Hout vervaardigde vele mechanische onderdelen en zijn technische ervaring en ondersteuning zorgde ervoor dat nagenoeg zonder problemen week in week uit gemeten kon worden.

Loek Penders stond altijd met electronische hulp en advies bij en vervaardigde vele componenten. De automatisering van de mengkoeler was voor een belangrijk deel zijn werk.

Jos van Amelsvoort en *Wil Delissen* zorgden immer op tijd voor de totaal 18000 liter vloeibaar helium en 80000 liter vloeibare stikstof zonder welk dit onderzoek nooit uitgevoerd had kunnen worden.

Rene Sanders en *Rini Verbruggen* verzorgden een groot stuk onderzoek omtrent stromingsmetingen en viscosimetrie gedurende hun afstudeertijd.

Ton Voncken verzorgde de afsluitende metingen aan de viscositeit.

Willian Draisma verzorgde de programmatuur die nodig was bij de automatisering van de mengkoeler.

Voorts werd veel steun ondervonden van de hulp van afstudeerders van de Hogeschool Eindhoven en stagiairs die participeerden in het onderzoek, leden van de faculteitsinstrumentmakerij, glas- en fijninstrumentmakerij van de Centrale Technische Dienst, de overige groepsleden, het secretariaat, alsmede de medewerk(st)ers van de bibliotheek.

CURRICULUM VITAE

27 november 1959	Geboren te Oss.
juni 1977	Eindexamen HAVO aan het Maasland College te Oss.
juni 1979	Eindexamen Atheneum β aan het Maasland College te Oss.
mei 1986	Doctoraal examen natuurkundig ingenieur aan de Technische Universiteit Eindhoven. Afstudeerwerk verricht in de groep Turbulente Transportverschijnselen onder leiding van Ir. C. Nieuwvelt.
juni 1986-juni 1990	Werkzaam als wetenschappelijk assistent aan de TUE in de groep Lage Temperaturen onder leiding van Prof. dr. H.M. Gijsman.
december 1990	Werkzaam als wetenschappelijk medewerker bij TNO-TPD, sectie Bouwkundige Systemen, afdeling Klimaatbeheersing, te Delft.

STELLINGEN

behorende bij het proefschrift van
J.C.H. Zeegers

1 De frequentieafhankelijkheid van de door Nadirashvili gemeten viscositeit in ^{4}He II is niet het gevolg van de vrije fononlengte in de vloeistof.
Z.Sh. Nadirashvili, D.S. Tsakadze, Dependence of ^{4}He II viscosity properties on oscillation frequency. J. of Low Temp. Phys. 37(1979)169.

2 Trillende-draad-viscosimetrie met draden waarbij de boogstraal veel groter is dan de draaddiameter kan alleen uitgevoerd worden in een trillingsarme opstelling.

3 De kritische snelheid in annulaire buizen ligt veel lager dan de waarde die men op grond van een criterium gebaseerd op product van snelheid en sleufbreedte zou verwachten.
Dit proefschrift, hoofdstuk 4 en 5.

4 Het getal van Reynolds speelt bij de eisen voor een goede werking van een trillende draad viscosimeter een ondergeschikte rol zolang de uitwijking klein is ten opzichte van de draaddiameter.

5 De theorie van Stokes voor de kracht op een oscillerende oneindig lange cilinder mag ook toegepast worden voor grote waarden van de viskeuze penetratiediepte, mits de uitwijking klein genoeg is.
N. Amin, Low frequency oscillations of a cylinder in a viscous fluid. Quart. J. of Mech. and Appl. Math. 4(1988)195.

6 In tegenstelling tot wat Chen beweert, gaat het begrip "added mass" niet terug tot Stokes' beschrijving in 1851, maar was het reeds in 1786 bekend bij Dubuat.
S.S. Chen, M.W. Wambsganss, J.A. Jendrzejczyk, Added mass and damping of a vibrating rod in confined viscous fluids. Trans. ASME, J. of Appl. Mech. 43(1976)325.
P.L.G. le Chevalier Dubuat, Principes d'Hydraulique et de Pyrodynamique verifiés par un grand nombre d'expériences. 2$^{\text{ième}}$ *éd. (1786), Ch. 7.*

7 Doordat stromingsverschijnselen in ^{4}He worden bepaald door de interactie van de normale en superfluïde component, via een wervelkluwen, is het zeer de vraag of de stabiliteitstheorie op grond van de Hall-Vinen-Bekharovich-Khalatnikov-vergelijkingen een oplossing zal geven voor de instabiliteit van stroming in buizen en tussen roterende cilinders.
C.F. Barenghi, C.A. Jones, The stability of the Couette flow of helium II. J. of Fluid Mech. 197(1988)551.

8 Ondanks het grote doorstroomoppervlak (7 cm^2) van de warmtewisselaars in de 500 mmol/s mengkoeler van Niinikoski, zal de minimumtemperatuur die deze koelmachine bereikt bij een circulatie groter dan 150 mmol/s bepaald worden door wederkerige wrijving.
T.O. Niinikoski, Dilution refrigerator for a two-litre polarized target. Nucl. Instr. and Meth. 192(1982)151.

9 Interpretatie van stromingsvisualisatie is moeilijker dan men in eerste instantie denkt.
M. Kurosaka, P. Sundaram, Illustrative examples of streaklines in unsteady vortices: Interpretative difficulties revisited. Phys. of Fluids 29(1986)3474.
I. Gursul, P. Lusseyran, D. Rockwell, On the interpretation of flow visualization of unsteady shear flows. Exp. in Fluids 9(1990)257.

10 Het bouwen van een helium-tunnel in Nederland zou serieus overwogen moeten worden.
A.W. Epstein, Cool breeze, a helium superwind for windtunnel experiments. Scient. Am. 262(5)(1990)12.

11 Door het locale stromingsprofiel van de normale component in rekening te brengen kan een belangrijke uitbreiding van numerieke simulaties van wervelkluwens worden gerealiseerd.

12 De aerodynamica van treinramen zou verbeterd moeten worden.

13 Kwaliteitsaanduidingen in muziek- en filmencyclopedieën zijn misleidend.

14 Het hebben van een omvangrijke onderwijstaak werkt bij assistenten in opleiding demotiverend en is eigenlijk onacceptabel.

25 januari 1991